A NOVEL SONAR DEVELOPMENT PLATFORM: DUAL FREQUENCY SONAR BEAM SHAPING FOR ANGULAR LOCALIZATION

by

Murat Karadeniz

B.S. in Electrical and Electronics Engineering, 2003

Submitted to the Institute for Graduate Studies in
Science and Engineering in partial fulfillment of
the requirements for the degree of
Master of Science

Graduate Program in Electrical and Electronics Engineering

Boğaziçi University

2006

ACKNOWLEDGEMENTS

I sincerely thank to my advisor Prof. H. Işıl Bozma for her confidence in me and for the assistance she provided through my research.

I am grateful to Prof. Ömer Cerid for the discussions we made and his guidance on Ultrasonics and Electronics over the year I spent on this project.

I would like to thank to Prof. Yekta Ülgen and Assoc. Prof. Yasemin Kahya for serving on my thesis committee.

I also would like to mention the name of Atmel Corporation for providing me engineering samples, and Megatek Eletronik for helping with the mechanical constructions used in the experiments. Finally, I would like to thank to Michael Bernstein, for preparing a custom VB version of his Universal Scope Library for me.

Finally, without the love and support of my family, this thesis would not even have been possible. Thank you for everything.

ABSTRACT

A NOVEL SONAR DEVELOPMENT PLATFORM: DUAL FREQUENCY SONAR BEAM SHAPING FOR ANGULAR LOCALIZATION

This thesis presents a complete airborne ultrasound system inspired by both underlying physics and biological sonar. First, a completely new hardware platform is designed and developed. This design supports an extendible and flexible sensor topology. Next, the associated firmware is designed and implemented. This software provides all the lower-level communication among the distributed sensors and the host processor while employing a new bus arbitration technique. An accompanying PC development environment is created. The result is an unique integrated system that holds the promise of providing research and development platform for future sonar work without requiring changes in the hardware and software infrastructure. This is demonstrated in the problem of finding angular position. As is well known, sonar sensors are capable of finding radial position of a target object quite precisely, however they have very low angular resolution. Previous work has proposed methods that are based on multiple sensors and hence are relatively complex. This thesis proposes a novel approach based on only a single transducer. This approach is based on dual frequency beam shaping. Experiments serve to demonstrate that even with minimal hardware, and hence processing power and cost, angular accuracies of order 0.5 degrees are easily achievable.

ÖZET

YENİ BIR SONAR GELİŞTİRME ORTAMI: AÇISAL KONUMLANDIRMA İÇİN ÇİFT FREKANS İLE SONAR HÜZMESİ BİÇİMLENDİRME

Bu tez çalışmasında, biyolojik sonar sistemlerinden ve altında yatan fizik ve akustik teorisinden esinlenen hava ortamında çalışan tam bir ultrason sistemi ortaya konmuştur. Öncelikle, bütünüyle yeni bir sonar donanım platformu tasarlanmış ve gerçeklenmiştir. Hazırlanan tasarım, genişletilebilir ve esnek bir algılayıcı eşgüdüm mimarisine sahiptir. Sonra, bu mimariyi gerçekleyecek gömülü yazılım hazırlanmıştır. Bu yazılım dağıtılmış algılayıcıların kontrolünü ve birimler arası alt seviye iletişimini, yeni bir veriyolu denetimi ile sağlamaktadır. Sonuç, köklü bir donanımsal ve yazılımsal değişiklik gerektirmeden gelecekteki sonar araştırmalarını icin temel oluşturacak benzersiz bir tümleşik sistemdir. Bu, açısal konum bulma sorununda gösterilmiştir. Çok iyi bilindiği gibi, sonar algılayıcıları bir hedef nesnenin uzaklığını oldukça hassas bir şekilde belirleyebilmektedirler, fakat açısal ayrım güçleri çok düşüktür. Önceki çalışmalar tarafından önerilen yöntemler birden çok algılayıcı tabanlı olup, oldukça karmaşıktırlar. Bu tez çalısması tek bir algılayıcıya dayalı bir yaklaşım önermektedir. Bu yeni yaklaşım iki frekanslı sonar hüzme biçimlendirmeye dayanmaktadır. Deneyler, asgari donanım, maliyet ve işlem gücü ile, 0.5 derece seviyesinde açısal doğrulukların kolaylıkla elde edilebileceğini göstermektedir.

TABLE OF CONTENTS

LIST OF FIGURES

LIST OF TABLES

LIST OF SYMBOLS/ABBREVIATIONS

E	Expected value
H	Directional factor
k	Wavenumber
α	Attenuation coefficient
θ	Bearing angle
σ	Standart deviation
ADC	Analogue to Digital Converter
CPLD	Complex Programmable Logic Device
DDS	Direct Digital Synthesis
DMA	Dynamic Memory Access
EMI	Electromagnetic Interference
FIFO	First In First Out
FIR	Finite Impulse Response
FPGA	Field Programmable Gate Array
HRTF	Head Related Transfer Function
ILD	Inter-aural Level Difference
IPD	Inter-aural Phase Difference
ITD	Inter-aural Time Difference
PZT	Piezoelectric Transducer
Q	Quality factor
SPL	Sound Pressure Level
TOF	Time of Flight
UART	Universal Asynchronous Receiver-Transmitter
UC	Microcontroller
US	Ultrasound
USB	Universal Serial Bus

1. INTRODUCTION

This thesis aims to develop a complete ultrasound system – inspired by both underlying physics and biological sonar. It is an effort at this intersection – towards developing an ultrasound system that can serve as a robust, flexible and extendible study platform for further sonar research and applications without requiring any modifications. This is achieved through the implementation of a unique integrated system that incorporates completely new designs in its electronics as well as its accompanying operational software. A novel sonar analysis algorithm that is biologically motivated and is based on the physical properties of the sonar transmission is then developed and evaluated on this system.

1.1. Acoustics

Acoustics may be defined as the generation, transmission, and reception of energy in the form of vibrational waves in matter [1]. As the atoms or molecules of a fluid or solid are displaced from their normal configuration, an elastic restoring force arises. It is this elastic restoring force, coupled with the inertia of the system, that enables matter to participate in oscillatory vibrations and thereby generate and transmit acoustic waves. Most phenomena (such as diffraction, refraction, reflection etc.) that can be observed in acoustics also occur in other modalities such as optics. The audible sound frequency range is between 20 Hz to 20 kHz. Frequencies above 20 kHz are called ultrasonic frequencies [1]. The ultrasonic signals are mostly used in the range 40 kHz to 120 kHz. The interested reader is referred to [1] for a detailed presentation of acoustics.

In particular, the strongly specular (mirror-like) nature of the reflected acoustic waves become prominent in most of systems – both biological and engineered and commonly known as time-of-flight (TOF) systems. Here, radial distance is estimated using this property along with the known speed of sound in the associated medium. Next, the attenuation of air medium is approximately proportional to the square of sound frequency. The penetration of sound into higher ranges is hindered – hence

making it a rather short range sensor. This range also determines the usable types of transducers. The transducer characteristics have a strong impact on the received signals and thus the resulting system and algorithms.

1.2. Biological Systems

Many biological systems utilize ultrasonics as a means for sensing their environment. On land, vision and hearing are the most effective senses for long range interaction. Under water, vision loses its effectiveness and auditory sensing becomes the only long range tool for navigation and survival. Dolphins and whales use ultrasound for range measurement, target identification and also for communication [2]. In the air, bats use ultrasonic waves throughout their navigation in the darkness of caves. In 1794, the Italian natural philosopher Lazzaro Spallanzai identified the bat's sixth sense being based on hearing but his findings were rejected in favor of a theory related to flying by touch [2]. It was only in the mid-20th century that serious research has been conducted and acoustic theory has been re-accepted [2]. Since then, biologists have established that the evolution path of echolocating bats seems to occur from passive hearing to active hearing (echolocation) [3]. Therefore, it is wise to examine the problem of spatial localization in passive hearing systems. Human hearing sense is a hot topic under active research for years. Its performance and sources of difficulties will give us insight before resorting to the active hearing problem at hand.

1.2.1. Human Audition

Human audition is a passive binaural system with two stationary ears positioned along the two sides of the head. The head provides a frequency and distance dependent masking to sound waves and thus has a related transfer function (HRTF). The effect of the head is very pronounced for nearby sound sources ($< 1m$) or for high frequency sound sources. External ear and ear-drum provide directional filtering or gain and spectral modification on received sound. Inter-aural level differences (ILD), inter-aural time differences (ITD) (inter-aural phase difference (IPD) can be classified as a sort of ITD) are two major mechanisms which provide auditory cues to localize the sound

source in passive hearing. According to generic belief, ILD, ITD and IPD are related to the horizontal direction of the sound, and spectral changes are related to the vertical direction of the sound.

When a sound source is relatively distant from the head, the auditory cues are roughly independent of distance. At distances beyond 1 m, the HRTFs that characterize the relationship between the sound generated by the source and the sounds reaching the left and right ears of the listener, vary only by a constant scaling factor that is inversely proportional to the distance of the source. The interested reader is referred to [4] for a comprehensive review of the literature on auditory localization for distant sources. The auditory cues associated with the direction of the source, including ITD, ILD and directional filtering by the external ear, are all roughly independent of distance [5]. In the region within 1 m of the human head, the situation is totally different. When a sound source is located near the head, the ratio of the distance from the source to the near ear divided by the distance from the source to the far ear decreases. Due to this, an increase in the ILD occurs as distance decreases. In addition, the effects of head masking at the far ear are enhanced when a source is located near the head (A sound screen is more effective when it is closer to the sound source). As a result of these two effects, the ILD produced by a source at a direction outside the median plane of the listener increases monotonically as the source approaches to the listener's head. For a 3 kHz source at 90° (where 0° corresponds to the median plane of the listener), for example, the ILD measured increases from 12 to 40 dB as a source distance decreases from 1 m to 12 cm [6]. Even at 500 Hz where the ILD for a relatively distant source never exceeds 5 to 6 dB, the ILD for a source near the head approaches 20 dB. The masking effect of head increases with increased sound frequency. This is due to the fact that at low frequencies, sound will diffract around the head whereas at high frequencies, sound will reflect off the head. In contrast to the dramatic changes in ILD for close sources, the ITD remains roughly independent of source distance. IPDs have been shown to dominate the judgements of source direction for humans [7]. For nearby sources, IPDs give roughly the same spatial information as ILDs. This is inconsistent with the idea that IPDs are perceptually more important than ILDs because they are naturally more reliable. However, the mapping between ILD and source direction varies with source

distance and environment, suggesting that robust computation of source location may be simpler using IPD cues than ILD cues [8]. Quantitatively, the precision of human's spatial localization of the sound source is about 5° in average in elevation and azimuth. Spatially, our most succesful spatial localization is directly in front (0° azimuth) with a maximum accuracy of 1° . The minimum audible angle increases as sounds are moved towards the axis of the ears, where it reaches a maximum of ± 10 degrees [9].

1.2.2. Echolocating Bats

Echolocating bats are auditory specialists [10]. In the course of evolution, they moved further and enhanced their passive hearing system into an active system. In their daily life routine, through the darkness of caves and through the cluttered environments of the forests, they complete their essential tasks such as prey detection and capture, spatial orientation and localization with the use of their single most advanced sensor, ultrasonic sonar. Periodically, they produce ultrasonic vocalizations and listen to the echoes reflected from the objects around them. One cycle of this operation is called *echolocation*. Echolocation is a rather short ranging system since the sound waves traveling through the air get attenuated. The big external ears of bats provide an acoustic gain like the antenna gain. As an example, the acoustic gain of the pinnae of Rhinolophus rouxi is 24 dB. The prey's size is comparable to their ultrasonic sound vocalization's wavelength. They can catch prey in mid-air with high catch probabilities. These capabilities indicate the presence of a very accurate and sophisticated biological sonar system. Biologists have been investigating bats for decades. Their findings have motivated engineers who have then set out to design sonar systems that can replicate or mimick at best such performance.

The most relevant classification of echolocating bats is done according the variety of their echolocation signals as [3]: i) Constant frequency (CF) bats that generate long, narrow band calls; ii) Quasi-CF bats that generate narrowband shallow frequency modulation (FM) calls; iii) FM bats that generate broadband steep frequency sweeps during calls and iv) CF/FM mixed bats that generate composite calls each made up of an initial CF section and following downward sloped FM section [11]. CF bats use long

narrowband CF signals in combination with doppler shift compensation which then enables the detection and decoding of prey specific modulations (glint patterns) in the echoes which is then utilized in the classification of fluttering insects in a cluttered environment. Studies also suggest that due to their long duration, CF echoes deliver flow field information revealing the position of targets while the bat is in motion [3]. FM bats attain more precise time markers due to the chirp caused time compression of received echoes after processing. Chirp signal generation is adapted to radar applications with great success, allowing increased SNR together with good time resolution. Broadband calls also excite different diffraction modes of pinna and thus contribute to te determination of the target elevation information.

The duty cycle, pulse duration, intensity, frequency range of the ultrasonic vocalization are all adaptive in nature. They are controlled in part by the bat's sensorimotor system (adjustments of the pinna, head aim, flight path and features of subsequent sonar vocalizations). Bat's habitat has direct impact on sonar vocalizations too. We can distinguish three main types of bat hunting environments: in the open, between and along vegetation, and close to and within vegetation and the ground [3]. Interactions with the background and a possible masking of prey echoes by clutter necessitate sonar vocalization changes. There is also general relationships between foraging and echolocation behaviour that are consistent among different bat species. Foraging behaviour consists of the following stages:

- Search flight (before detection of prey)
- Approach flight (pursuit after detection of prey)
- Capture of prey
- Retrieval of prey.

These stages are correlated with distinct phases in echolocation behaviour: search, approach, and terminal phase followed by a pause. In the approach and terminal phases, pulse duration and pulse interval decreases as the proximity to the target decreases, while bandwidth (for FM bats) and sweep rate increases. While pursuing insects, the reduction in pulse duration serves to avoid an overlap between outgoing

signal and the echo returning from the prey. Furthermore, the bats are observed to stop emitting signals several centimeters before they reach the prey [11]. Detection of prey occurs in pipistrelle bats at distances of 1.14-2.20 m [11]. The search cone extending from the bats mouth is up to 150° wide. The pipistrelles catch their prey in mid-air, either with the tail membrane alone or by funnelling it with a wing onto the tail membrane. The mean flight speed of pipistrelles foraging in open space in straight search flight ranges from 4.2 to 7.1 m/s and differed between species, larger bats flying faster than smaller one. Flight speed characteristically drops from 4-7 m/s in search flight to 1.5-3.5 m/s during pursuits. flight speeds of insects caught by pipistrelles ranges from 0.5 to 1 m/s for small, mosquito-sized insects up to 3-4 m/s for medium-sized moths [11]. In an experiment detailed in [12], radiation patterns of the 55, 75 and 95 kHz components in frequency-modulated sounds emitted by the grey bat (Myotis grisescens) were studied. The main beam was emitted 5-10° downward from the eye-nostril line. The radiation angle at one half of maximum amplitude was 38° lateral, 18° up and 50° down at 55 kHz, 34° lateral, 8° up and 32° down at 75 kHz, and 30° lateral, 5° up and 25° down at 95 kHz. At 95 kHz, two prominent side lobes were present.

It is generally accepted that FM bats estimate the target object's range from echo delay. For big brown bats, it has been seen that their range resolving power is much shorter than the shortest periods in the bat's sounds [13]. In their experiments, bats can separately perceive the delays of two concurrent electronically generated echoes arriving as little as 2 microseconds apart, thus resolving reflecting objects as close together as 0.3 mm in range. As the bats pulse trains are 2000-4500 ms long, the echoes overlap. In order to distinguish the time delays of overlapping echoes, the bat has to recover information regarding the very small delay separation that was transferred into the spectrum when the two echoes interfere with each other, thus explicitly reconstructing the range profile of targets from the echo spectrum. Resolution of delay seems extremely sharp just for capturing isolated flying insects which suggests that the bats biological sonar images are of higher quality to suit a wider variety of orientation tasks, and that their sonar echo processing is more sophisticated than has been suspected.

It is believed that most bats use ILD to estimate the target azimuth as the human

does. Behavioral studies have shown that FM bats make use of the morphology of the pinna to extract vertical cues from the echo [14]. Experiments reveal that pinnae alter the vertical angle of maximum sensitivity over different frequencies of the frequency sweep. Studies on 3D localization with elevation estimation are rather new and there is no consensus on bat's solution to this problem. In the case of CF bats, the azimuth angle estimation is thought to be done using ILD. CF bats cannot make use of any special multi-frequency cues for elevation estimation. Behavioral studies indicate that they use a sensorimotor behavioral approach to estimate the target elevation: they move their pinnae in vertical direction over in an arc from +15° to -15° [15]. Some researchers in robotics have tried to mimick this behaviour to their biomimetic sonar systems and steer artificial ears to locate the sound source [16]. The steering of external ears allow for controlled directional filtering of the environmental sound stimulus. We believe that orienting the ears to the direction of interest reduces the head related masking in that direction. This is supported by our observation that the positioning of the ears on the head for ear steering animals is also different from non-ear steering animals. The implications of this observation will be discussed later on in this thesis.

1.3. Ultrasonic Transducers

The US transducer is assumed to be *reversible* [1] which means that it has the same directional properties regardless of whether it is in a transmission or reception mode. There are basically two major categories of transducers:

- Electrostatic
- Piezoelectric

The electrostatic transducer is simply a large and thin parallel plate capacitor. One plate is rigid while the other is made of a thin gold-plated plastic foil. This special foil is pressed with its non-metallic face against the other rigid grooved backplate. On the backplate, concentric grooves are engraved. A high bias voltage (150 V or more) is applied, so that the foil is firmly pressed against the ridges of the grooves. When a signal is applied to the transducers, the voltage changes produce attractive/repulsive forces

between the plates, which make them oscillate with the applied signal's frequency. In the reverse mode, when ultrasonic waves arrive at the transducer face, the foil oscillates, modulating the capacitance of the parallel plate capacitor. One such transducer is the commercially available Polaroid transducer which is used in most robotics applications as shown in Figure 1.1. The advantage of this type of sensor is that it can transmit and

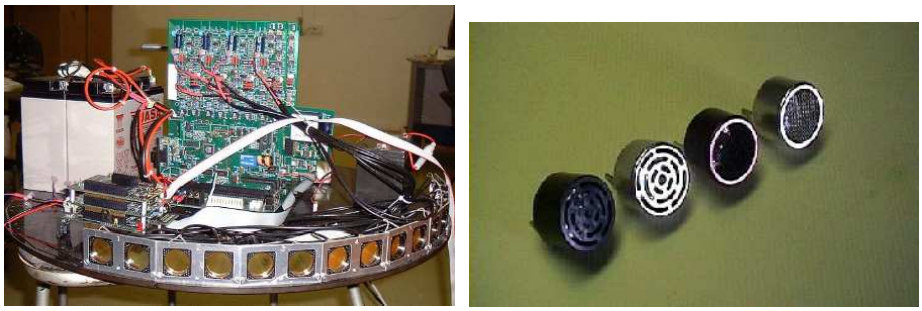

Figure 1.1. Left: Polaroid electrostatic transducers of the DSP Sonar Ring by Lindsay Kleeman; Right: Open type piezoelectric ultrasonic transducers

detect a wide range of frequencies. Its major disadvantage is that the voltage across the plates need to be in the order of hundreds of volts. Furthermore, the instantaneous current requirement is very large too. As an example, the Polaroid transducer needs approximately 300 V across the plates and draws a peak current of 2 A. For larger robots, such a power consumption may be acceptable but it is certainly detrimental for small scale robots with limited battery capacity. Furthermore, the aperture size is relatively large which results in highly directive beams. They have a narrow main lobe beam angle and multiple sidelobes since the the transducer aperture size is considerably bigger than wave length. The side lobes become more pronounced in large pulse count transmit packets. As the tranducer excitation resembles a mono-frequency one, the occurence of sidelobes are revealed. (The pulse needs to be wide enough to include enough frequency components so that it actually is 40 kHz e.g.). If the pulse is made very short (as in the order of a few wavelengths of the transducer center frequency e.g.), then the transducer would not see the signal as a 40 kHz wave but as a wide spread of frequencies and it would not resonate, which would mean that we would not get a signal strong enough.

The second available type of transducers is piezoelectric transducer (PZT), as shown in Figure 1.1 (left). The main part of this transducer is a small piezoelectric crystal which has been cut to resonate at ultrasonic frequencies. Piezo crystals are capable of converting electrical energy to mechanical energy and vice versa. The internal construction of a "bimorph" PZT is shown in Figure 1.2. The PZT bimorph is a two-layer wafer made of poled PZT material – arranged in such a way that it bends from convex to concave as an AC voltage drive is applied across its terminals. This brings about big displacements in the center of the element. To couple the vibrations to the air load and give the PZT a mechanical load, a lightweight cone about 7 mm in diameter is attached to the center of a load matching plate which is bonded to the bimorph. The cone has a fundamental vibration mode at the bimorphs loaded resonance. To produce more output, the bimorph is mounted over a $1/4\,\lambda$ cavity [18]. When voltage is applied across the elements pins, the upper red element gets longer while the bottom blue one shortens, causing a bending in the bimorph material. Changing the polarity causes the opposite bending to occur. The maximum displacement of the vibrational movements is in the center of the element where the cone is mounted. This way, the cone experiences maximum displacements, increasing transmitting SPL level. Most air PZT transducers can be driven with up to 20 V root mean square (rms) drive voltages and SPL levels about 125 dB (measured at a distance of 30 cm and relative to standart reference value of 20 uPa) can be easily generated in the air. Unlike the electrostatic transducers, piezo crystals are very frequency selective. A piezo crystal can be thought as a bandpass filter with a very tight pass-band and high output impedance. They generally have one resonant frequency where the electro-mechanic energy conversion efficiency is very high. On the other hand, frequencies other than this resonant frequency do not convert well. Many variants exist:

1. Open type PZTs. They offer better sensitivity, but are for indoor use only (See Figure 1.1 (right)).
2. Closed type PZTs. They can be used in outdoor applications, and are dust & water proof
3. Asymmetric Field PZTs. Their beam pattern is asymmetric in the vertical and horizontal directions. (Used for example as parking sensors in cars)

4. Tx only PZTs. These PZTs are optimized for transmitter mode of operation.
5. Rx only PZTs. These PZTs are optimized for receiver mode of operation.

A transducer with high selectivity has some key advantages as well as some limitations under operation. The key advantages of PZTs can be listed as:

- Small size – multiple transducers can be put closer to match to the requirements of transducer array topology used in active phased array beam-steering and beam-forming applications or in micro-robotics platforms with good sensor coverage [19].
- Rugged construction (closed type ones are extremely environment proof).
- Higher immunity to electromagnetic interference.
- Economic cost
- Wide beam angle - Let it be noted that although most of the previous work see this as a disadvantage, we argue that this can be advantageous as will be explained in the sequel.
- Easier drive electronics
- Very low power consumption – As PZTs are made of crystal and operate at resonance, they require dramatically less power to produce the same SPL with electrostatic transducers. Drive voltages are an order of magnitude smaller, with current on the order of milliamps.
- High frequency selectivity. The detector itself helps in filtering out the noise produced by other interference sources.
- Use of separate transducers for Tx & Rx Operations offers better SNR.

After a comparative analysis, the PZTs are selected as the US sensors to be utilized in this thesis project. With audible sound transducers, limiting ourselves to the sound transmission case at first, the directivity of the transducer is intentionally controlled with the selection of an appropriate aperture size for the specific task, during the problem definition and hardware implementation phase. For a sound frequency of interest, the right aperture size is determined to satisfy the directivity needed. However, the sound being generated is rarely of mono-frequency, and usually a range of frequencies

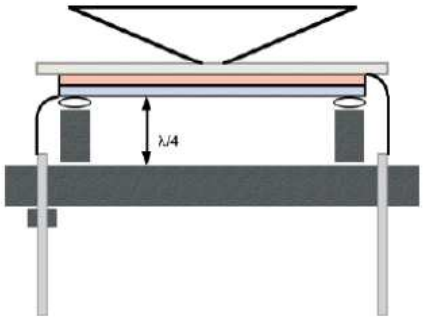

Figure 1.2. The internal construction of a bimorph piezoelectric transducer

centered around some center frequency is to be handled by the transducer. The unintentional and undesirable consequence is that different frequency components of the transmitted sound signal are transmitted to points off the acoustic axis of the transducer with different emphasis. This results in frequency dependent distortion. Furthermore, the sound content cannot be distributed equally to the space to be vocalized. Speaker cabin designers therefore split the wide frequency range to be covered using cross-over circuits and use multiple aperture size speakers covering smaller frequency ranges to achieve similar directivity over a wider overall frequency range and a more homogenous sound reproduction throughout the space. A similar problem occures for sound receivers.

1.4. Ultrasound Electronics

The ultrasound sensor configurations that have been reported fall into one of three categories as listed below in the order of increasing complexity:

- Circular ring topology with multiple Polaroid transducers as a belt for the robot [20].
- Pan(&tilt) head mounted single/dual transducer pair topology [21].
- Phased array topology (in either linear, planar or complex array arrangements of sensors) [22], [23].

The number of transducers and their spatial arrangement in space are both determined based on whether the required sensor coverage is two or three- dimensional. In the pan(&tilt) configuration, two transmitters and two receivers are used for two-dimensional sensing. For three-dimensional sensing, the number of transmitter and receiver transducers are both increased to three. Impulse like short pulse trains are used with high SPL levels and highly directive transducers to compansate for the poor signal-to-noise ratio of impulsive pulses [24].

The sampling is usually done with 12 bit ADCs at 1 MHz, and simultaneous sampling is used in multi-aural configurations. Most sonar system developers use Polaroid type transducers with high directivity and high voltage (300 V) drive. In most of the systems, the acquisitions of received echoes are done with data aquisition boards connected to the data bus of industrial/commercial PCs. However, self-contained sonar systems with internal signal processing capability using DSPs have also been reported [21].

1.5. Ultrasound Sensors in Robotics

Sensors are very important for autonomous systems. The mobility and task completion performances are highly related with the quality of the environmental data their sensors can provide and at what rate they can sustain this. The sensor information is mostly used to generate a geometric model of the environment, which is then used by the robot as it navigates through the environment. The mobility tasks such as localisation, path planning, obstacle avoidance and map building & maintenance are all achieved with sensory information. In less structured environments, more information need to be collected at high rates to accomplish the mobility tasks. This is where some researchers claim that sonar has severe limitations. Some favor other types of sensors such as infrared, laser, camera and microwave systems for mobile robotic platforms. Despite some disadvantages, ultrasound sensors have many advantages, which make them popular sensors. The low cost, low power operation and low processing power requirements are some of their advantages. The high object reflectivity, high measurement time and low information content are some of its disadvantages.

The half beamwidth angle θ_0 of a transducer is defined as [25].

$$\theta_0 = \sin^{-1}(\frac{1}{a}0.61\lambda) \tag{1.1}$$

where $\lambda \in R^+$ is the wavelength of the ultrasonic beam in the air medium corresponding to the driven frequency, which is also the resonance frequency of the ultrasonic transducer in hand, and $a \in R^+$ is the aperture size of the transducer. It is well known that using a single stationary transducer, the angular position of the target object cannot be estimated with a resolution better than the full beamwidth angle $2\theta_0$. Consequently, when a range reading is made using the time-of-flight (TOF) method, all that is known is that the object is somewhere on a spherical cap subtending a cone of angle θ_0 and radius r and origined at the transmitting/receiving transducer [25]. Most approaches have this perspective and use narrow beam Polaroid type electrostatic transducers with 15-20° full beamwidth angle in order to keep the ensonified spherical cap small and have better angular resolution for one transducer. This has the added advantage that a smaller portion of the sensed environment is ensonified with full strength, and thus its acoustic brightness level is enhanced with respect to the nearby reflectors. One such transducer is the Polaroid transducer with 50 kHz resonance frequency and 20 mm aperture size, which has a half beamwidth angle θ_0 of only 11.97°. The major disadvantage of such a highly directive ultrasonic beam is that it acts as if it is looking through a key hole to the world, and the beam has to be steered to the region of interest. Consequently, large area coverage may be either time-consuming or require additional hardware. Different approaches have been proposed in order to overcome this shortcoming. For example, a 360° coverage around the robot body is obtained by employing multiple narrow angle transducers in a circular ring configuration [20], [26]. For most sensor topologies, the sensing is assumed to be limited to the two-dimensional workspace. The reflecting surfaces are assumed to be continuous and smooth in the vertical direction. An alternative approach is to mount the transmit/receiver transducers on a motorized pan and tilt base and scan the environment [21]. However, in real-time applications, such an approach may also prove to be too slow. In contrast, some researchers, although relatively few in number, have chosen to work with US transducers with wide beam angle [27].

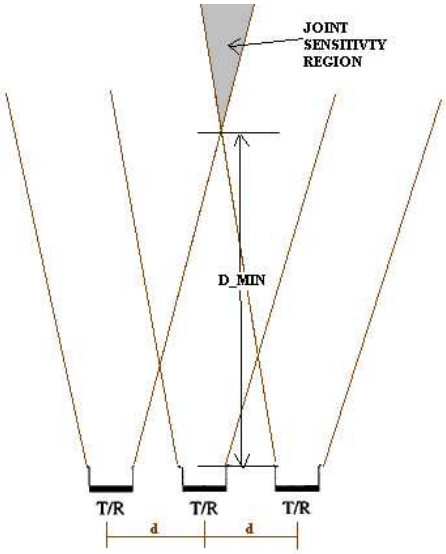

Figure 1.3. The joint sensitivity region for 3 sensor linear array configuration

The angular position (azimuth and elevation) of the target is estimated using again multiple transducers and triangulation. In two-dimensional workspace, the positional uncertainty can be reduced by using at least two transducers. In three-dimensional workspace, more transducers are required. However, this is still restricted since localization is possible only in a limited region known as the joint sensitivity region where the sensitivity regions of the separate transducers of the combined sensor group overlap [25]. As this joint sensitivity region starts at a distance from the combined sensor group, there is a dead zone up to the start of joint sensitivity region where it is not possible to estimate the angular position, as shown in Figure 1.3. For a group of three transducers seperated by $d \in R^+$ from each other, the distance D_{MIN} between the central transducer and the start of the joint sensitivity region is shown to be [25]:

$$D_{MIN} \approx \frac{d-a}{\tan(\theta_0)} + \frac{a^2}{\lambda} \tag{1.2}$$

As an example, for a set of 50 kHz transducers with $a = 20$ mm and with $d = 10$ cm, D_{MIN} is 43.6 cm. The narrow beam US transducers worsen the compromise between the dead zone's extent and the required minimum transducer separation for accuracy in target azimuth estimation. One approach is to position the receiver/transmitter

pairs close to each other [28] regardless of the fact that greater separation between the transducers brings better angular resolution. Alternatively, the combined sensor group are moved adaptively in the direction of the target object as to ensure that the target falls within the joint sensitivity region [25]. An improvement in SNR also follows which increases the accuracy of TOF measurements. The most important shortcoming of multi-sensor array configuration is that the transducers are spatially apart which creates ambiguities and introduces error. As the separation between sensors of the multi-sensor sonar system is in the order of multiples of the wavelength, when reflections have specular character, there will be error in the positional estimate. Furthermore, issues such as sensors alignment calibration and sensor to sensor matching of the sensor group pose challenges and require validation.

Binaural biomimetic sonar system mimic biological findings in their attempt to overcome these problems. In ITD based systems, in order to take advantage of binaural (or tri-aural) sensors, the arrival times from the two (tree) receivers need to grouped into pairs (triples) based on their source object. The time axis spread of these pairs (triples) bring about the famous 'correspondence problem'. This problem belongs to the class of inverse problems, most of which are ill-posed, and require additional constraints in order to have a unique solution. Unfortunately, the specular nature of reflections make it very hard to find such constraints. Consequently, most researchers restrict their applications to indoor environments with well defined target structures in order to alleviate the problem. However any complexity of the environment may easily cause correspondence errors. The correspondance problem is addressed by minimizing the spread of the pairs (triples) and hence reducing angular resolution. The use of ILDs for estimating the spatial location of the target object has also its own inherent difficulties. The binaural configurations are asymmetric in 3D and biased to the horizontal plane. The most reliable information that can be extracted is the azimuth angle estimate. ILD value is dependent on the target distance and elevation angle estimate requires additional effort. The ambiguities occuring in ILD returned azimuth estimates are attempted to be solved with i) orienting (in a sensorimotor behavour manner) the binaural sensor head (with vertical neck movements), reducing the elevation effect, or ii) taking multiple measurements at different angles and combine them. A recent

study speculates that bats use multiple HRTFs that correspond to different ultrasonic vocalization frequencies by combining them to reveal binaural cues for localization in azimuth and elevation [10].

Another important limitation of the ultrasonic sonar implementation for robotic applications is the effect of the transmission path non-linearities on the transmitted pulse and received echoes. The sound velocity is a function of transmission medium properties such as temperature, and partly relative humidity and pressure. Turbulent air motions greatly effect the predictive sound propagation characteristics of air. Similarly, the dust and humidity content of air modify the magnitude of dispersion causing a frequency dependent attentuation per distance on the pulse-echo spectral components. The reflective properties of the target object (the target strength) and the general specular character of sonic pulse reflections add to this. Multiple reflections are a frequent natural problem and difficult to detect and discard. Increasing the transmit SPL magnitudes above some limit to reach distant targets can end up with saturation of the air column in front of the transducer, and deviations from linear acoustic theory may start to arise.

Finally, let it be noted that in most applications, very short pulses of the resonance frequency are transmitted. A broad frequency range is covered due to short pulse train length in time. During the transmission and reception, frequency dependent distortion occurs and the sound content cannot be perceived equally in the space. The received echo shape changes for differing angular directions due to spectral modification. In another acoustics implementation field, speaker cabins are designed to alleviate this problem by splitting the wide frequency range using cross-over circuits and using multiple aperture size speakers covering smaller frequency ranges. Both result in improved matching between directivities over a wider overall frequency range and a more homogenous sound reproduction throughout the space. In sonar applications, matched filtering type signal processing requires pre-stored template sets parametrized for different angular directions and distances [29]. All together, the pulse shape and amplitude are difficult to model, process, interprete and to get advantage of as an additional stimulus dimension. The quest in the sonar analysis part of this project is

after a new method (and a system utilizing it) adressing some or preferably most of the issues identified above.

1.6. Sonar Analysis

The nature of the transducers promotes operating them at a single frequency, at its natural resonance frequency ω_0. This is a common practice to maximize the energy efficiency and SNR of the US system. However, here we choose another path and operate it away from ω_0, to sense the direction to the target. As will be explained, this will enable sensing the direction to the target

In TOF systems, the aim of the sonar data processing is to extract the arrival times of the echo pulses. From the echo arrival times, range and bearing of reflecting objects can be estimated by using the speed of sound and receiver geometry. In most applications, the bearing is estimated with triangulation using a minimum of 2 receivers. The target type, i.e whether it is a plane, an edge, a corner or a cylinder etc.) is done using two transmitters. If multiple transducers are fired, some sort of pulse coding is applied to outgoing pulse trains [29]. Advanced TOF systems go beyond the thresholding method and use matched filtering by template matching the incoming echoes to a stored template set to increase echo detectibility and positioning accuracy by better estimating the arrival times. Matched filtering is one of the inspirations coming from radar systems. In matched filtering, the arrival time is estimated by cross correlating the received echo with an echo template pre-stored in the processing unit. The templates are parametrized with respect to angle, range, environment variables and transducer specifications. They are shifted across the echo waveform to find the maximum correlation. Some matched filtering based analysis uses very short sonar pulse trains [24]. Others use barker code utilizing longer pulse trains which are shown to increase the SNR [30].

Sensor array based *beamforming* is elegant and widely used in underwater applications, but requires many receivers, good processing power and has an important implication in airborne sonar implementations: In airborne ultrasonics, it is very diffi-

cult to construct a sensor array system corresponding to underwater applications. This is due to the fact that in traditional beamforming, the scale of the phase shift monitored between received echoes corresponds to the wavelength of the transmitted wave burst. As the velocity of sound in air is much lower than in water and the wavelength of ultrasonic sound is much shorter, we have to observe the phase shift of the envelope of the burst instead of the phase shift inside one cycle [23]. Beamforming is not widely used in airborne sonar implementations. Beamsteering by electronic means is adapted by some researchers [22], however the slow speed of sound makes this implementation impractical for most robotic applications. A unique advantage of beamsteering could be a possible discrimination of target objects which are equidistant from the sonar sensor in the main lobe. Other sonar systems currently cannot achieve this.

1.7. Problem Statement

This thesis attempts to reassess all the design parameters and possibly adapt alternative novel strategies and methods. In particular, the goal is to develop an ultrasound system with the following features:

Hardware: The hardware should be an integrated system that supports multiple transducers and multiple frequency excitation.

Firmware: The accompanying software should enable flexible programming and access to the hardware as well as the analysis of the incoming signal.

Sonar Analysis: Consider a single transducer system with an excitation frequency $\omega \in [\omega_{min}, \omega_{max}]$. Supppose there is an object at an unknown radial position r_o and angular position θ_o. The sonar analysis algorithm should compute the angular position θ_o – taking advantage of the newly developed integrated system.

1.8. Contributions of the Thesis

The contributions of this thesis are multifold:

Hardware-Firmware: A novel design that can embed upto 128 wide beam angle

transducers and allows multiple-frequency excition has been developed and realized in both hardware and software.

Transducers An effective use of wide angle and frequency dependent directivity nature of ultrasound transducers.

Sonar Analysis: A physics-based and biologically inspired approach for computing angular position. This approach is based on dual frequency beam shaping and has the following features:

- The correspondence problem is eliminated,
- The dead zone before the joint sensitivity region is eliminated,
- It has increased immunity to environmental noise and system parameter effects by using relative measurements.

1.9. Thesis Outline

The outline of the presentation is as follows: In Chapter 2, the hardware design of the airborne US system is presented. We first determine a list of hardware performance criteria, and build a sophisticated hardware subsystem that satisfies these criteria. Following, in Chapter 3 the details of the software backend is given that makes all the system operational. Our sonar signal processing approach is explained in Chapter 4. Comprehensive experiments and their associated results are presented in Chapter 5 along with a discussion that evaluates the proposed sonar analysis method together with system configuration using quality metrics. Finally, the thesis concludes with a brief summary and comments on future work in Chapter 6.

2. HARDWARE DESIGN

2.1. Design Criteria

The hardware design is an extremely crucial part of an ultrasound system as its capabilities and limitations dictate the properties of the transmitted and received sound signal as well as the post-processing that can be applied. The developed platform should be maximally flexible and extendible as to enable future extended studies. In our attempt to achieve this aim, a systematic study of the related literature was conducted as has been discussed in the previous chapter. In this study, we have seen, the US community have addressed a wide variety of design tasks with diverse hardware configurations, mostly custom built for the specific sonar implementation. Partially motivated by this investigation, a short set of requirements as listed below provided the general guidelines of the design considerations.

1. Flexibility: The hardware and low level software shall be generic and be customized by a higher layer software during the application.
2. Extendibility: It should have development platform sophistication as to minimize hardware intervention or worse a redesign during development. The number of transducers supported must be easily changeable. For example if one starts with a data acquisition board with a single chip simultaneous sampling ADC, say with 4 inputs and 500 ksps sampling rate and want to increase the sonar transceiver count, the project is doomed and redesign is required before further continuation is possible. In conjuction, reconfiguration through software should be supported.
3. Robustness: The hardware should be mechanically robust and have provisions for a protective casing.
4. Remote connectibility: It shall be easily connected to a pocket PC platform and remotely operated.
5. Economics: Hardware should have cheapness perspective. A cheap sensor with a cheap electronic hardware backend can be commercialized for a mass market.

2.2. Design Details

The following factors are of consideration in the design of hardware topology.

- Modules - Central Host Interface
- Topology of Modules

2.2.1. Modules - Central Host Interface

The connection of the computing and development platform was initially designed to be through the compact flash (CF) interface of commercial pocket PC. The CF interface is a different form factor of the more familiar PCMCIA interface. It allows parallel 16 bit word data transfers at rates up to 20 Mbytes/s, and is the widest bandwith interface of pocket PC platforms, and this is probably more than we need. Its memory mapped mode is easy to handle with some glue logic circuitry using a complex programmable logic device (CPLD). Later this design decision was changed to accommodate the regular PC platforms as well. In this perspective, the connection interface was modified to Universal Serial Bus (USB) revision 1.1 – as it can be utilized in interfacing to both pocket PCs and PC platforms. This mode supports data transfer rates up to 12 Mbps. USB supports single-drop peer-to-peer serial communications between a host and a slave device. Electrically, the communication is done through a bidirectional balanced differential pair. In addition, power can be provided to the slave device (max 500 mA, 5 V). Up to 127 devices can be connected to a host port, however since the USB communication is peer-to-peer, intermediate hub devices are required, which contain up to 4 down-stream ports and 1 up-stream port and repeat/reroute and restructure the packets and a tree structure needs to be established to accept connections from many USB devices to a single host port. This tree like USB bus topology is illustrated in the Figure 2.1 [31]. In parallel with the physical layer specification, a full software specification is required in order to ensure the universality and plug-and-play operation smoothness of the bus. Device drivers are needed at the host side which makes the utilization of this interface challenging at the startup phase.

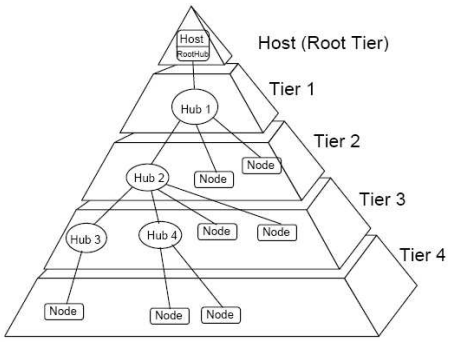

Figure 2.1. The USB bus topology

2.2.2. Topology of the Modules

The topology of the modules is designed to enable decentralization in the sense that the sensor modules are to embed some processing 'intelligence'. We planned to make use of distributed intelligence at sensor nodes and pre-process the signals at the sensor sites before transferring them to the main host. This is one step closer to the idea of fully embedded intelligent US sensors. Once the sonar signal processing algorithm is finalized, the data transfer to the central host node can be completely eliminated. In this perspective, the central node serves as a research and development environment. In this manner, the maximum data transfer rate of 12 Mbit/s stops to be limiting as compared to 20 Mbyte/s of the CF interface. Let it be noted that this is very different when compared to almost all the hardware that has been reported where sensor modules are not 'intelligent' and raw data stream is usually fed through a high bandwith interface like PCI using DMA. Hence, any increase in their numbers loads the bandwidth.

The sensor modules could be connected together using a USB-based network. However, this is not selected since the implementation of such a network is extremely cumbersome and there is a need for intermediate USB hub stages in order to build a whole USB connection tree: i) the cabling gets complicated, ii) the bus overhead of intermediate hubs is costly, iii) the reliability drops due to increased module count, iv) every sensor node needs USB slave capability which increases sensor node cost and v) the synchronization between the USB devices is impossible due to the inherent

peer-to-peer topology of communication. A simpler and better choice is to use a serial multi-drop half-duplex RS485 bus. RS485 is a physical specification (there is no specification on software layer, which we take advantage of) for an industrial bus and is very common in the data acquisition world. In RS485, voltage-mode differential signaling is used to transfer information over long distances. Using a single differential pair, the data can be transferred bidirectionally in a half-duplex manner. The single cable pair visits every bus node, and every slave receives from the master the same data packets simultaneously, making the synchronization between sonar modules using broadcast like packets possible. The nodes can become driver or receiver under software control. The software layer should be able to manage master to slave communication, and avoid collusions. The RS485 can support 12 Mbps with ease using termination resistors at the ends of the bus cable in order to reduce reflections [32].

2.2.3. Overall Hardware Topology

The overall hardware topology is as shown in Figure 2.2 and in Figure 2.3. A 4-wire cable carries the RS485 differential pair, power and ground to the sonar modules. The sonar modules are replica of each other and may differ only in the addon module attached to them. One of the sonar modules carries the USB interface module and connects to the main node PC through USB 1.1 . The other modules carry the external memory addon module and have a 32 kbytes memory for locally buffering the sonar data. Local buffer memory ensures that the precision sampling does not get affected from other modules on the bus or the operating principles of the central host (PC or pocket PC). Let it be noted that operating systems on these platforms are not truly real time operating systems and hence guaranteed latency and throughput on the USB bus is not ensured. The inner workings of USB also contains delays and latency issues [33].

The multi-drop bus type serial connection gives us the tools to meet the extensibility and robustness items of our starting short list of system requirements.

1. Economics: Off-the-shelf components are used for each module.

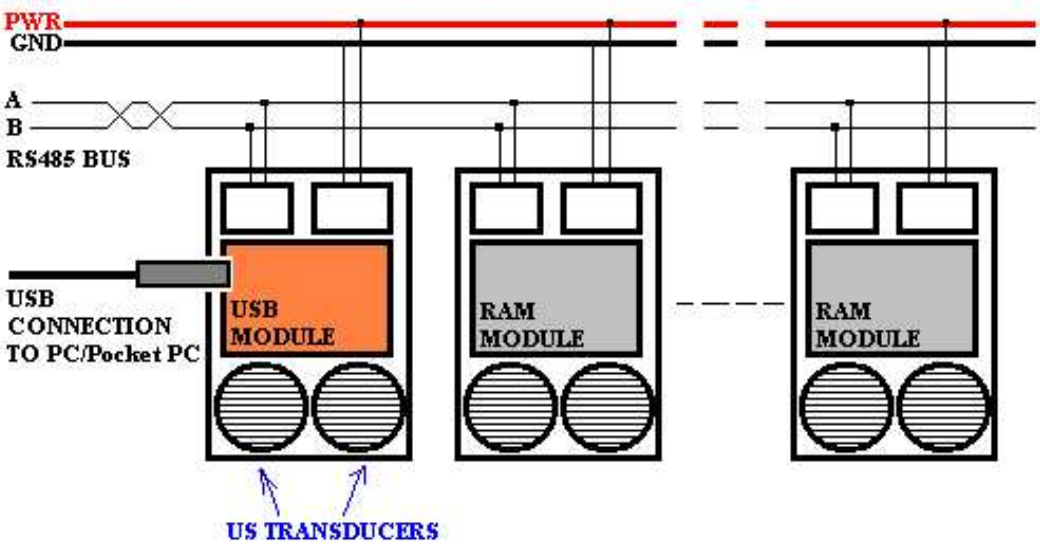

Figure 2.2. Hardware design topology

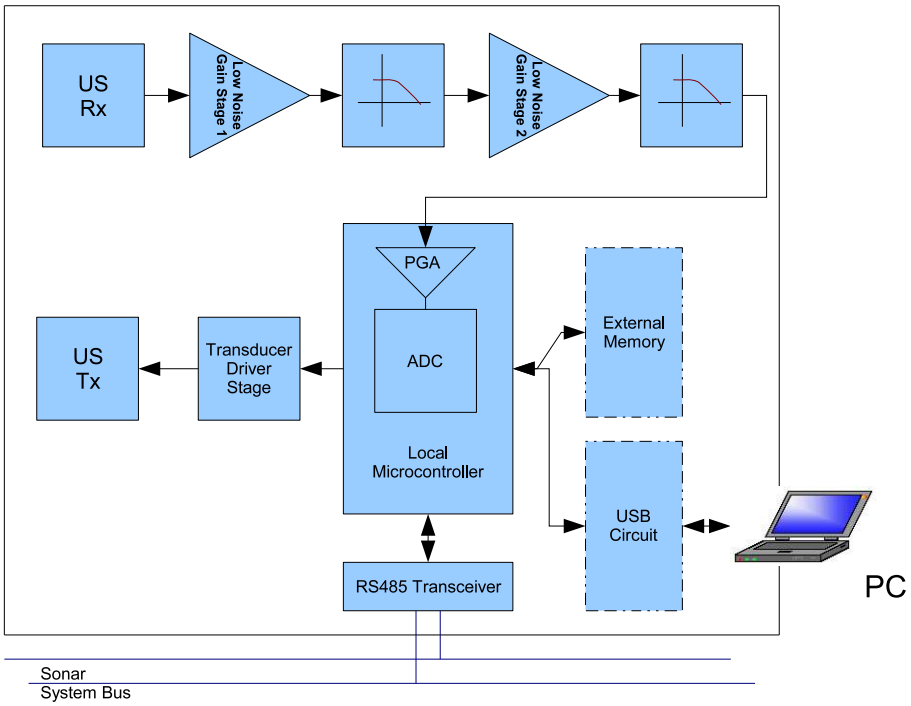

Figure 2.3. Hardware block diagram

2. Extendibility: We achieve extension through replication, which is a very smooth process during algorithm development stage, making hardware redesigns unnecessary when one limit is reached. Up to 32 sonar modules with standart RS485 transceivers or 128 modules with $\frac{1}{4}$ load transceivers can be interconnected.
3. Robustness: Every module is self contained in terms of receive and transmit func-

tionality, signal conditioning, signal digitization, and data compression. Replica sonar modules can be synchronized to do simultaneous sampling of the incoming echoes. The digitization is done locally at the reception site. The output of ultrasonic receivers is very small and of high impedance and it is better in terms of signal purity and reliability to amplify this sensitive signal and digitize right near the transducer, and transfer the acquisition data (also locally processed) in digital format to the central node. As an example the DC motors on the current robotic platform draw discontinous currents of about 26 A each from 24 V batteries during start and they could easily distort the weak sensor signals.

4. Flexibility: Having *multiple parallel sequential machines* (the microcontrollers on the sonar modules), which operate in parallel and simultaneously after a key synchronization call, is invaluable. This makes the system extremely flexible. For example, in one widely used array signal generation method known as *beemsteering*, the transducers of a linear or planar array are intentionally fired with fixed time shifts between successive array elements to steer the overall beam front in the space to some angle [22]. Traditionally, this is implemented via a custom built circuit or a FPGA configuration to generate the steering control signals and these are built for one array size. In our case, we write a few line codes to the common firmware of sonar modules and allow a software programmable beemsteering from the central node PC, which can then independently activate/deactivate the firing of a specific transducer in the array, add totally independent $\pm$ delay before the firings, allowing a much greater control over beamsteering without the time spent on FPGA implementation or custom built circuitry. Furthermore, the programming of paralleled sequential machines in software is considerably easier than developing custom hardware or reconfigurable logic. There is enough time to accept a few additional clock ticks – taking advantage of the slow travelling speed of sound in air medium. In summary, the parallelism of a set of modules each of which is sequential enables an ease of development and expansion as well as faster implementations when compared to a full custom FPGA solution.
5. Remote connectibility: Remote connection to a pocket PC or desktop PC is possible via the USB interface.

2.2.4. Microcontroller Selection

A sophisticated 8 bit microcontroller is used in every sonar module. The AT90PWM3 microcontroller from Atmel Corporation has been chosen. This device is rather new. It is a special design chip for motor control and electronic balast jobs but its high level of integration and performance peripherals brought it into our attention. In particular, its following properties contributed to its selection:

- The microcontroller with a high clock frequency (16 MHz) and a single cycle core. Timers and power stage controllers in the device can even switch to 32 MHz or 64 MHz operation using an internal PLL circuitry. This high clock rates ensure that we have enough sub-cycle resolution during sonar wave generation and acquisition and good syncronization between the modules.
- Powerful timer peripherals which will be utilized during sonar firings and echo acquisitions.
- Built-in high speed 10 bit ADC. ADC will be used to digitize the incoming echoes.
- Built-in programmable amplifier with steps x1, x5, x10, x20, x40. It will allow compensation of the dramatic attenuation in received signal strengths due to geometric spreading.
- High speed UART (2 Mbps is possible with 16 MHz clock). It will handle RS485 bus communications.
- Built-in comparator with resistor array to adjust comparison voltage. For analog signal processing.
- Built-in 10 bit DAC. Can be used with DDS (Direct Digital Synthesis) type transmit transducer drive.
- Low price (it is sub-dollar).

2.2.5. Design of Modules

The first ultrasound module prototype consists of 3 separate boards:

- Sonar module mainboard

- Memory expansion addon board for sonar module
- USB connectivity addon board for sonar module

The use of add-on boards allows the sonar modules to take less space. The PCB designs are in 1 layer to reduce the production cost. The interface connector of the addon boards is compatible with the expansion connector on MCBv3 Motor Control Board which was designed as part of another project during the first year of the author's MS studies. This platform is used as an intermediate development platform for the sonar system. Also the microcontrollers in both systems use the same instruction set and system-on-chip architecture which saves prototyping time.

2.2.5.1. Sonar Module Mainboard. A short review of the mainboard design is provided in the sequel. Please refer to Figure 2.5, 2.6, 2.7 in order to see the described components. Figure 2.4 shows the mainboard CAD design.

The functionality of the mainboard is centered around the AT90PWM3 microcontroller (uC). It is programmed in-circuit through the programming connector J8. Serial Peripheral Bus (SPI) signals MOSI, MISO, SCK and the reset line RST# need to be overtaken by the external programmer and the resistors R1, R2, R26 ensure that their onboard use does not interfere with the programming of the device.

The internal data memory of the device is 512 bytes. As its size could pose a limitation on the length of the data memory, external memory extension capability is added to the board. J7 is the standart digital expansion connector on the mainboard. Memory expansion card can be attached here. Alternatively, the USB connectivity addon board can also be attached here. An 8 bit port and 4 additional I/O pins of the uC are brought to J7. Regulated digital power (DVCC) is also supplied to the addon modules through J7. Digital Ground (DGND) nets are split between the data port pins to reduce current loop areas of the fast switching signals.

Since the board is a mixed signal board, great care has been given to keep the

digital switching noises (internal and external to the uC) low. Series termination resistors R4 to R10 are used to increase the rise and fall times of the data bus signals and limit their high frequency content. A parallel connection of 10 nF, 470 nF SMD ceramic capacitors and 10 uF electrolytic capacitor close to each power pin of the uC provide a low impedance charge supply to the fast uC over a wider frequency range and a good decoupling. The beads L1 and L2 provide isolation at the noisy nodes and separate the two power pins at high frequencies. SMD components are used where possible, to keep the circuit parasitics down and reduce PCB size. C5 serves to decouple the analog reference level and provide a cleaner reference voltage to the internal ADC. Resistors R11 and R12 provide the option to selectively use a reference voltage level other than the AVCC. C4 eliminates unexpected resets to the uC.

U12, a DS18S20 device from Maxim, is a high precision digital thermometer with 1-Wire communication interface. It is used to provide temperature measurement with an accuracy $\pm$ 0.5°C in the temperature range -10°C to +85°C. The speed of sound is highly sensitive to air temperature and U12 will serve to make a first order compensation of the air temperature in the calculations. In the PCB, it is positioned between the Tx and Rx US transducers, outside the protective packaging.

U8 and components surrounding it do serve to the RS485 bus connectivity. U8 is a standart RS485 transceiver IC. The UART receive and transmit nets RS485_RX, RS485_TX and an additional I/O net RS485_DIR for the direction control connect to U8. The led D3 indicates that the current unit is on the bus and transmits data. 2 connectors J4 and J5 are used to connect the sonar module to the bus and complete the chain.

An observation of the bats will quickly reveal to the observer, that the timing, duration, the frequency content, and the intensity of sonar signals used by the bat to probe the environment directly effect the information available to its acoustic vision system. Bat makes use of adaptive sensorimotor behaviours, where they continuously control the pinna orientation, head aim, and features of sonar vocalizations to sharpen their vision [35]. To mimic their vocalization capabilities, the complexity of the trans-

mit hardware is increased.

- A 16 bit timer peripheral is utilized to generate the transmit control pulses.
- The transmit frequency can be selected in 200 Hz steps, the number of pulses is programmable, different frequency pulses can be used to make up a mixed frequency transmit packet.
- A push pull driver implemented with discrete components (components around Q8, Q7 and Q6) provides the heavy duty square wave US transmitter drive.
- The square wave drive is widely used for PZT type transducers and the single ended drive is based on information given in [34] where it is concluded that there is no measurable difference for PZTs, whether driven bipolar or single-ended, for the same V_{rms} value.
- A separate transducer is used as a transmitter, increasing the SNR and also making the measurement of very short distances possible (due to reduced forward masking).
- The transmit drive voltage level and thereby the intensity is digitally controlled using an 8 bit PWM generated DAC output.
- Transmit voltages from 8 V up to 40 V are software selectable.
- A step up converter circuitry built around MC34063 is used to generate the transmit voltages higher than the battery supply minus 2 diode drops.
- Since the operation of switching power controllers is too noisy for most analog data acquisition boards, the step up converter is planned to be shutdown during the echo acquisition phase.
- The pulse-echo type operation of sonar allows such optimizations, not only in hardware also in software.
- Two rather big output capacitors C14 and C15 can store enough charge for one pulse generation.
- The use of switch mode supply for the transmit voltage increases the power efficiency of the active sensing. Another option would be supplying a high voltage all of the time, and driving the transducer using high voltage high slew rate power opamps, which would be less power efficient, since for a low drive level, most of the energy from the supply would be dissipated as heat by the opamp.

- The air column in front of transmitter has the tendency to saturate at high drive levels and corresponding high SPL levels (above approximately 125 dB) and we may get out of the linear acoustics field of audio [18]. Intensity control will give us the choice at what SPL level to operate, and the chance to analyse the effects of transmit intensity on parameters of interest. Intensity control can be also interesting when we want at some instance of operation to use weak pulses, because the proximity to the target object is so close and we want higher update rates for the closer objects, so reduce crosstalk from background objects and shorten the 'US in air dead time' [3].
- A scaled version of transmit drive voltage HV_TX is brought to analog input PD6 in order to measure instantaneous transmit supply voltage level.

U2 and U13 generate the digital power for uC and negative supply for the receiver pre-amplifier respectively. Using discrete components, a very low noise positive voltage supply for analog circuitry has been built using NE5534 low noise opamp and low noise buried zener LM329.

The analog input stage consist of 2 AC coupled non-inverting jfet-input amplifier stages. Capacitors C53 and C55 roll off the AC gain at higher frequency and increase stability. R63 and R52 do the DC biasing at the ADC input, R51 and C58 provide a clean supply to DC bias network. The network D8-R53-C57 builds an optional half cycle rectifier/integrator with loss, in case we want to process the envelope but not the wave content of the received echoes. The comparator input can be converted to an output pin in software and the integrator capacitor can be quickly discharged to increase the detectibility of close echoes.

With the exception of the microcontroller, all the circuit components are off-the-shelf components which makes it easy to find and buy components for new replica sonar modules.

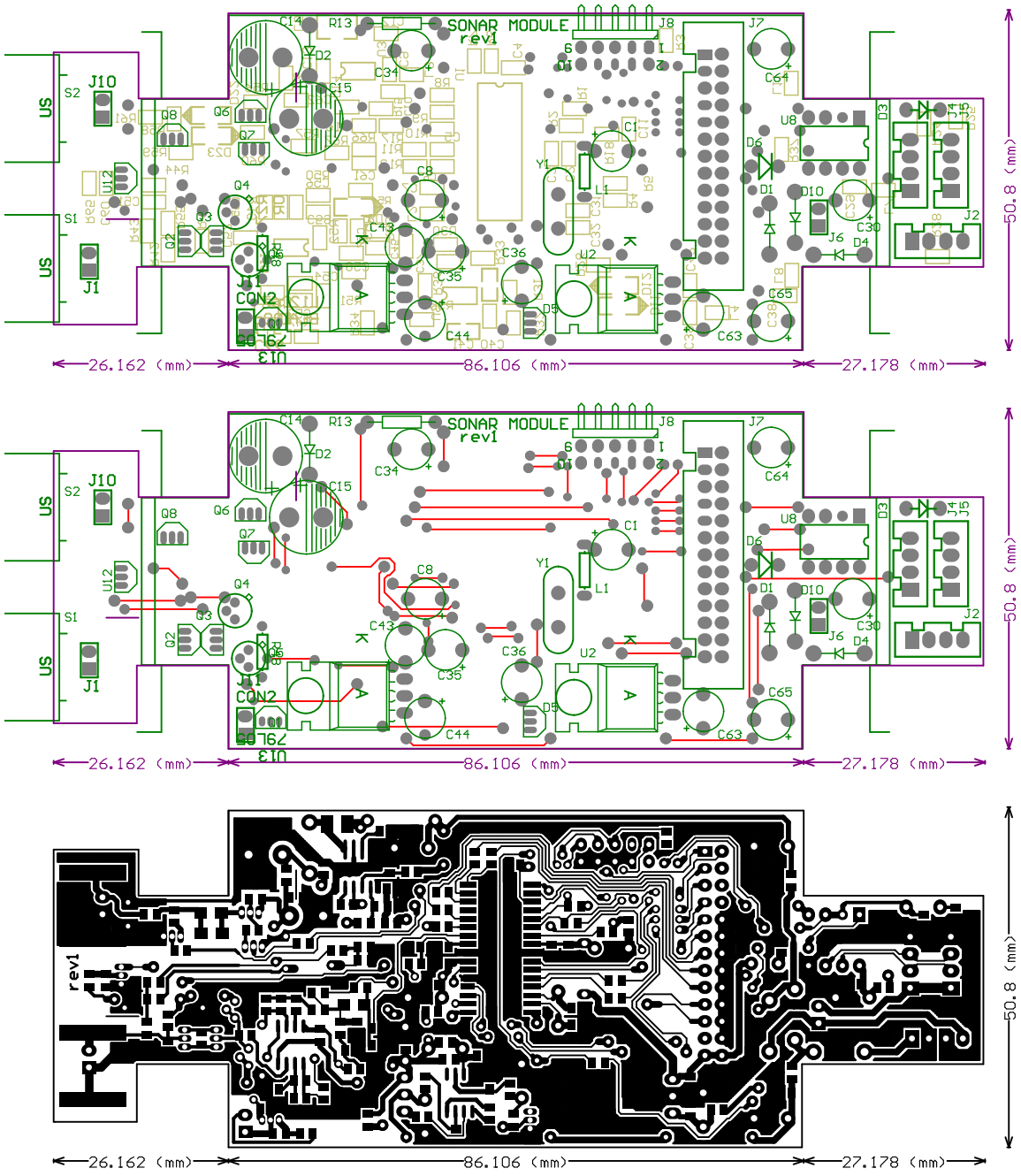

Figure 2.4. Sonar Module Mainboard - CAD design snapshots - top & bottom overlay; top layer & top overlay; bottom layer

2.2.5.2. Memory Expansion Addon Module. The Memory Expansion Module (Figure 2.9) carries an 8 bit 32 Kbyte SRAM device. The uC does not have a native external memory interface. The 8 bit data port alternately transfers the address high-byte to latch U5, address low-byte to latch U4, and the data from the activated memory location or to activated memory location of SRAM U6. The 4 I/Os control latch enable

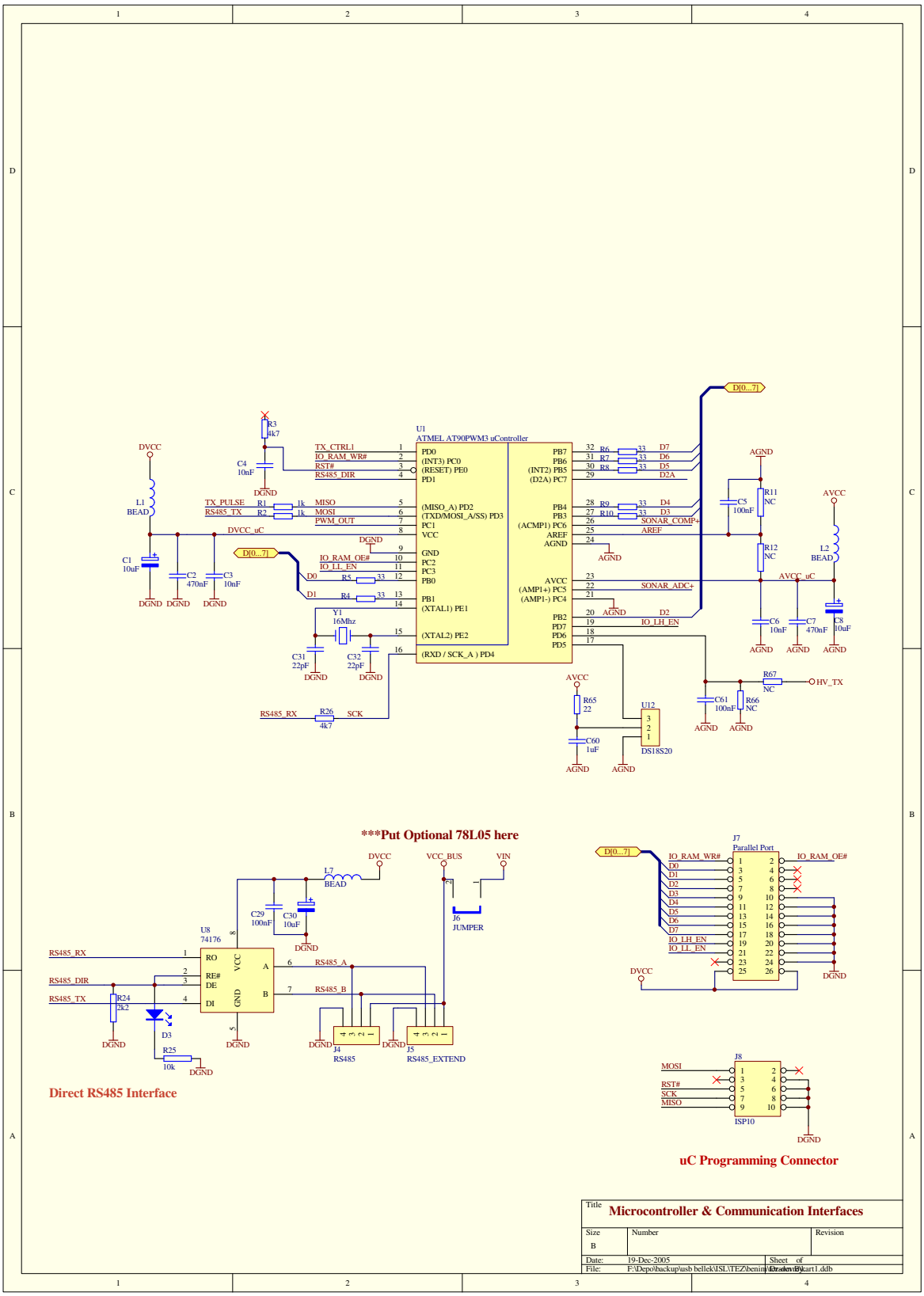

Figure 2.5. Sonar Module Mainboard - schematic page 1 of 3

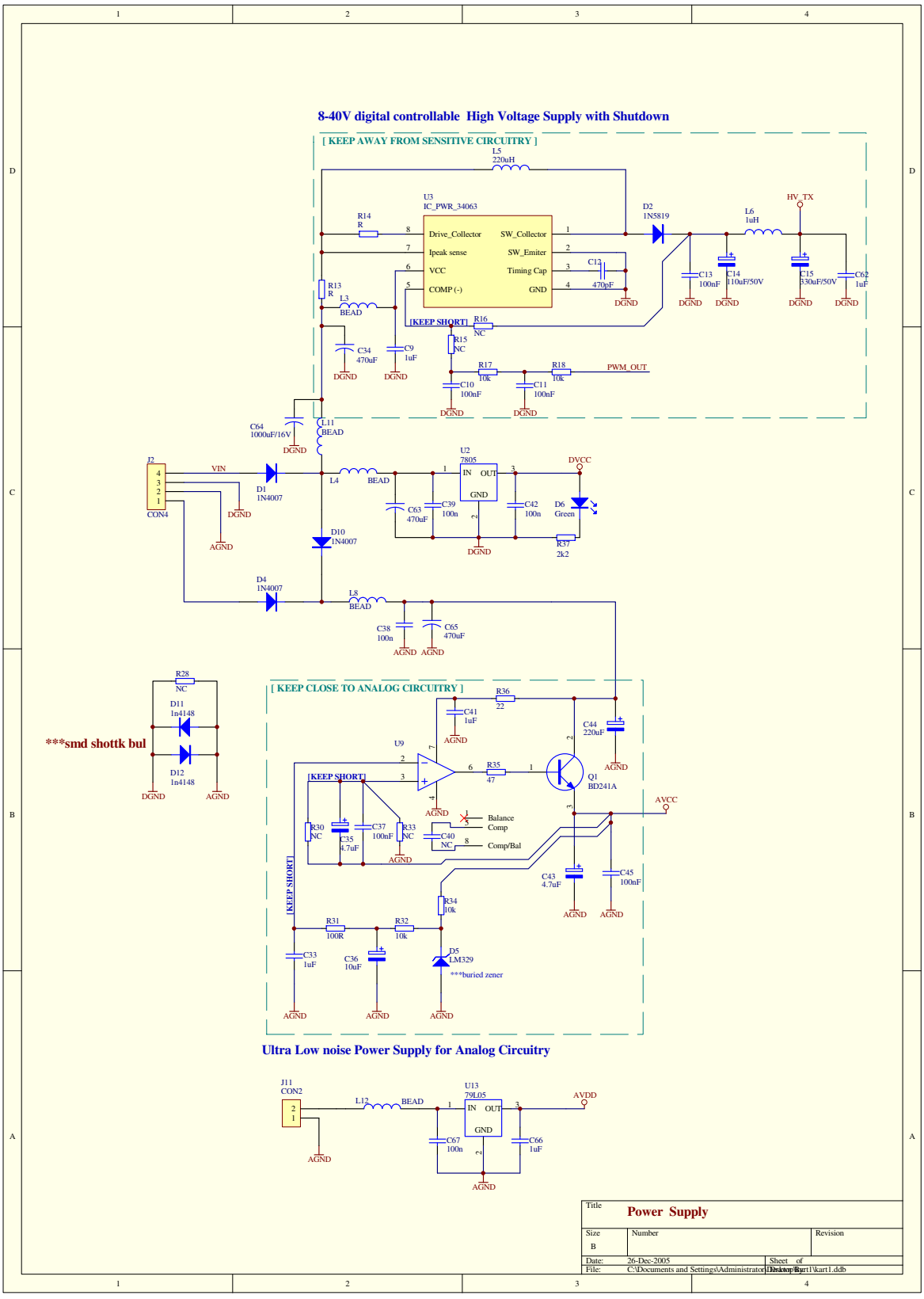

Figure 2.6. Sonar Module Mainboard - schematic page 2 of 3

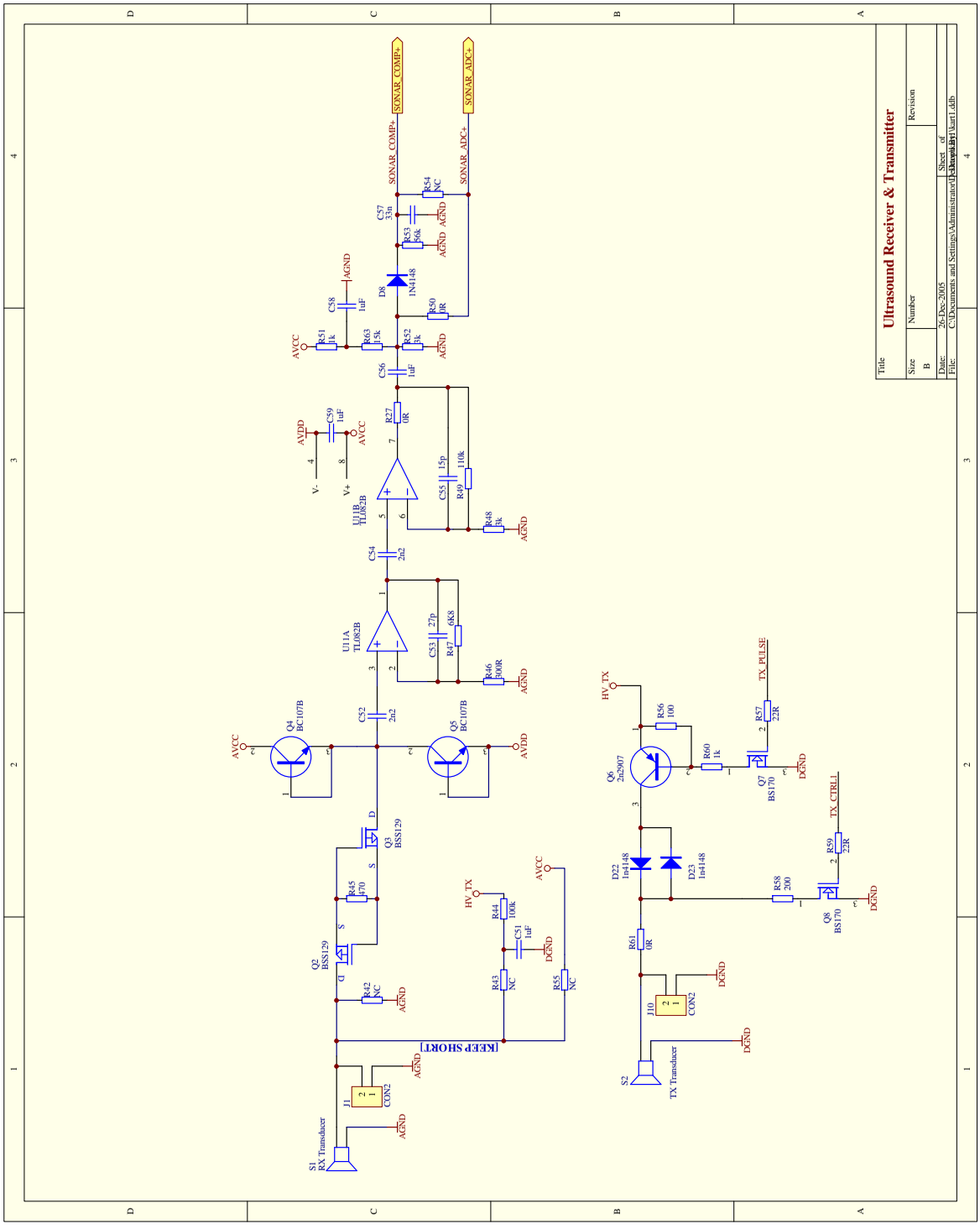

Figure 2.7. Sonar Module Mainboard - schematic page 3 of 3

and RAM write/read control and output enable control lines. The latch enable signal to high latch (LH_EN) is at the same time used to put the SRAM device into sleep mode, to reduce the current consumption of the unit when the master deactivates the unit in software. Two leds D9 and D7 are connected to two data port pins and are used as user debug leds when the memory is not accessed. Adequate power supply decoupling is provided to the CMOS ICs. Figure 2.8 shows the Memory Expansion Addon Module's CAD design.

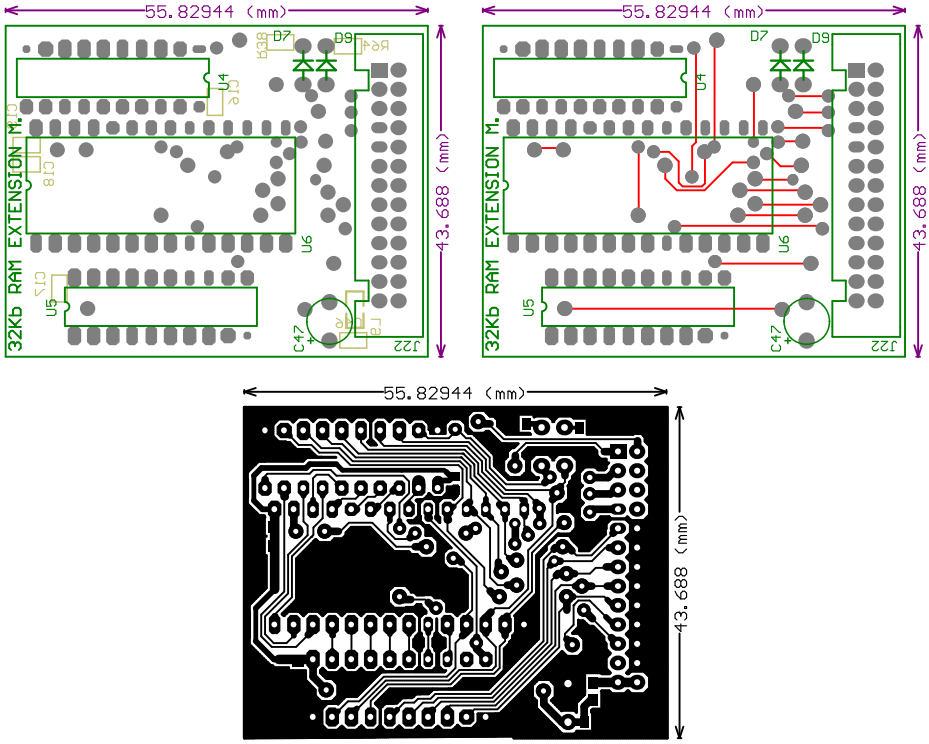

Figure 2.8. Memory Expansion Addon Module - CAD design snapshots - top & bottom overlay; top layer & top overlay; bottom layer

2.2.5.3. USB Connectivity Addon Module. The USB module is designed around the FT245BM USB FIFO device from FTDI corporation. This device contains necessary logic for USB to internal FIFOs bidirectional data transfers and has a physical parallel port to access these FIFOs, so that nearly full USB 1.1 bandwith can be utilized. Tx buffer size is 384 bytes and Rx buffer size is 128 bytes. The availability of company made virtual comport driver and higher performance DLL type driver greatly simplifies the software design. Device drivers are not only available for PC platforms but also for WindowsCE which is the operating system of pocket PC. Using this device we have a

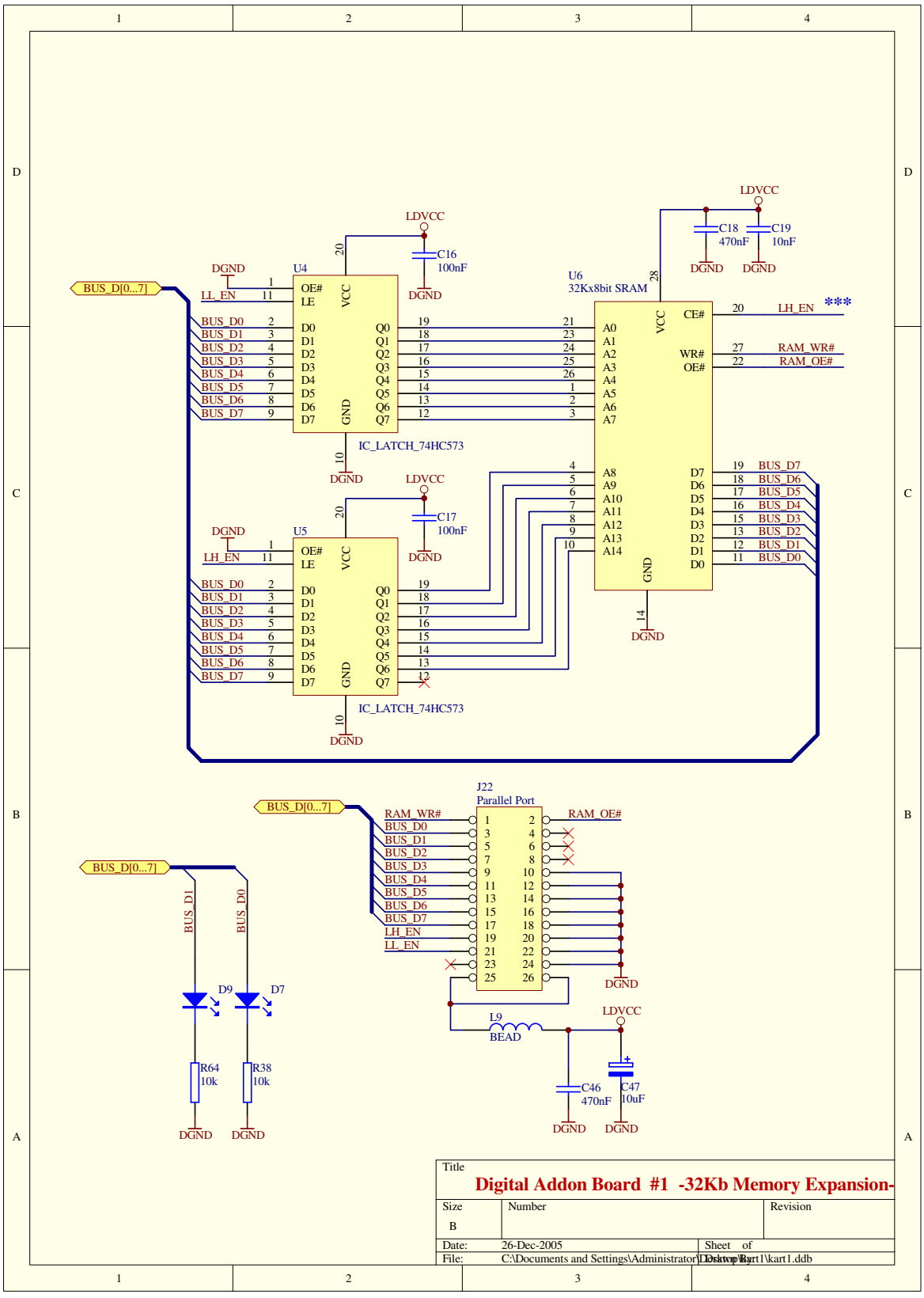

Figure 2.9. Memory Expansion Addon Module - schematic page 1 of 1

solution ready for PC and pocket PC platforms.

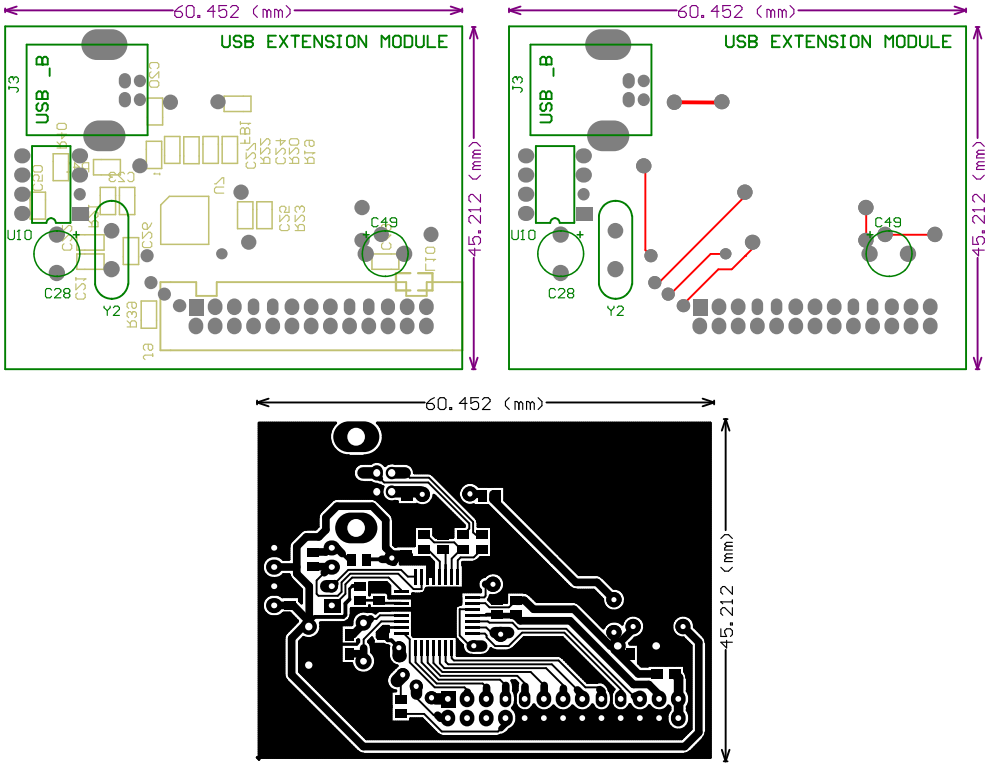

Figure 2.10. USB Connectivity Addon Module - CAD design snapshots - top & bottom overlay; top layer & top overlay; bottom layer

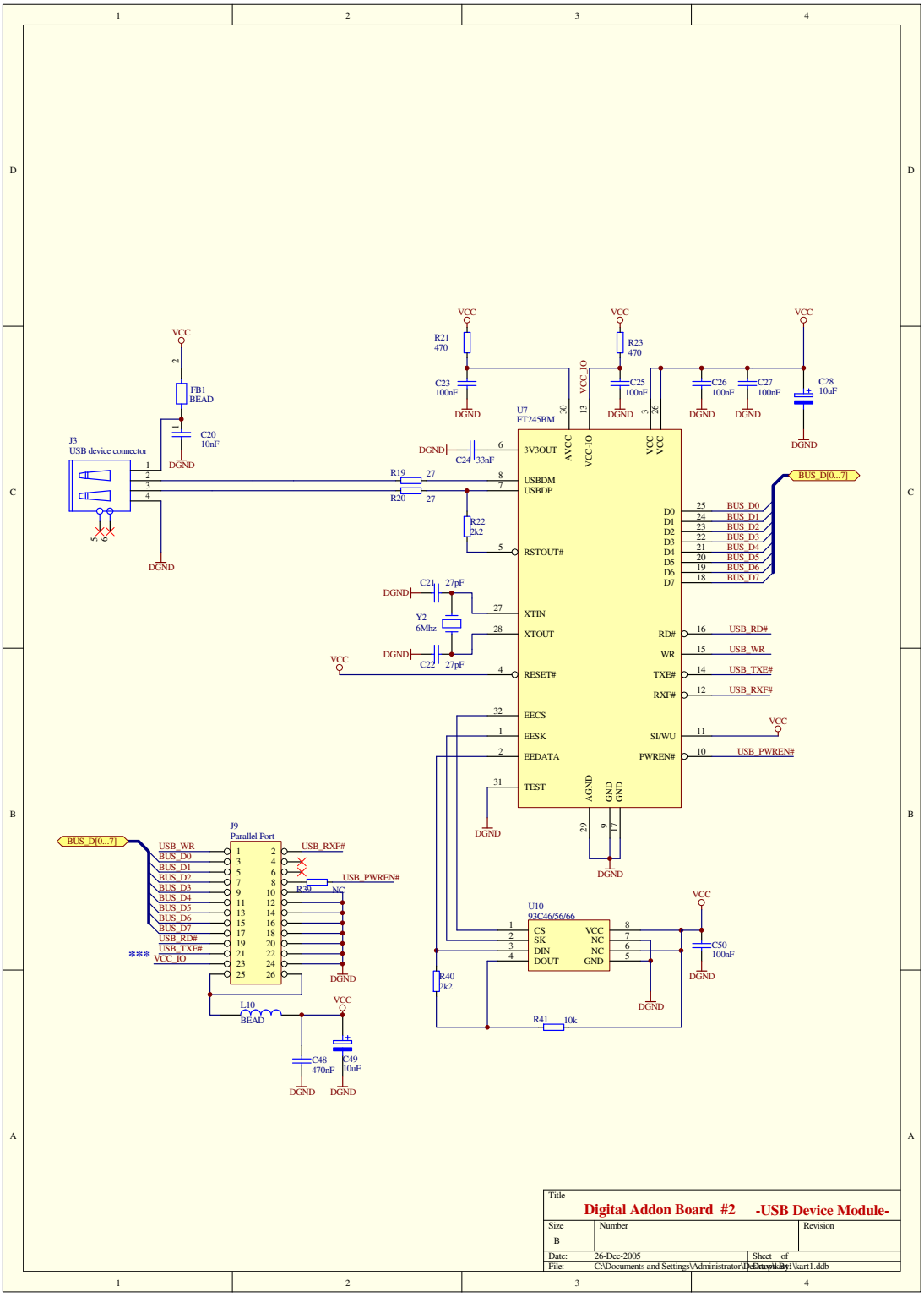

Figure 2.11. USB Connectivity Addon Module - schematic page 1 of 1

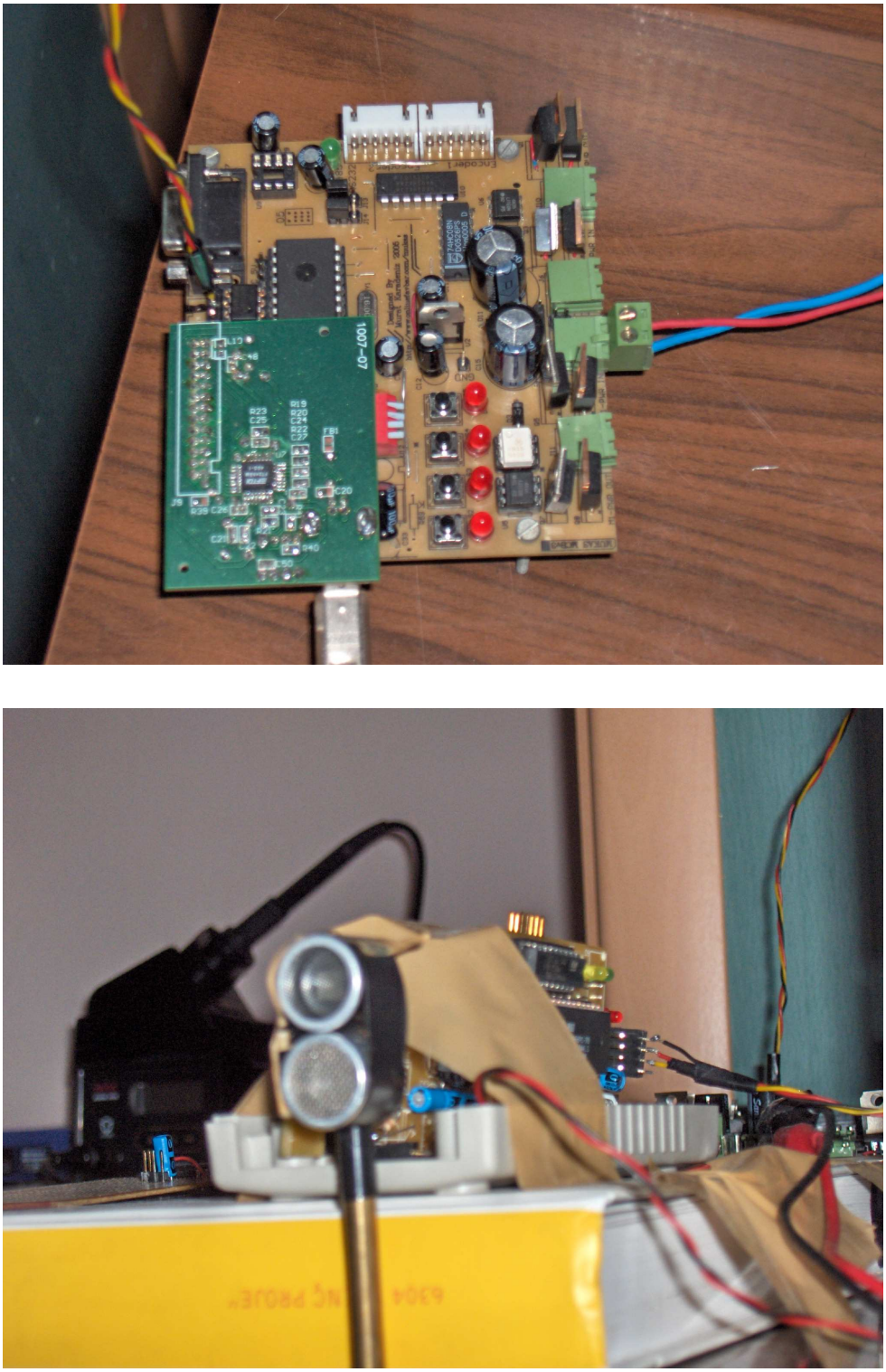

Figure 2.12. Top: USB module on the MCBv3 board - connections to the PC through a USB cable and to the sonar module through a hand made twisted pair cable are visible; Bottom: Sonar Mainboard and Memory Expansion Addon Module attached to it during an experiment

3. SOFTWARE DESIGN

The software of US Integrated Development Environment (IDE) is required to have the following properties:

- Decentralization to multiple units as firmware of embedded systems,
- Proper execution of timing critical tasks such as US signal generation and acquisition in firmware,
- Interfacing the whole US system to a non-RTOS environment,
- Fulfilling the software requirements of an IDE platform.

As is explained in the sequel, satisfying all these properties simultaneously has proven to be intricate and thus challenging. In order to be as modular as possible, the separate components have been identified as: i) The embedded system software, ii) The PC IDE software and iii) The communication protocol. In the rest of this chapter, the design of each component is explained in detail.

3.1. Embedded System

The embedded system software is stored in the flash based program memory inside the microcontroller. This software is referred to as the embedded system firmware (or more simply the firmware) since it is rarely updated when compared to software on PCs and thus requires different considerations than traditional PC software programming. As the firmware directly interacts with embedded systems hardware, it can cause malfunction of hardware or even damage it. Hardware and firmware should be co-designed as the hardware specifications are directly affected by software specifications. Improvements in cost, size and performance of the hardware are mostly due to a succesful firmware specifications and implementation.

The AT90PWM3 device contains 8 kbyte (4 kword) of program flash memory and 512 byte of data memory. Its C language optimized instruction set allows efficient

use of this limited capacity. The AVR GCC Open Source C compiler has been used [36]. The following table lists the separate source files of the firmware:

Table 3.1. Firmware Source Files List

n	$filename$
1	comm_rs485.h
2	comm_rs485.c
3	ext_ram.h
4	ext_ram.c
5	timer.h
6	timer.c
7	usb_ft245bm.h
8	usb_ft245bm.c
9	ultrasound.h
10	ultrasound.c
11	delay.h
12	global.h
13	main.c
14	mouse_lib.h

The operation of the firmware is as follows:

- Upon power up, the firmware waits 5 ms long for the power supplies to stabilize and then starts the device initialization in the following order: i) The ports, ii) The external memory, iii) The timer peripherals, iv) RS485 bus interface and finally v) The ultrasound related startup configuration.
- The use of external memory requires the testing the external memory module by a test procedure in the firmware. The whole memory space is filled with a pattern and a read-back is done to verify that every memory location can be read and written without error. If a faulty location is detected, the test is terminated and a 'memory fault flag' is raised in a flags register that can be read remotely so that the operator is informed of the fault.
- In the idle loop, a software operating properly indicator led (led D9 on ext. mem-

ory module) is flashed every 1 second indicating that there is no code run-away. The sonar modules expect the central host node to make bus synchronization calls (as explained later in communication protocol section) at least once every 4 seconds. If if this is not the case, the respective sonar modules begin to flash led D9 every 250 ms. Hence, the associated connection problems can be easily traced.

- All the sonar operations are done in interrupt routines in order to ensure that no other interrupt source interferes with the current timing critical operation.
- Initially, USB connectivity module was connected to a MCBv3 board's expansion connector. The firmware of MCBv3 board has an added option for making it act as an USB to RS485 translator board – that can be selected from command line using a terminal software such as HyperTerminal. This repeater was used during the initial phases of the software design and development. The same option can be directly given to the sonar module without any problem by simply changing the relevant pin and port definitions in file $usb\_ft245bm.h$. The reception of data bytes from USB bus is detected by an hardware interrupt, and the uC device services them in an interrupt routine. The rate of arrival of data bytes from USB bus can be faster than the uC can service them. However, the existence of a receive FIFO buffer inside FT245BM eliminates data loss.
- The US pulses are generated directly using a 16 bit timer peripheral of the uC which is configured to run as a modulo counter with a remotely selected counter maximum value. The 'toggle a timer output pin on timer overflow' feature is enabled so that 50% duty cycle programmable frequency pulses are generated without a time jitter due to firmware. During US pulse generation, the firmware counts the number of pulses generated asynchronously. When the programmed number of pulses is generated, the firmware interrupts the pulse generation. A second pulse train is generated after the first pulse train with the same operating principles but with different frequency and pulse settings. For each pulse train, the transmit frequency can be changed in 200 Hz steps. The pulse count can be varied from 0 to 127 in increments of 1. A 0° or 180° phase shift can be inserted between the two pulse trains, so the second train of pulses can act as anti-pulses if desired.

- A programmable sub-cycle startup transmit delay (in increments of $\frac{1}{3200000}^{th}$ of a second) can be inserted before the transmission of the pulse train. This will enable beamsteering with no additional custom hardware. This transmit delay increment corresponds to a steering angle increment which can be computed as follows: Consider a transducer separation d between array sensor centers and assume that the transducers are configured for progressive time delay of τ seconds across the array. According to steered angle θ_0 formula for the beam from a linear phased array [1],

$$\sin\theta_0 = \frac{c\tau}{d} \tag{3.1}$$

  For example, if $d = 6$ mm and $\tau = \frac{1}{3200000}$, then accordingly the major lobe is steered to an angle of 2.4°.
- Every sonar module can be *transmit active* or *transmit inactive* and can be totally suspended.
- When the central host sends the 'new cycle' broadcast type packet to the sonar modules, they respond asynchronously to the incoming packet and each of them behaves according to their own independent configuration. If a unit is transmit active, it first sends out the configured pulse trains and then synchronizes to other units (which may transmit pulse trains with different frequency, pulse count or startup transmit delays) with the help of an asynchronous *Post-Tx Synchronization Interval*. This guarantees that the succeeding echo samplings are made simultaneously among sonar modules.
- A programmable sampling start delay after Post-Tx Synchronization Interval allows phase sweeps and a way to investigate the effect of starting phase of sampling with respect to the incoming echo, and the effect of finite sampling rate on various signal parameters. As an example, digital storage oscilloscopes use a phase sweep feature to increase the sampling rate above the physical ADC's sampling rate for repetitive signals.
- The samples are successively written to a local memory buffer, which can be then retrieved by the main node PC. This way, the undeterministic effects of the non-RTOS operating system and non-real-time USB bus is isolated from the sampling

period (in terms of timing).

3.2. PC IDE Software

As seen in Figure 3.1, the PC software is made up of three main windows.

The PC IDE software is implemented using Visual Basic. The ease of developing a graphical user interface (GUI) and portability to a pocket PC platform for which the Embedded Visual Basic compiler is available, both make it an attractive programming language.

3.2.1. Bus Manager Window

The top left window in Figure 3.1 is the bus master window. It provides a GUI for the lower level functions of bus management and for debugging purposes such as:

- Debugging bus packets,
- Learning the unique 24 bit CPU ID of a new connected sonar module or other bus module,
- Learning the device descriptors of the bus module with a given CPU ID. Device descriptors include Device Class, Firmware Verison and Firmware Built Date which are handy when one is dealing with black box components with embedded firmware.
- Suspending or resuming bus operation,
- Configuring the bus settings,
- Accessing directly the internal memory space of the bus modules,
- Sending standart leds packet to blink the leds on a specific board, so that it can be located among multiple bus modules on the bus.

3.2.2. Sonar System Driver Window

The top right window in Figure 3.1 is the sonar driver window, which is responsible from the whole sonar system.

When the sonar driver window is opened, it first reads the 'sonar.ini' file for getting the CPU ID's of the registered sonar modules and then scans the bus if they are available. Then in the 'Sonar Units' list, the accessible sonar modules are shown with their CPU ID's and the unaccessible sonar modules with an additional $< NA >$ label at the beginning.

Any unit can be selected from the list and then by pressing the 'Advanced...' button, 'Advanced Unit Settings' window is opened, where user can configure an extensive list of operational parameters (See Figure 3.2). Since software configuration can change the whole behaviour of the sonar system, the current settings are stored to a 'sonar.ini' file to be able to recall an old system configuration and pass configuration data to the Matlab software during algorithm design.

The content of the ini file looks as follows:

```
[UNITS]
UNITCOUNT=2
UNIT0=6,7,8
UNIT1=6,7,9

[UNIT0-CONFIG]
SUSPEND=1
TXACTIVE=0
TXVOLTAGE=7
TXLENGTH=0
TXFREQ=40000
```

ANTIP_ LENGTH=32

ANTIP_ FREQ=42553

REVERSE_ ANTIP=0

USE_ VARGAIN=0

VARGAIN=40

BUFFER_ DEPTH=249

WOI_ START=0

WOI_ STOP=70

USE_ COMPRESSION=0

TXDELAY=0

[UNIT1-CONFIG]

SUSPEND=0

TXACTIVE=1

TXVOLTAGE=34

TXLENGTH=0

TXFREQ=42553

ANTIP_ LENGTH=32

ANTIP_ FREQ=42553

REVERSE_ ANTIP=0

USE_ VARGAIN=0

VARGAIN=5

BUFFER_ DEPTH=2049

WOI_ START=0

WOI_ STOP=2049

USE_ COMPRESSION=0

TXDELAY=3

Sonar System Driver Window also contains the controls for 'the Sonar Signal Viewer Window', and controls for various signal generation and analysis tasks.

3.2.3. Sonar Signal Viewer Window

The Sonar Signal Viewer Window functions as a near real time (it is updated after every echolocation cycle) digital oscilloscope which can show echo returns for three separate sonar modules simultaneously. It allows to quickly gain insight into the sonar signal waveforms, and during experiments it is a great tool for setting up the environment and detecting anomalies.

3.2.4. Advanced Unit Settings Window

The functions of the Advanced Unit Settings Window is self explanatory from the Figure 3.2. The settings 'WOI-Start Position' and 'WOI-End Position' serve to determine the lower and upper bounds for the *window of interest* in the local buffer memory of the sonar module. The unit will transfer only this window's content when requested from the central development unit. There are many more functions of the PC IDE software, that are not mentioned here, due to limited space. They are provided in detail in an user's guide.

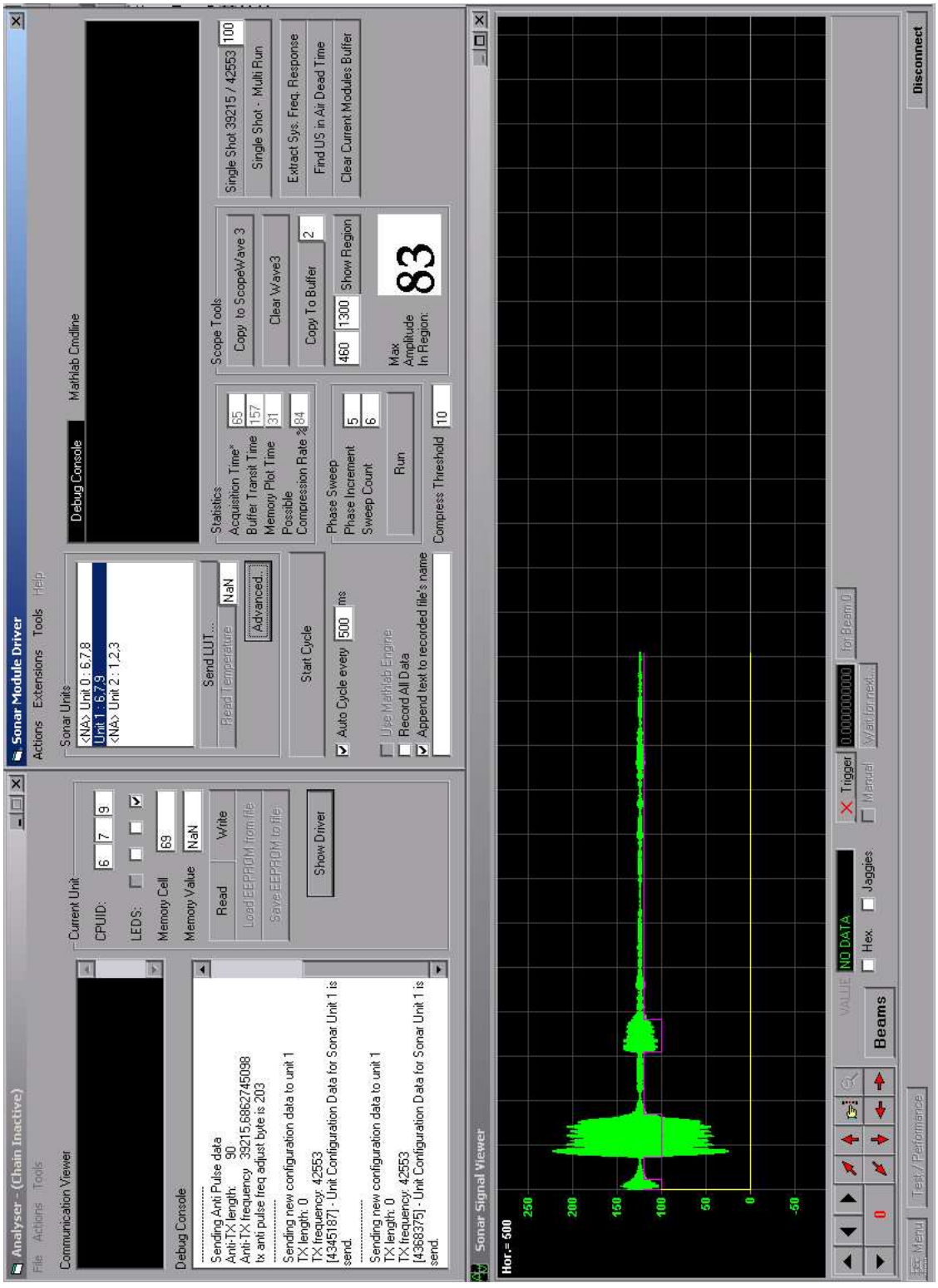

Figure 3.1. Integrated development environment - overall PC software

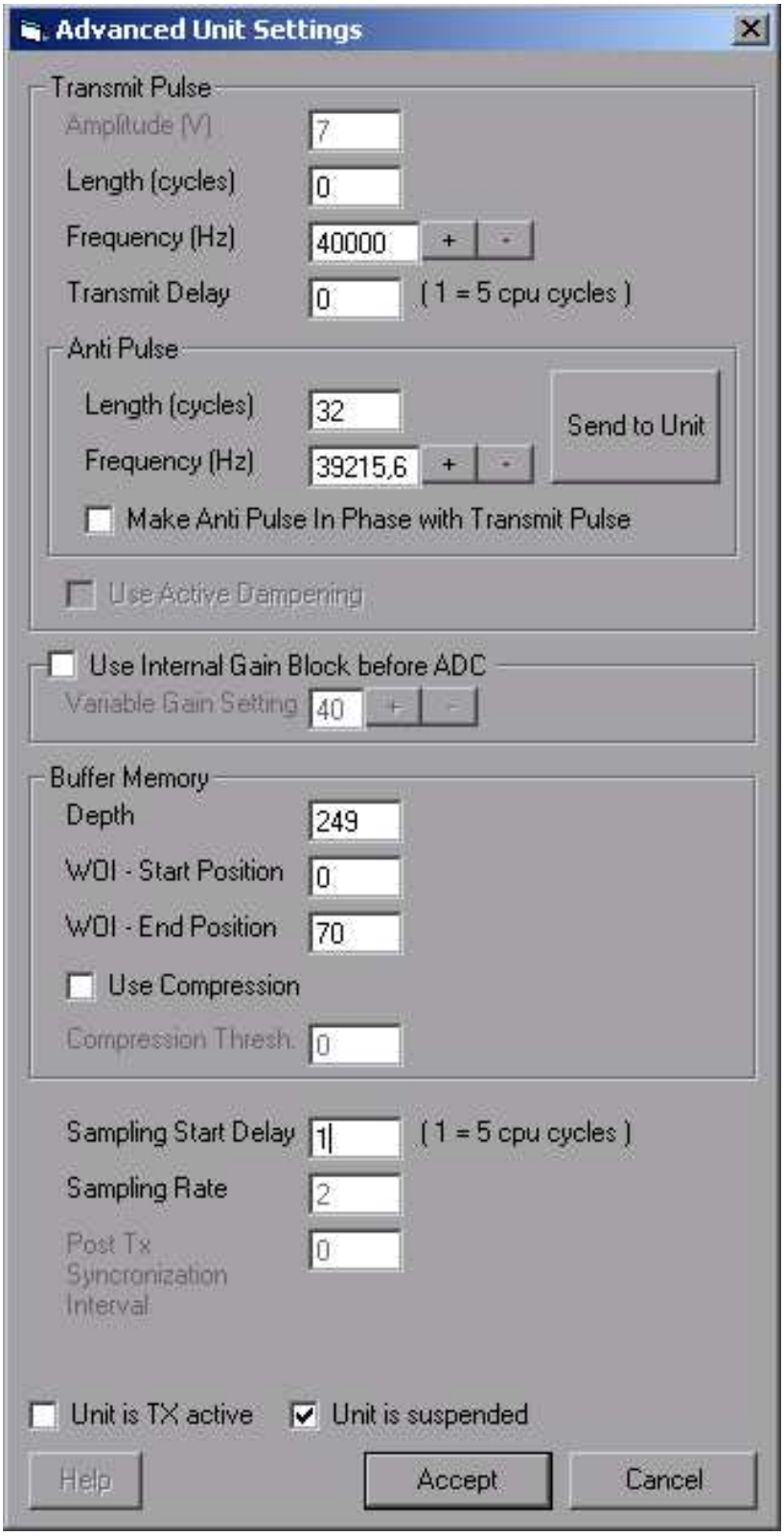

Figure 3.2. Integrated development environment - Advanced Unit Settings Window

3.3. Communication Protocol

The reliability, and the guaranteed latency of the inter–module communication of the distributed sonar system are of prime importance. The used physical bus standart has no mandatory software specification and therefore there is no pre–generated (and accessible with or without a fee) software layer available. Special features of the design like 'Synchronization over the communication channel' necessiates a custom build software layer from scratch. The communication is done in packets. The need for packets first arises from the fact that the communication speed is in the Mbps range and means for providing data integrity and for detecting errors are required. The packet structure resembles the TCP/IP packets used in telecommunication networks. The handling of the packets are custom, partly resembling the USB bus inner workings and are partly unique. The structure of a packet is shown in Figure 3.3. Since the data is 8 bits long and is transferred with 8 bit words, the start of a packet is identified with a unique header, that comprises of a special byte ordering. The use of 3 bytes in the header gives a combination that has occurance probability of $\frac{1}{16000000}$, which is quite low and proved itself very robust during field uses. The fourth byte in the packet carries the unit specific $time - slot$ that is assigned to a unit by the master during the bus initialization step. Its function will be explained in the sequel. The byte 'packet type' tells the packet's receiver, what type of data it carries or what function does the packet serve. There are two classes of packets: i) generic packets that every unit on the bus should be able to respond to, whether its a sonar module or not, and ii) packets that are function specific. The 'packet size' byte carries the number of bytes making up the whole packet. The three bytes following it carry the unique 24 bit unit identifier 'Chip ID' of the slave unit that should process the packet, in cases where the packet originates from the master unit and is not a broadcast packet. The master generated packets either belong to the class $MASTER\_TO\_SLAVE$ or to the class $MASTER\_TO\_ALL$. The master generated packet belongs to a class that is identified by the slave sonar modules by constantly checking the time–slot byte of the incoming packets. Time–slot 0 is always assigned to master–to–slave accesses and time–slot 1 is assigned to master's broadcast calls, accessing every unit simultaneously. The variable length data payload section of the packet is followed by a single byte static data delimiter. The checksum

of the packet bytes 4, 5 and 6 is calculated and appended to the packet. Finally, every byte of the packet is xored with each other and the result is appended to the end of packet. Xoring is a primitive alternative to the CRC16 standart. The calculation of CRC16 checksum would be slow if implemented in software due to lack of a hardware CRC calculator in the local microcontrollers. The author's idea to use time–slots is a

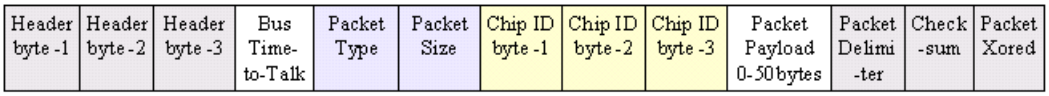

Figure 3.3. The structure of a communication packet

novel approach in half duplex bus implementations. In traditional implementations, there is a master that has the ownership of the bus, and only the master can initiate communications on the bus. It is done so that there will be no collusions. This exclusive right of the master requires the sequential polling of every slave unit on the bus. The time it takes to complete one polling cycle grows linearly with unit count, and can deterioate the responsiveness of the inter-module interactions by increasing latencies. However the devised time-slot mechanism solves these problems. The operation of the time–slot mechanism is as follows

- Slave units are allowed to initiate communication. For this, a method to eliminate collusions is needed.
- During the initialization of the bus, every sonar module that was previously introduced to the master and registered, is accessed one by one, and timeslots between 2 to 130 are assigned to them.
- The master generates periodically 'synchronize your watches' broadcast packet.
- After receiption of this packet, sonar modules simultaneously reset their software communication timers to assigned timeslot value times the time for 32 bits (3.2 bytes * (1 start bit + 8 data bits + 1 stop bit)) at the rated communication speed
- Any unit that has a waiting interrupt type bus access and communication need, waits until its communication timer expires before starting communication.
- While waiting, when a sonar module starts transferring data, the other units with higher valued timeslots detect the appearance of the standart packet header on the

bus. Recently mentioned 32 bits time corresponds to the packet header time plus some security buffer time. The waiting modules postpone their communication timers by one packet time.

- Master starts a new operation cycle by generating a new 'synchronize your watches' broadcast packet and the operation continues.

The resulting design turns out to be a low overhead bus management scheme with extremely low latencies. The CPU load of the bus trafic is minimal, since the bus is managed with silences instead of polling packets which generates interrupts at distributed nodes, even if they are not part of the current communication. Any unitialized sonar module (an erroneous CPU reset by an EMI event may cause this during run time) can be detected by the master, and can be joined back to the bus.

The generic packet types are well defined and the sonar bus can be utilized also by other non-sonar modules, custom designed for the robotic platform or experimentation needs. As an example, within the PC IDE software, support for optic mouse positioned experiment obstacles has been given, where new optic mouse interpreting microcontrollers are attached to the sonar bus. This way the obstacle position data acquistion can be done without human intervention, increasing experimentation speed and reducing human introduced errors during manual position measurements.

4. DUAL FREQUENCY BEAM SHAPING

This chapter presents a novel algorithm for angular localization. First, the theoretical formulation is presented.

4.1. Theoretical Formulation

The ultrasonic transducer is modelled as a vibrating piston with an aperture size of equal to its radius $a \in R$ [1]. Let us note that this is only an approximation as no real life transducer behaves totally like a piston within an infinite baffle, however the prediction is suprisingly reliable when transducer is excited with a narrow band signal with frequency $\omega \in R^+$ input signal [37]. According to planar piston model for the far field ($r \gg a$) , a transmitting transducer located at the origin and excited with frequency ω generates a pressure level $P_T : R \times SO(1) \times R | R \rightarrow R$ at the target location as measured by radial distance r and bearing θ as measured from the acoustic axis at time t whose intensity is as shown in Figure 4.1(left). The function P_T is modelled as consisting of two terms:

$$P_T(r, \theta, t, \omega) = P(r, t, \omega) H(\theta, \omega) \tag{4.1}$$

The function $P : R \times R \times R \rightarrow R$ models the on-axis pressure as a function of radial distance r, time t and excitation frequency ω. It is parametrized by a number of underlying physical properties:

$$P(r, t, \omega) = 0.5 j \frac{1}{r} p_0 c U(\omega) k(\omega) a^2 e^{j(\omega t - k(\omega) r)} \tag{4.2}$$

Here, $p_0 c$ is the characteristic impedance of the air medium, the function $U : R \rightarrow R$ is the amplitude of velocity of the transducer membrane vibrating radially with the frequency ω. The term $k : R \rightarrow R$ is the wave number and is a function of ω as $k(\omega) = \frac{\omega}{c_P}$. For a non-dispersive medium, $c_P = c$ where c is the adiabatic speed of

sound. Let us note that in the acoustics literature, the argument ω is omitted in the U and k terms for mono-frequency formulations. This standard will also be adapted in the sequel. The phasor term $e^{(\omega t - kr)}$ indicates that it is a traveling wave moving in the direction of increasing r with a frequency ω. It represents the instantaneous phase of the sinusoidal oscillation at a space point r at time instant t.

The function $H : SO(1) \times R \rightarrow R$ is the directional factor. It is defined as:

$$H(\theta, \omega) = \frac{J_1(k\,a\sin(\theta))}{k\,a\sin(\theta)} \tag{4.3}$$

where J_1 is the Bessel function of the first order of the first kind and k is the wavenumber as discussed previously. Let it be noted that the half beamwidth angle θ_0 corresponds to the first null of the directional factor [1] . The directional factor H is always normalized so that its maximum value is 1 which is attained when $\theta = 0°$. The sound beam is shaped in the angular directions by the directional factor term as shown in Figure 4.1(right). It consists of pressure lobes separated by nulls called pressure nodes. The set $\{\theta \mid H(\theta) = 1\}$ represents the acoustic axes of the transducer [1]. In a single transmitter case there is only one major lobe centered around the single acoustic axis line.

The term $k\,a$ is a measure of the ratio of the wavelength of the sound wave being generated/received to the aperture size of the transducer. Hence, its value is an indicator of the directivity of the transducer. Hence, the directivity of the sonar system can be controlled by choosing a transducer of an appropriate aperture size. For $k\,a << 1$, there is only one major lobe and there are no side lobes. Increasing $k\,a$ values makes the major lobe span a smaller angle and hence the number of side lobes are increased which then steal part of the raditated energy. This can then interfere with the major lobe returned range information and is therefore usually not desired. This is illustrated by example shown in Figs. 4.2-4.3. Here, two real life tranducers are used: the first one is a transducer with wide angle PZT with 40 kHz resonance frequency and approximately 7 mm aperture size, and the second one is an electrostatic transducer

[1]There is no standard definition for the beamwidth, so the first null of the directional factor is considered to give the half beamwidth angle throughout this thesis.

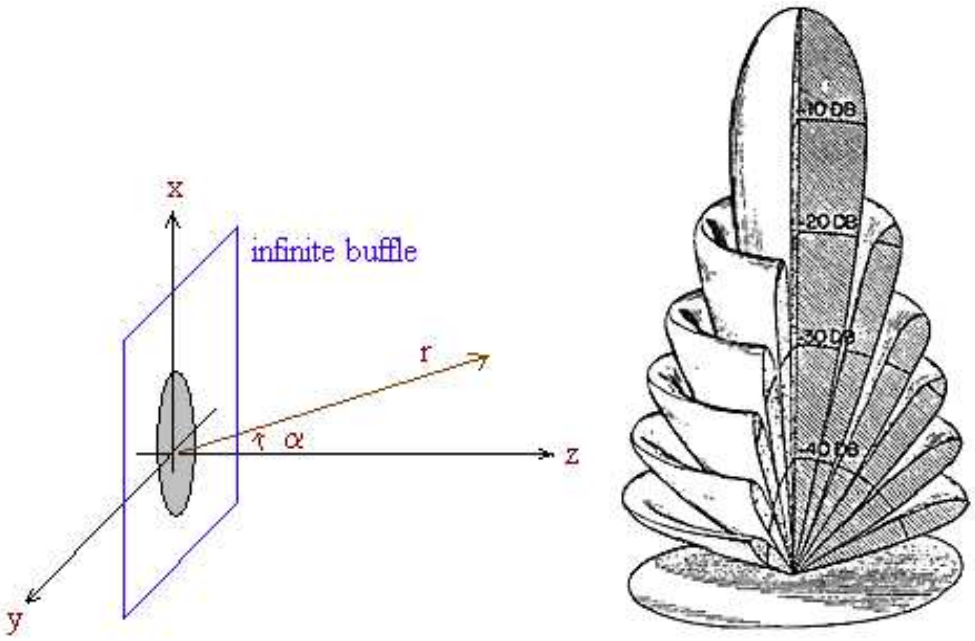

Figure 4.1. Left: Planar circular piston model; Right: The beam pattern of a plane circular piston in 3D

with 50 kHz resonance frequency and 20 mm aperture size. The figures show the beam patterns and system beam patterns (transmission of pulse and reception of the echo beam patterns superimposed together). Finally, let it be noted that the frequent appearance of the $k\,a$ term in acoustics literature has motivated the dual-frequency beam shaping appoach to be presented.

4.2. Algorithm

Let us assume pulse-echo operation with the following constraints in order to restrict the initial parameter space:

1. Ultrasonic sound reflections are of direct nature, and multiple reflections are ignored. Therefore the outgoing sound energy toward the target object leaves the transmit beam pattern through the same point as the incoming echo sound energy's point of penetration into the receptive beam pattern.
2. A single reversible transducer is used for both transmission and reception. Thus, the directivity function H_T for the transmitter and H_R for the receiver are the

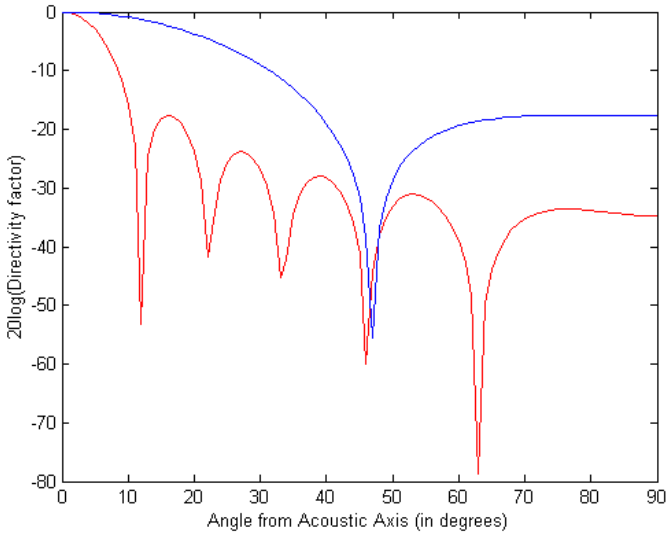

Figure 4.2. Comparison of transducer beam patterns in dB scale: Polaroid transducer (bottom curve) and PZT (top curve)

same; namely $H_T = H_R = H$.

3. There is no dispersion. (It will be included and compensated at a later stage)
4. Reflective target surface is a planar surface whose physical dimensions are greater than the wavelength of the sonar signal.
5. Far field conditions exist: $r \gg a$.
6. The environment is stationary.

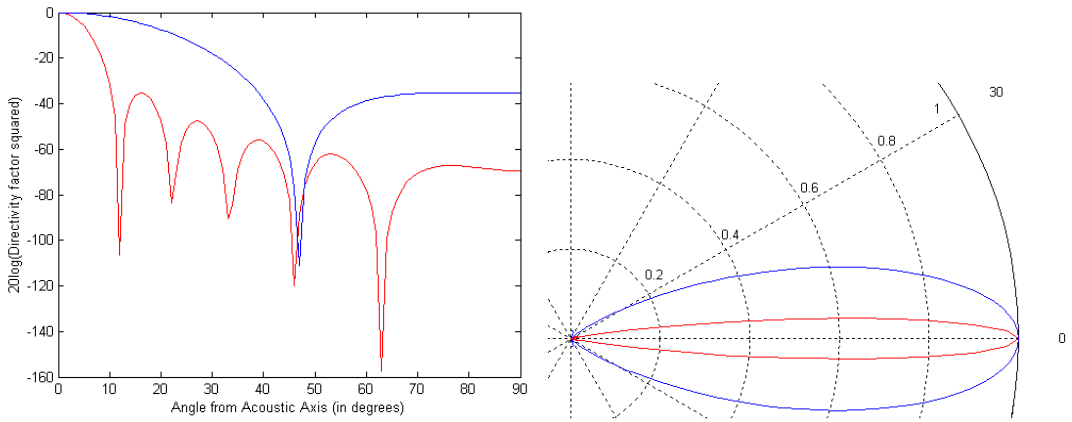

Figure 4.3. Left: Comparison of system beam patterns in dB scale: Polaroid transducer (bottom curve) and PZT (top curve); Right: Beam patterns in Polar diagram (in linear scale): Polaroid transducer (dotted lines) and PZT (outer, blue)

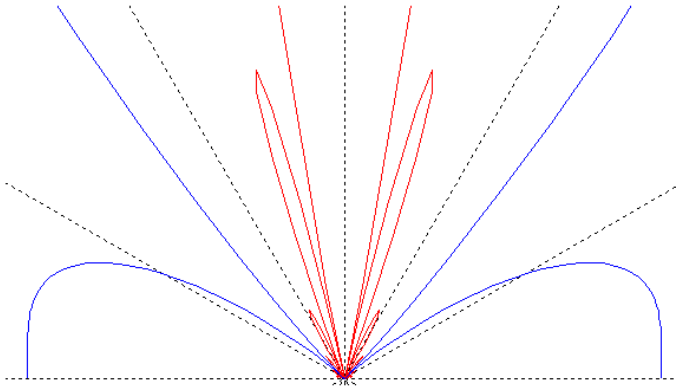

Figure 4.4. Side lobes comparison in linear scale: Polaroid transducer and PZT

With these assumptions in effect, let us recall that the pressure field of the transmitter is:

$$P_T(r,\theta,t,\omega) = P(r,t,\omega)H_T(\theta,\omega) \text{ for } r \gg a \tag{4.4}$$

The transmitted signal is subjected to a directional beamforming as determined by H_T.

Following, the sound wave propagates to the target object and is then reflected back. The returned echo is scaled according to the target strength which is a function of the target object's shape and surface properties. The reflected sound wave undergoes another geometric spreading in the return path which is denoted by the factor $\frac{1}{4\pi r^2}$. Finally, it is subjected to a secondary directional filtering by the receiving transducer as determined by the H_R directivity function. Hence, the pressure at the receiving transducer is then

$$P_R(r,\theta,\omega,t) = P(r,\omega,t)H_T(\theta,\omega)S\frac{1}{4\pi r^2}H_R(\theta,\omega) \tag{4.5}$$

Now, with a reversible transducer, the directional factor terms are equivalent and are equal to

$$H_R(\theta,\omega) = H_T(\theta,\omega) = H(\theta,\omega) = \frac{J_1(ka\sin\theta)}{ka\sin\theta} \tag{4.6}$$

In order to extract an angular position information from the received and measured pressure amplitudes, we should be able to eliminate the known and unknown/hard-to-quantize parameters other than the angle terms from the equation. Of prime importance is the parameter r, specifying the distance between the sensor and the target object, because it scales the amplitude of the measured echo in a range of up to 60 dB in the useful range of the ultrasonic transducer. Secondly, the target strength is an unknown/hard-to-quantize parameter and its inclusion in the equation makes the angular position information hard to extract.

Let's define $P_{R,max} : R \times SO(1) \times R \rightarrow R$ as $P_{R,max}(r, \theta, \omega) = max_t P_R(r, \theta, t, \omega)$ as the maximum amplitude in the mono-frequency snapshot of the sinusoidal echo sound wave. For two successive transmissions from the same single transducer with two different frequencies ω_1 and ω_2, selected to be close to the natural resonance frequency of the transducer, let us consider the ratio $\gamma : SO(1) \times R \times R \rightarrow R$ as

$$\gamma(\theta, \omega_1, \omega_2) = \frac{P_{R,max}(r, \theta, \omega_1)}{P_{R,max}(r, \theta, \omega_2)} \tag{4.7}$$

In case of a short delay between the the consecutive trains of the two frequency beams, the sound speed c does not change appreciably and the terms c in the nominator and denominator in the equation for γ cancel each other, which will be quite a big gain of the formulation. It is also assumed that for closely chosen w_1 and w_2 the changes in the target strength are ignorable.

Using equations 4.2-4.6 and substituting in equation 4.7

$$\gamma(\theta, \omega_1, \omega_2) = \frac{U(\omega_1)k(\omega_1)}{U(\omega_2)k(\omega_2)} \frac{H^2(\theta, \omega_1)}{H^2(\theta, \omega_2)} \tag{4.8}$$

The detectability of the angular position related cue we introduce into the traveling sound pulses/echoes and its relative size to the real world deviations from the underlying assumptions in the formulation will define the accuracy of the angular position estimate.

Here the first group of multipliers are mainly transducer characteristics and transducer's operating point specific parameters and the second term is the ratio of the directivity factors squared. For $w_1 < w_2$, and for the cone angles confined in the main lobe of the transducer beam pattern, the ratio term $\gamma(\theta, \omega_1, \omega_2)$ is bigger than one and increases monotonically with increasing cone angles. From the measured $\gamma(\theta, \omega_1, \omega_2)$ value, we will be able estimate the cone angle θ to the reflecting target object. The solution set will be a circular area enclosed by two co-centric circles drawn by $\pm$ standart deviation around the mean cone angle θ on the sphere surface with radius r.

To illustrate how the ratio function γ looks like, for two different frequency pairs, 39215 Hz - 42553 Hz and 37558 Hz - 44692 Hz, this ratio term is plotted:

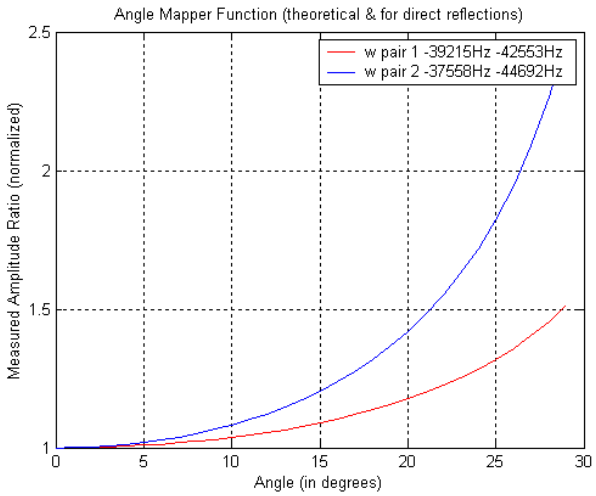

Figure 4.5. Plot of Equation 4.8 as a function of angular position

4.3. Choosing the Frequency Pair

The choice of the specific frequencies of the pair has been made to meet the following criteria:

1. The two frequencies of one pair should be close to the resonance frequency f_0 of the transducer, so that SNR and received echo amplitude does not drop dramatically. Received echo amplitude also has an effect on the level of the quantization noise introduced by the ADC during digitization process.

2. The two frequencies of the pair should be as separate as possible. This criteria contradicts the first criteria – a tradeoff exists in their choice.
3. The initial choice of what type of transducer and which aperture size to use, has a great impact on the performance of the method being developed. For an improved angular position resolving power at a specific cone angle θ, it is possible to operate in the fast changing (sensitive) portion of Bessel function J_1, by either increasing k or a. Thus, the method promotes the use of highly directive, big aperture size Polaroid transducers (the function curve rises more quickly for them, increasing angular position estimation accuracy), but we insist on using it with wide angle PZT transducers to maximize other robotic application specific performance metrics. Hence, the product $k\,a$ is not allowed to get big.

The first two criteria can be met only after the system response is extracted. To make this analysis, a frequency response analysis feature is added to the IDE software. Since the frequency response is also a function of the environmental setup and reflecting target object's bearing, an on-axis target object has been used, and while extracting frequency response for different hardware configurations (tuned and detuned transducers), the environmental setup has been preserved. The Figure 4.6 illustrates the frequency response of the original untuned transducer pair.

From Figure 4.6, it can be seen that for frequencies very close to the transducer pair's resonance frequency, the ADC's input saturates causing the sine fitter algorithm to fail to correctly measure the maximum amplitudes. This is due to using a single gain setting through the whole frequency range and due to the high Quality Factor Q of the transducer, but it does not cause a problem since the frequency pair we will select will not be that close to the resonance frequency. After reducing the circuit gain, we have also seen that the exact resonance frequency lies near 40800 Hz instead of 40000 Hz, which is thought to be due to the production tolerances and the mismatch between the separate transmitter and receiver PZTs.

The frequency pair 39215 Hz - 42553 Hz is the first choice with the current design of the system. Most of the experiments has been conducted using this frequency pair.

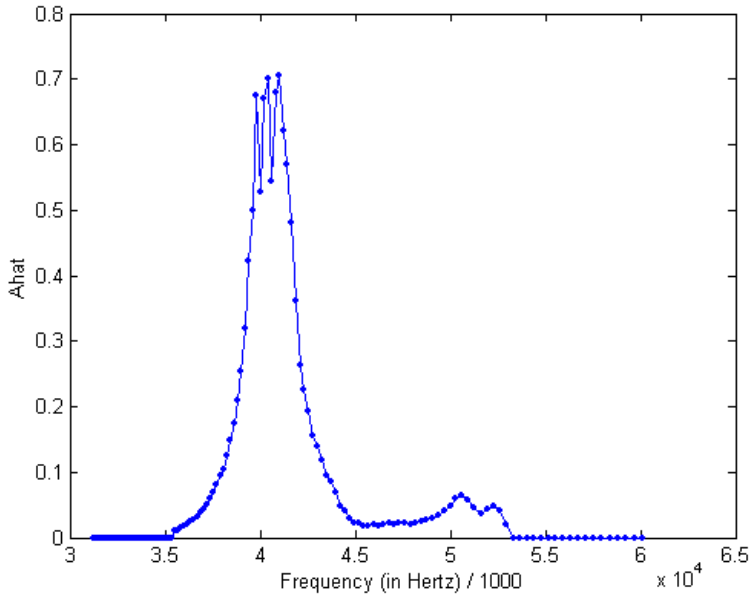

Figure 4.6. System frequency response that is extracted with untuned transducers for an on-axis planar target

After some study, we also discovered that we could increase the separation between the two frequencies of the pair some more without reducing the signal amplitudes much, via *transducer* detuning. The second frequency pair 37268 Hz - 44692 Hz has been attained after this analysis.

4.4. Transducer Detuning

To have the best possible resolving power for the bearing of the target object, we have investigated ways to achieve an increased bandwidth out of highly resonant piezo transducers – without resorting to higher bandwidth but also highly directive electrostatic transducers.

The piezoelectric transducer is a mechanically resonant system, because of the stiffness and mass of the piezoelectric material. Due to the piezoelectric effect, these mechanical properties show themselves as electrical equivalent properties. For example, the measurable electrical resonance frequency at the transducer terminals is equal to the mechanical resonance frequency of the piezo material. The mechanical properties mass, stiffness and damping can be represented by a coil, capacitor and a resistor. The

electrical equivalent model looks a lot like the well-known model for a crystal, which consists of a series arrangement of coil L_s, a capacitor C_s and a resistor R_s, which is paralleled by a single capacitor C_p [38].

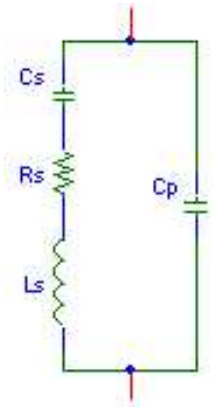

Figure 4.7. Electrical equivalent model for a crystal

As described in [38], the addition of an external inductor in parallel with the transducer, turnes the piezoelectric transducer into a component with two resonance frequencies and the bandwidth can be increased. To test if this is really the case, a 6 mH inductor has been constructed and connected parallel to the receiver. Four TDK make 1.5 mH SMD inductors are connected in series, to take advantage of their built-in electromagnetic shielding. The input of the pre-amplifier and the transducer's output are both of high impedance and this node voltage is amplified with high gain, so inductors should be connected with great care not to inject electromagnetic pollution to the signal to be amplified from external electromagnetic field sources like monitor, lighting, etc. The frequency response of the same enviromental setup with the receiver detuned is given in the Figure 4.8.

The frequency pair 37268 Hz - 44692 Hz has been selected from this frequency response curve. The Figures 4.9, 4.10 illustrate the beam shaping we achieve with dual frequency operation:

The angular accuracy is directly proportional to the derivative of the γ function. The Figure 4.11 shows this derivative. From this figures you see that detuning will more than double the accuracy (at increased cone angles even more).

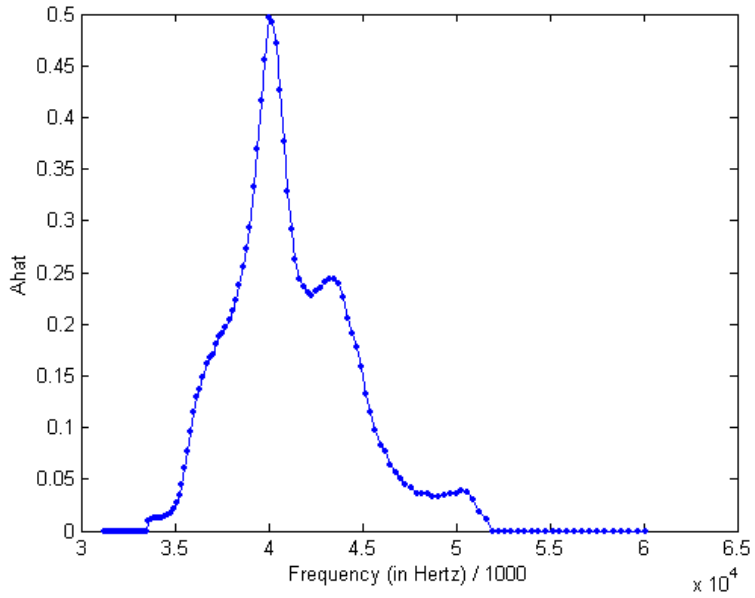

Figure 4.8. System frequency response that is extracted with detuned transducers for an on-axis planar target

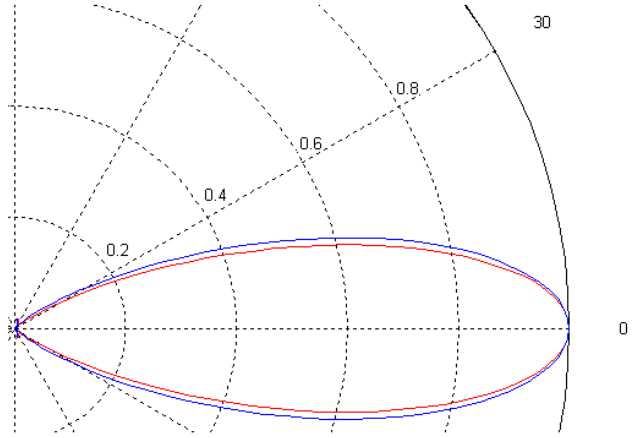

Figure 4.9. Polar diagram (in linear scale) of system beam patterns at 39215 Hz and 42553 Hz. 42553 Hz excitation results in the inner narrower beam.

4.5. Signal Processing

The incoming ultrasonic signal is externally pre-amplified and then input to one of the analog inputs of the sonar unit's built-in ADC. The rectification and low pass filtering option in the hardware is not utilized. The DC offset at the ADC input also needs to be measured as the pre-amplified signal is AC coupled to the input of the ADC and the DC operating point is set by a resistive network. Exact measurement

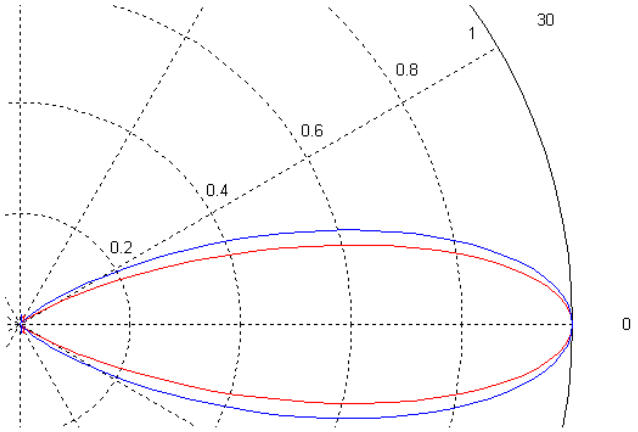

Figure 4.10. Polar diagram (in linear scale) of system beam patterns at 37268 Hz and 44692 Hz. 44692 Hz excitation results in the inner narrower beam.

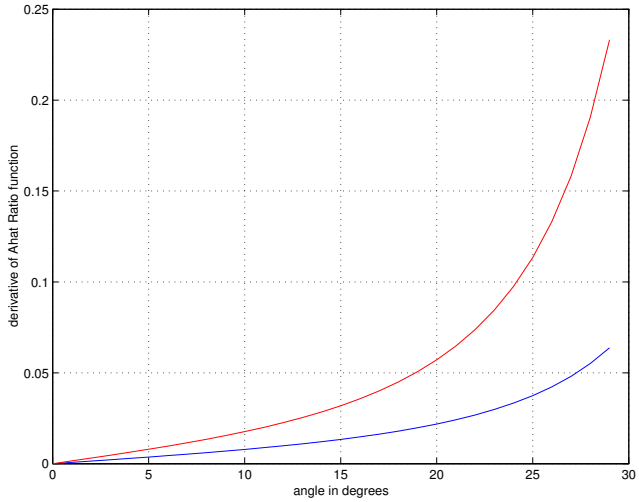

Figure 4.11. Derivative of the γ function versus target angle. The upper curve is for detuned transducer, the lower for simple transducer

of the AC circuit gain is not necessary for our spatial localization algorithm. The AC circuit gain is planned to be adaptively matched to the environment to compensate for distance and other attenuators.

The digitization is done in 8 bits and at a sampling rate 160363 samples per second (sps). The sampling rate is a multiple of the frequency of the external quartz crystal on the sonar module. The quartz crystal oscillator in the microcontroller generates the clock pulses for the synchronous operation of internal peripherals, the processing unit and the initial accuracy of the selected quartz crystal component. The capacitive loading at the crystal pins cause some deviation from the oscillation frequency printed

on the crystal. Digital domain signal processing is directly affected by the inaccuracies of the time base. In summary, there is imprecision in the frequency due to two factors: i) The sonar module generates the ultrasonic wave at a frequency not precisely known due to inexact crystal clock frequency, and ii) The sampling rate is not precisely known since it is a multiple of the crystal clock frequency. In order to alleviate the effects of both, the output of the ADC must be processed in order to improve the data. In literature, ADCs are usually tested by applying a pure sine wave to their inputs. Since the exact parameters of the resulting sine wave are very difficult to precisely obtain, the measured samples are interpolated to a sine wave. The ADC is then characterized by the analysis of the differences between the samples and the sine wave [39]. The parameters of the input which can accurately describe it by its amplitude, phase, frequency, and dc offset are determined from the series of output samples [39]. This method is described in IEEE standards 1241-2000 and 1057-1994. Curve fitting technique known as 4 parameter (4p) sine fit algorithm is used. 4p sine fit algorithm is a nonlinear least squares formulation with respect to frequency [40]. The algorithm is described in [40] by fixing the frequency and thereby converting the nonlinear LS into a linear one and finally doing a one dimensional optimization with respect to the frequency. The sampling rate estimate is updated. Following, 3p sine fit interpolation is used to estimate the frequency over a range of sample values. Let it be noted that the sine fit algorithm also helped in the signal processing as the phasor terms from the traveling wave equations are eliminiated. Moreover, sine fit algorithm has also a noise filtering characteristic.

After digitization, a 32 tap hanning window type low pass digital FIR filter is applied to the input samples series using information from [41]. Following, the parts of the input samples series where the absolute amplitudes of 5 successive samples all exceed a pre-determined threshold value are tagged to contain echoes reflecting from obstacles. The 3p sine fit algorithm is applied to the tagged sections so that the traveling wave phasor terms are removed from the equation and the maximum amplitude magnitudes are determined. Let it be noted, for practical purposes, once the sampling rate is determined, the use of 3p sine fit algorithm is preferred over 4p alternative for a static environment as it runs remarkably faster. The number of

samples used in the 3p sine fit algorithm has been determined after analyzing the bounds for harmonic distortion and noise errors for LS sine fit algorithms as discussed in [42]. Based on this study, 30 samples is used in the sine fit algorithm. This period contains approximately 8 periods of the fundamental frequency.

4.6. Dispersion Compensation

In the formulation so far, the absorption of the sound waves by the air has been ignored. A pulse train's acoustic energy is ultimately converted into thermal energy by lossy processes. The sources of losses can be grouped into two major classes: losses in the air medium and losses at the medium boundaries. Viscous losses (which can be treated as friction losses), heat conduction losses and molecular exchanges of energy belong to the first group. A primitive lossy model introduces a delay and associated relaxation time τ to modify the linear equation of state in the linearized wave equation theory [1]. The important consequence of absorption is that the phase speed c_p is not equal to c, but depends on the sound frequency. This makes the propagation medium *dispersive*. The term P in equation 4.1 should now be modified to include the effect of dispersion as [1]:

$$P(r,t,\omega) = 0.5j\frac{1}{r}p_0 cUka^2 e^{j(\omega t - kr)}e^{-\alpha r} \tag{4.9}$$

where α is the absorption coefficient. The traveling wave's phase speed is no longer the thermodynamic speed c of sound, but

$$c_P = c\sqrt{2}\left[\frac{1+(\omega\tau)^2}{\sqrt{1+(\omega\tau)^2}+1}\right]^2 \tag{4.10}$$

Recall that $k = \frac{\omega}{c_p}$ and in this form is known as the propagation constant. Consequently, the ratio γ function has a range dependency due to environmental effects – a consideration that has been ignored so far. This effect, although quite minor, is the dissipation of acoustic energy. Usually, the dissipation occurs so slowly, that it can be ignored for short distances. However, for increased accuracy and increased distances,

it should be rather taken into account. This primitive model is later extended to include the effects of viscous and thermal conduction losses additively and the classical absorption coefficient is developed [1].

$$\alpha = \frac{\omega^2}{2\rho_0 c^3}\left[\frac{4}{3}\eta + (\gamma_r - 1)\frac{\kappa}{C_P}\right] \tag{4.11}$$

where ρ_0 is the density of the fluid medium, η is the shear viscosity coefficient, κ is the thermal conductivity of the fluid, C_P is the heat capacity at constant pressure and γ_r is the ratio of heat capacities. For details on this material properties, the reader is referred to [1]. The classical absorption coefficient is in good agreement with experimental results for mono-atomic gases, but it falls short of the measurement results for polyatomic gases and the mixture medium air. In the air, the existance of CO_2 and water vapour causes dramatical deviatiations from classical absorption coefficient α. The theoretical approach of molecular thermal relaxation successfully gives close values with experimental data. In year 1993, the International Organization for Standardization defined the standart ISO 9613-Part 1 as the standart calculation of the absorption of sound by the atmosphere for pure tones (mono-frequency). This model assumes uniform meteorological conditions and specifies the attenuation coefficient as a function of frequency, temperature, humidity and pressure. The reference ambient atmospheric pressure, is that of the International Standard Atmosphere at mean sea level (101.325 kPa). The reference air temperature is 20°C. The range for frequency of the sound is (50 Hz to 10 kHz), for the temperature (-20°C to +50°C), for the relative humidity (10% to 100%) and for standart pressure (101.325 kPa) of the air. Formulae are also given for wider ranges (ultrasonic frequencies, lower pressure etc.) and for other not pure tones. According to ISO 9613-1, the accuracy of the calculated pure tone attenuation coefficients for atmospheric absorption is ± 20% in the 0°C to 50°C temperature range. The difference $\alpha(\omega_1) - \alpha(\omega_2)$ needs to be compensated. Figure 4.12, Figure 4.13 and Figure 4.14 illustrates the effects of humidity, temperature and pressure on $\alpha(\omega_1)$, $\alpha(\omega_2)$ and on $\alpha(\omega_1) - \alpha(\omega_2)$ for the frequency pair 39215 Hz - 42553 Hz.

In the environmental condition ranges specified by ISO 9613-1, a worst case anal-

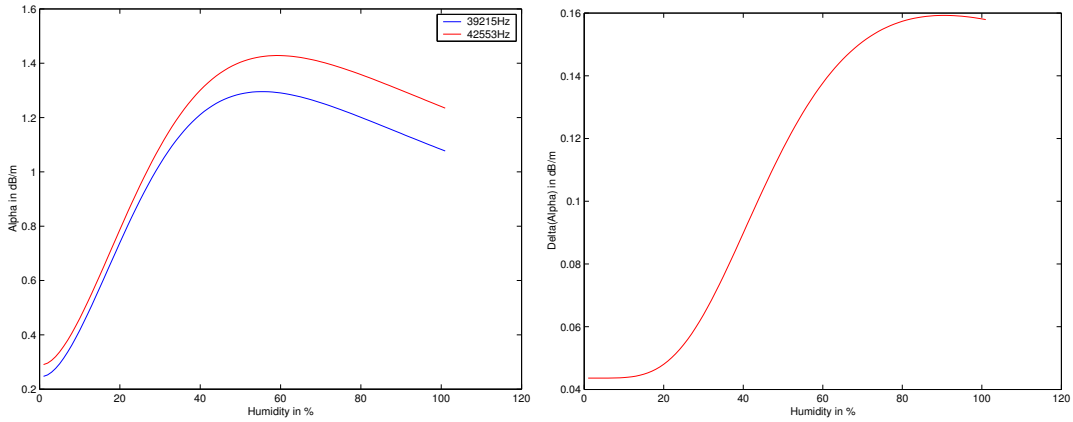

Figure 4.12. Effect of humidity on attenuations $\alpha(\omega_1)$, $\alpha(\omega_2)$ and attenuation difference $\alpha(\omega_1) - \alpha(\omega_2)$

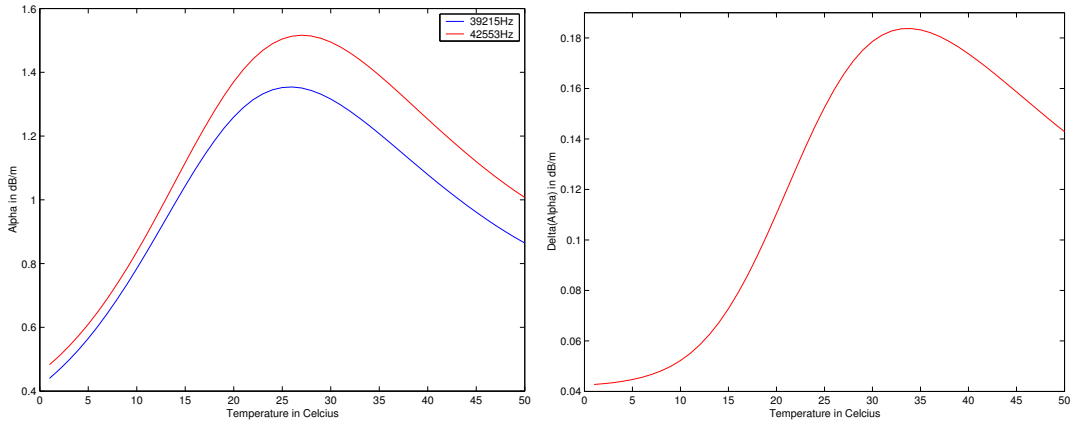

Figure 4.13. Effect of temperature on attenuations $\alpha(\omega_1)$, $\alpha(\omega_2)$ and attenuation difference $\alpha(\omega_1) - \alpha(\omega_2)$

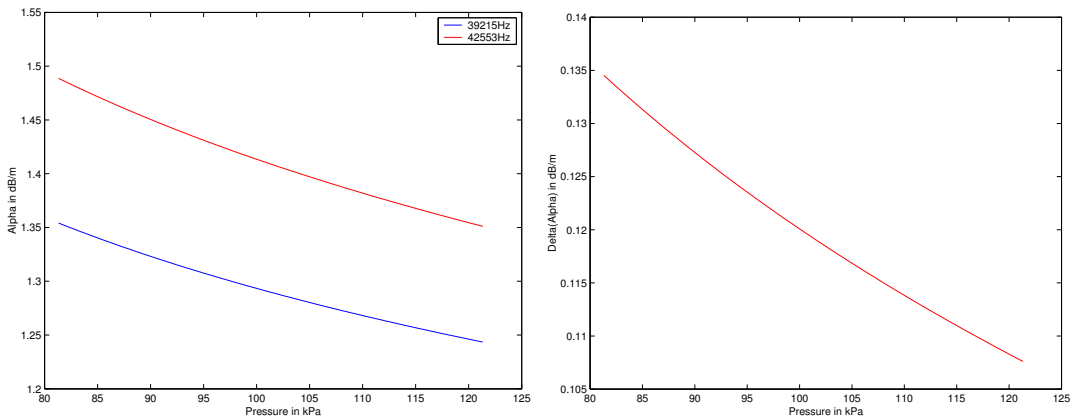

Figure 4.14. Effect of pressure on attenuations $\alpha(\omega_1)$, $\alpha(\omega_2)$ and attenuation difference $\alpha(\omega_1) - \alpha(\omega_2)$

ysis of α has been made and the following data have been found:

- $[\alpha(\omega_1) - \alpha(\omega_2)]_{max} = 0.1532$ dB/m, which occures at 33°C, 85 kPa, 85% humidity.
- $[\alpha(\omega_1) - \alpha(\omega_2)]_{min} = 0.0356$ dB/m, which occures at 0°C, 120 kPa, 0% humidity.
- $[\alpha(\omega_1) - \alpha(\omega_2)]_{nominal} = 0.0928$ dB/m, which occures at 20°C, 101 kPa, 40% humidity.

The outliners are 0.06 dB/m away from the nominal value. For 1 m of sound path, this number corresponds to a 0.69% effect on the γ. For 10 m of sound path, this number corresponds to a 7.1% effect on the γ ratio. It is the derivative of γ that translates an uncertainty in γ to an uncertainty in spatial location. Checking the data from Experiment #9, it can be said that the initial accuracy is potentially very high. We can use the $[\alpha(\omega_1) - \alpha(\omega_2)]_{nominal}$ directly for a first order compensation of the weak distance dependence of γ.

5. EXPERIMENTS

Using the Advanced Air Ultrasound Hardware and PC Software IDE designed, which is described in a detailed manner in the previous sections of this thesis, a series of experiments regarding bearing estimation have been conducted. The setups are as shown in Figure 5.1.

Figure 5.1. Top: System setup; Bottom: Experiment setup

5.1. Transient Signals

Experiments showed that there is a transient time at the beginning and at the end of every echo, where the frequency content, and the amplitude behavior differ as shown in the example of Figure 5.2. The transducers are of highly resonant character and their high Quality Factor Q is directly accompanied with a large decay time τ. First graph in Figure 5.3 shows that a pulse has been transmitted by driving the transducer at a frequency other than its natural frequency (39215 Hz instead of 40800 Hz) and the returning echo is captured. The first 720 samples embed the forced response region. The remaining samples represent the decay transient region with a decay time τ. The start of the forced response region is also worth paying attention to as it represents the superposition of the transient response of a damped oscillator at its natural angular frequency w_0 on the steady-state condition of the forced oscillation at w [1]. We can use this model since the piezo transducer has mechanically resonant structure and the phenomena can be explained with this. The solution of a linear second order differential equation driven by a signal $Fe^{j\omega t}$ is known to be of the form

$$x = Ae^{-\beta t}cos(w_0 t + \Phi) + \frac{F}{\omega Z_m}sin(\omega t - \Theta) \tag{5.1}$$

where A and Φ are determined by initial conditions. At the beginning of the development, the transmitter driver circuit was not taken into operation. Rather, the transmitter is driven by a square wave coming from a free I/O pin of the microcontroller. This has the consequence that the very first edges of the driving square wave are perceived as a step input due to high driving impedance of the regular I/O drivers. The transducer begins to ring and the A term becomes energized so that the associated natural response now decades with the same decay time τ. In a proper drive implementation, the low driver internal impedance ensures that A does not grow that much. Reducing the Q by adding a resistive damping will also reduce the decay time. DC coupling instead of AC coupling of the driver output to transducer may help. This initial mistake pushed us to analyze the underlying physics of oscillation and learn where to look inside the echo pulse train to find the feature of interest. During the experiments and analysis that follow, we didn't return and activate the on-board heavy

duty push-pull piezo driver stage but increase the number of cycles in an ultrasonic sound burst, to have enough time after the application of the driving force for the waveform to settle into the steady state. The second graph of Figure 5.3 shows the 4p sine fit algorithm returned frequency estimate divided by 1000 Hz. The third graph in Figure 5.3 shows 3p sine fit algorithm and 4p sine fit algorithm returned local maximum amplitude parameter together. It can be seen that after calibration, the 3p sine fit algorithm returns almost the same amplitude estimates except in the transient dominant regions as expected. The Figures 5.3 and 5.4 illustrate the analysis in greater detail.

5.2. Quick Demonstration

In this experiment, an experimental setup as illustrated in Figure 5.5 is used. In this mechanism, a planar object is rotated around the transducer pair. The frequency pair 38834Hz - 42328Hz is used. P_R measurements from three different angular positions are taken. The computed γ values are shown in Figures 5.6-5.8.

5.3. Statistical Studies

In order the investigate real-life performance, a series of statistical experiments have been conducted as detailed in this section.

5.3.1. Initial Experimental Setup

In this experiment, an experimental setup as shown in Figure 5.9 has been used with the following conditions:

1. A room volume of 2 m (d) x 2.25 m (w) x 2 m (h) has been emptied in order to minimize uncontrolled echoes.
2. At the center of the longer dimension (w) of this area, a table is used to raise the US sonar module about 80 cm above the floor level (See Figure 5.10).
3. The separate Tx and Rx transducers are stacked in the vertical direction and are

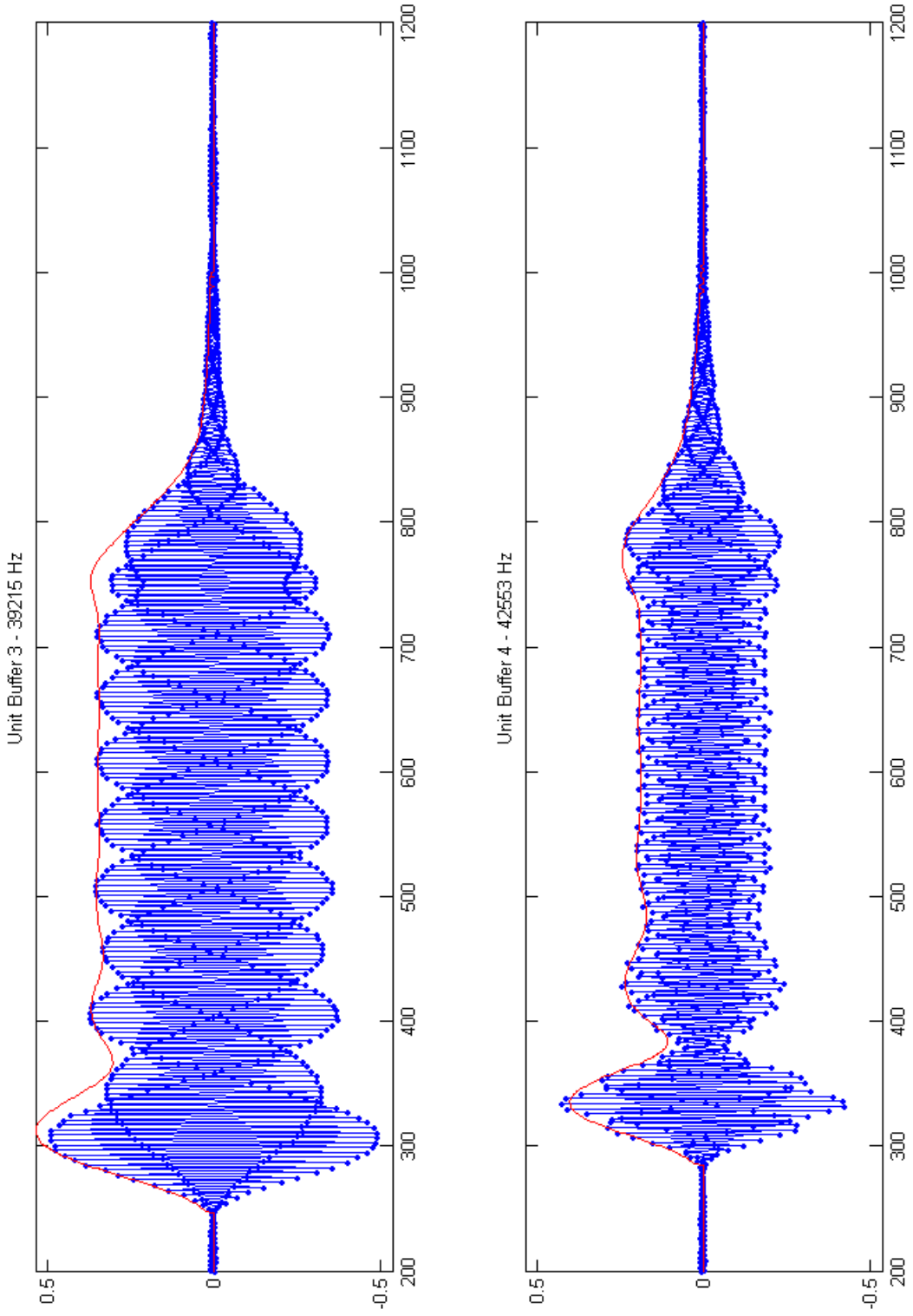

Figure 5.2. Input sample series for 39215 Hz and 42553 Hz sonar excitations

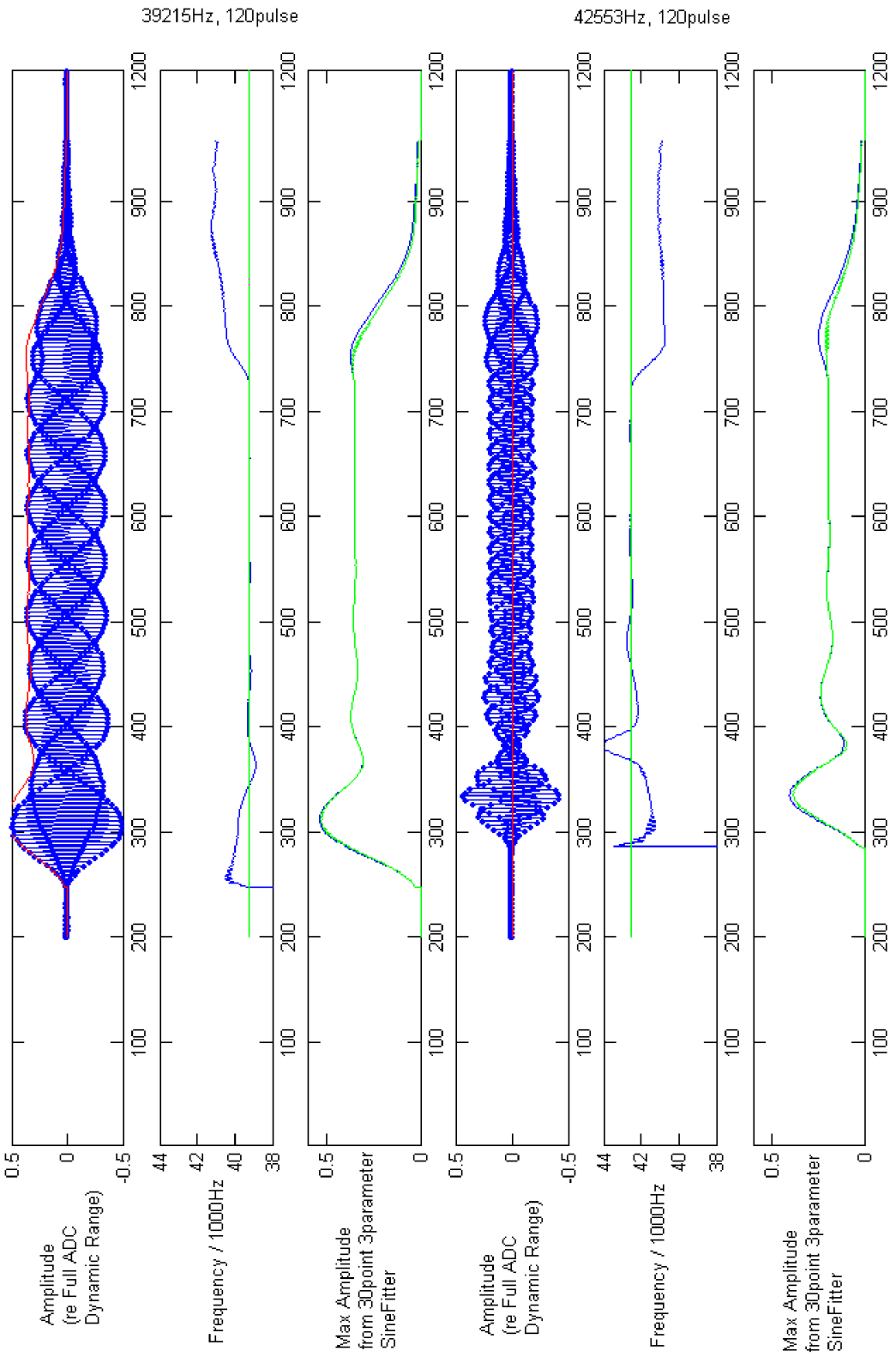

Figure 5.3. Input sine fit analysis for 39215 Hz and 42553 Hz sonar excitations

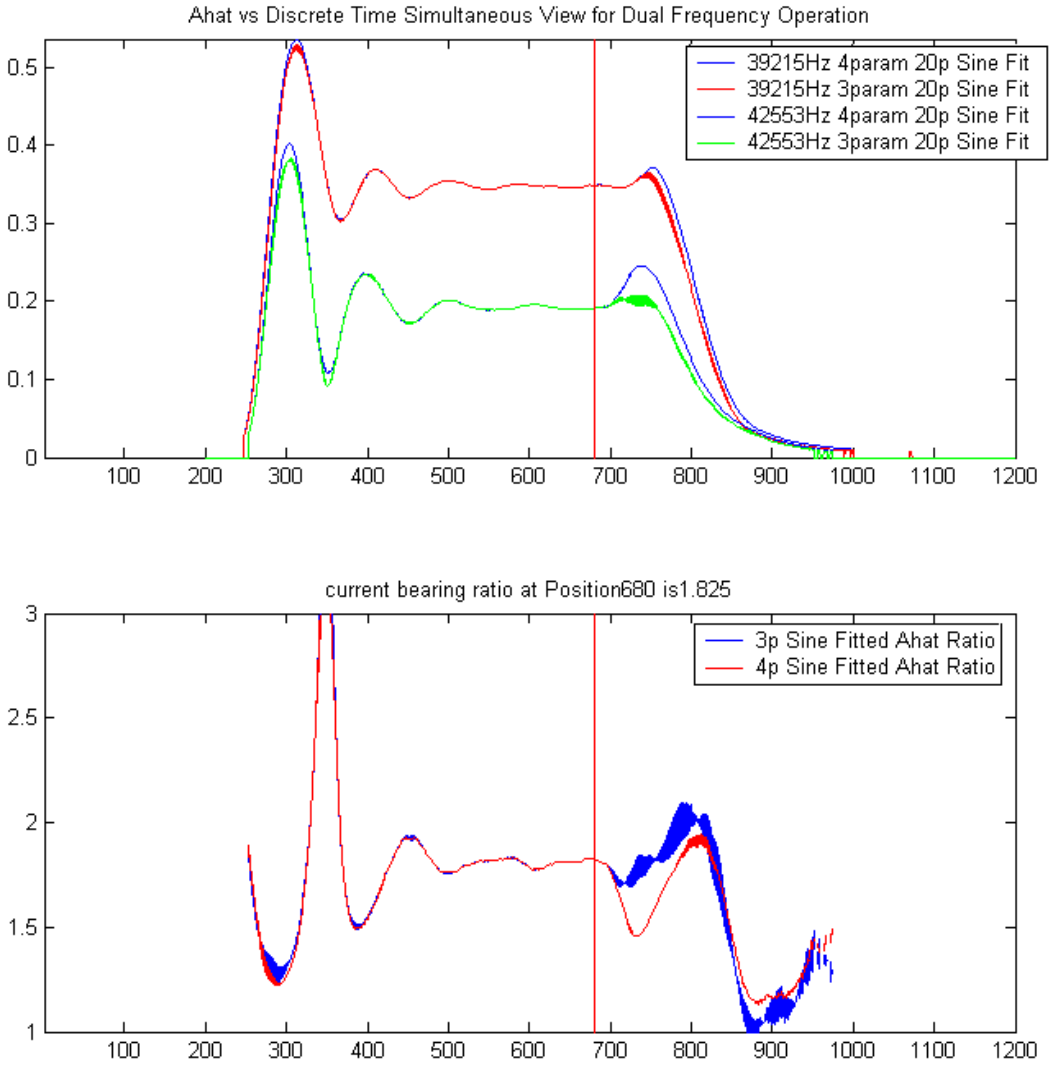

Figure 5.4. γ analysis for 39215 Hz and 42553 Hz sonar excitations

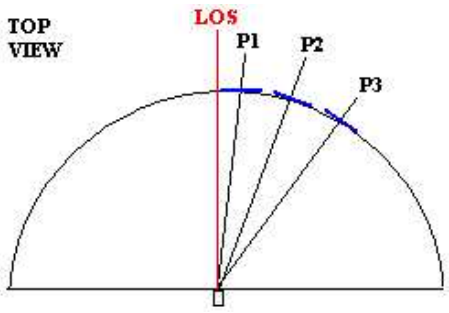

Figure 5.5. Angular positions of 3 demonstration points with respect to line of sight (LOS)

as close as possible to each other, approximating a single transducer.

4. A special mechanical apparatus has been constructed. In this apparatus, a pla-

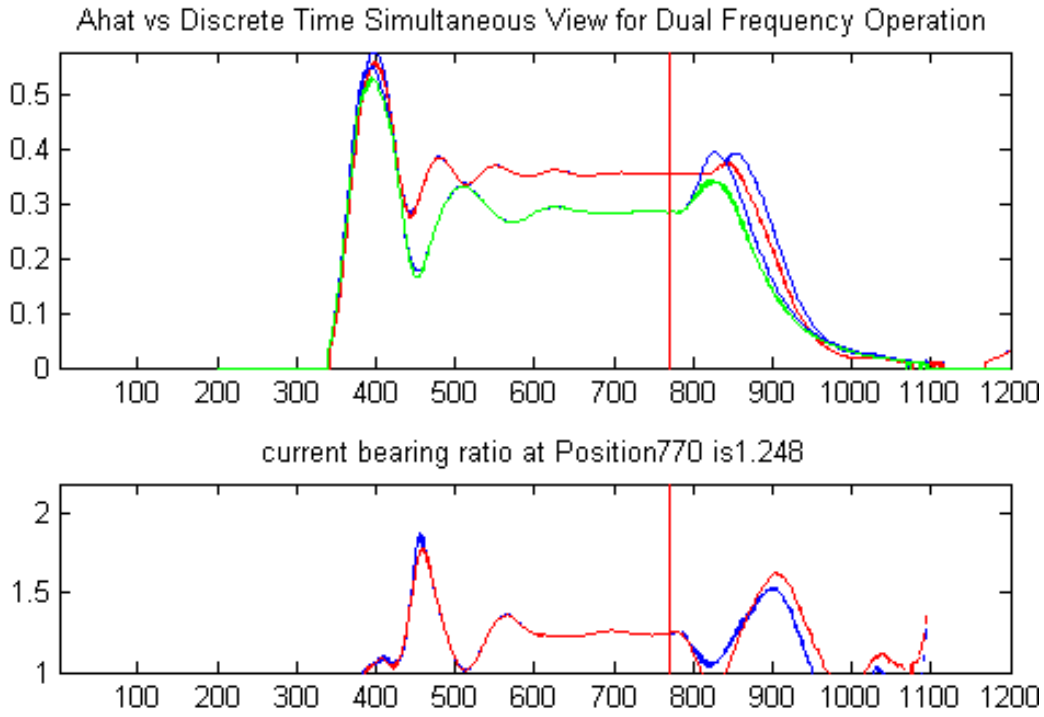

Figure 5.6. γ calculation for P1

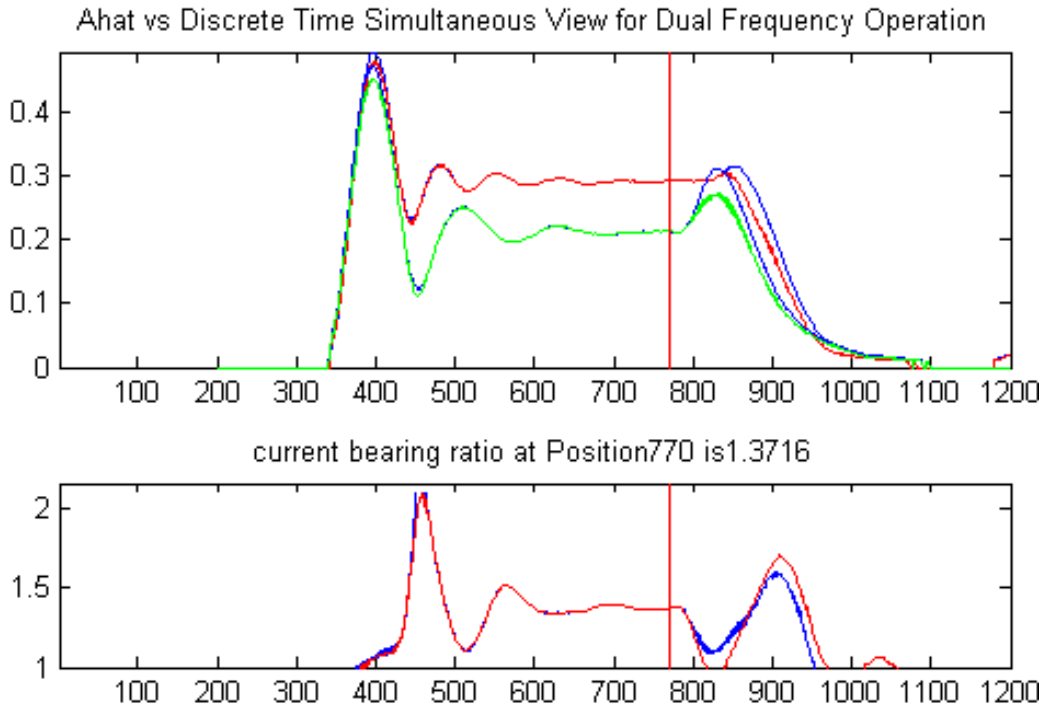

Figure 5.7. γ calculation for P2

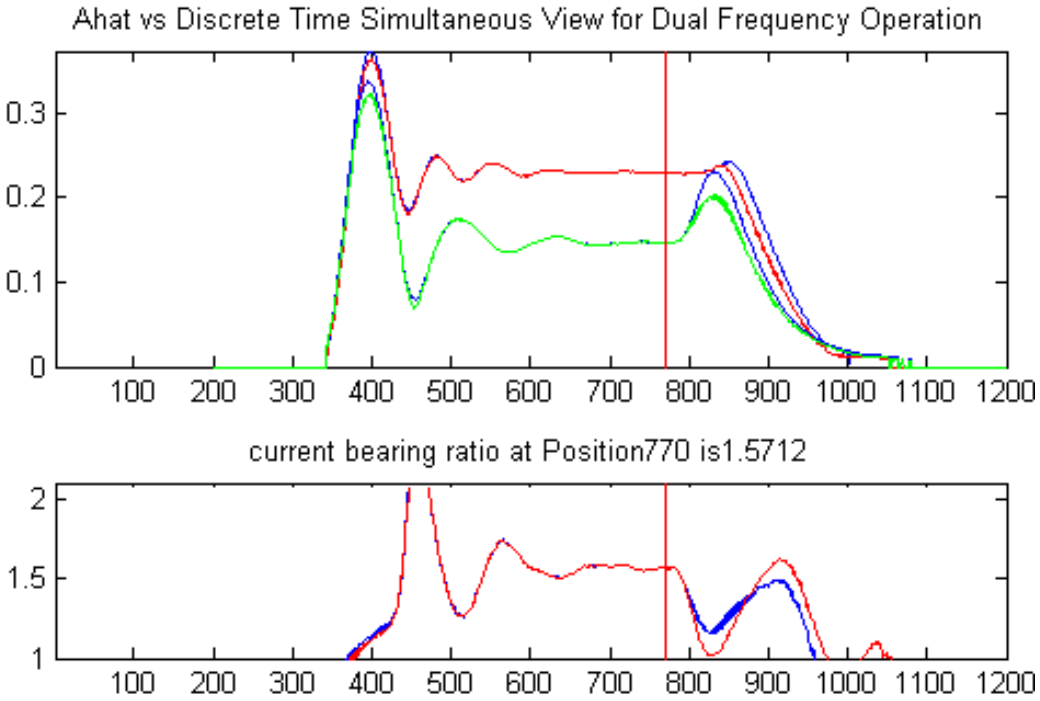

Figure 5.8. γ calculation for P3

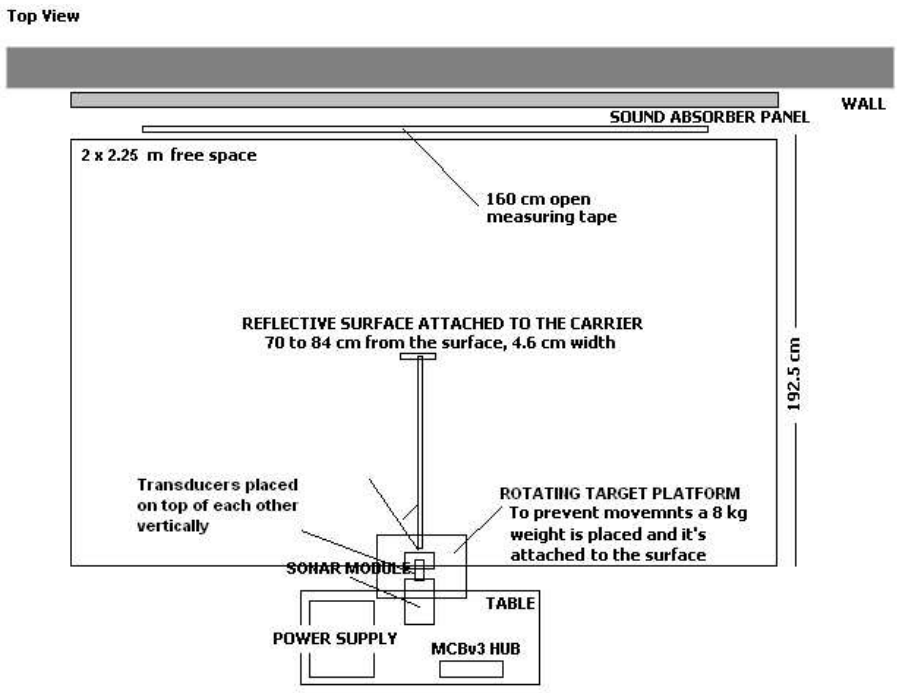

Figure 5.9. Drawing of the room setup for the experiment #8

nar reflecting target surface rotates around the sonar module on a circular path. Figure 5.11 shows its static base. It allows to test spatial locations with differ-

ent azimuth angles but fixed elevation (the elevation angle is approximately 0°). To eliminate any movements of the base during experimentation, metal weights totaling 8 kg is put on the base.

5. A reflecting target surface is used which is made of carton, and is 14 cm by 4.6 cm with its longer dimension oriented vertically. It is 88 cm away from the transducers at the center.
6. A laser pointer located close the center (to reduce errors) sends its beam onto a measuring tape, which is 192.5 cm away from the laser (See Figure 5.12). This way, we tried to minimize measurements errors. The black surface to the back of measuring tape is a sound absorber that quickly dampens the acoustic energy in the air.

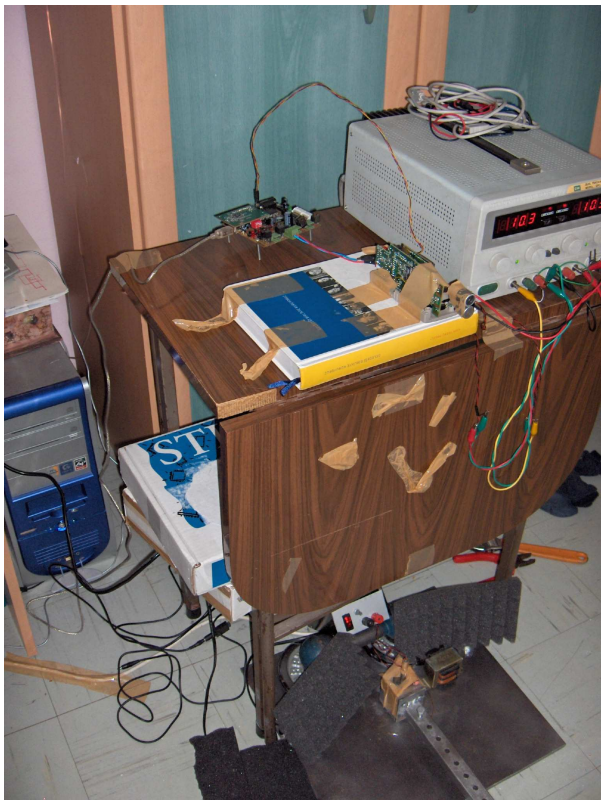

Figure 5.10. Table carrying the sonar module in the experiment

The results are as presented in Table 5.1. A close analysis reveals the following:

- The minimum value of $\mu(\gamma)$ occurs for the azimuth angle 0° as expected.
- The standard deviations $\sigma(\gamma)$ for various azimuth angles drop as the bearing is

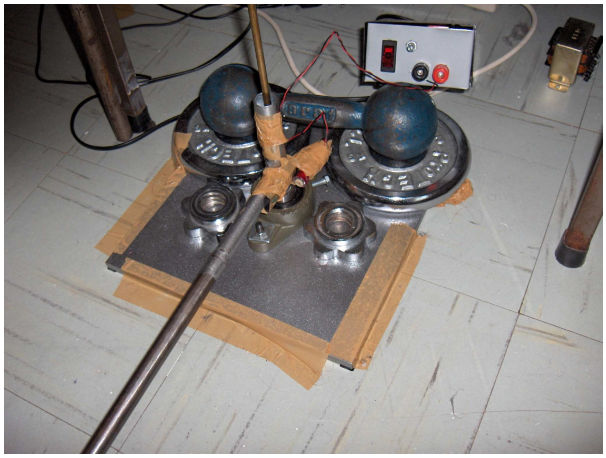

Figure 5.11. Base of the rotating mechanism used to position the target object to different azimuth angles

Figure 5.12. The laser beam is projected to a far measuring tape, to increase measurement accuracy

closer to 0° due to the increased signal amplitudes.

- It is observed that contrary to the expectations, the measurement obtained with $\theta = 0°$ does not have maximal amplitude. A careful examination of the ex-

periment setup reveals the error source: the two transducers are positioned at an angle with respect to each other. Consequently, there is a slight difference between their azimuth angle.

- When γ values at symmetrical (target position 10), but opposite sides of the center are compared, it is seen that the position range 10–17 behaves as expected. From position 10 to position 17, the rise in γ value is monotonic, with an expected curvature. Actually, the curvature is a bit higher than that the formula of γ estimates. This is due to the conical piston shape and the transducer shell which modifies the directivity from that given in the γ formula. The system behaves erratically in the Position range 1–10, which corresponds to the same side with respect $\theta = 0°$. After examining the mechanical apparatus, it has been observed that the rotation occurs with some unevenness in this range. Accordingly, the laser beam spot makes a noticeable vertical movement. The uncontrolled movements in the elevation direction are exacerbated with the controlled azimuth changes causing unexpected results in this range.

This experiment provides insight into the required modifications in the mechanical apparatus for improved experimental results.

Table 5.1. Results for Experiment #8

no	x[cm]	$\mu(\gamma)$	$\sigma(\gamma)$	max(γ)	min(γ)	$\mu(w_1)$	$\mu(w_2)$
1	6,2	1,8744	0,0234	1,9421	1,8031	0,0799	0,0426
2	23,5	1,8289	0,0166	1,8709	1,7631	0,1136	0,0621
3	26,5	1,8162	0,0203	1,8612	1,7666	0,1207	0,0665
4	30,5	1,7985	0,0175	1,8712	1,7604	0,1351	0,0741
5	33,5	1,8220	0,0172	1,8697	1,7793	0,1277	0,0710
6	36,5	1,8064	0,0210	1,8545	1,7490	0,1416	0,0784
7	41	1,7852	0,0144	1,8164	1,7476	0,1521	0,0852
8	50,5	1,7364	0,0148	1,7816	1,6946	0,1739	0,1002
9	61,5	1,7246	0,0126	1,7541	1,6923	0,1967	0,1141
10	68	1,7208	0,0140	1,7614	1,6801	0,2073	0,1205
11	72	1,7292	0,0159	1,7670	1,6862	0,2154	0,1246
12	76	1,7415	0,0167	1,7892	1,7022	0,2216	0,1272
13	81	1,7578	0,0171	1,8148	1,7200	0,2294	0,1305
14	88	1,7812	0,0143	1,8263	1,7511	0,2370	0,1331
15	104,5	1,8932	0,0137	1,9229	1,8554	0,2424	0,1280
16	122	2,03	0,0173	2,0837	1,9863	0,2262	0,1112
17	139	2,2222	0,0236	2,2827	2,1648	0,1968	0,0885

5.3.2. Improved Experimental Setup

Based on the insight gained from the previous experiments, a series of modifications in the setup are introduced in order to improve the accuracy of the measurements:

- The distance to the measuring tape is increased from 192.5 cm to 199 cm, to increase the measurement accuracy a bit more.
- The misalignment between the two transducers has been corrected as much as possible.
- The use of the laser pointer is improved.
- The analog gain of the circuit is increased in order to have a better utilization of the input dynamic range of the ADC.

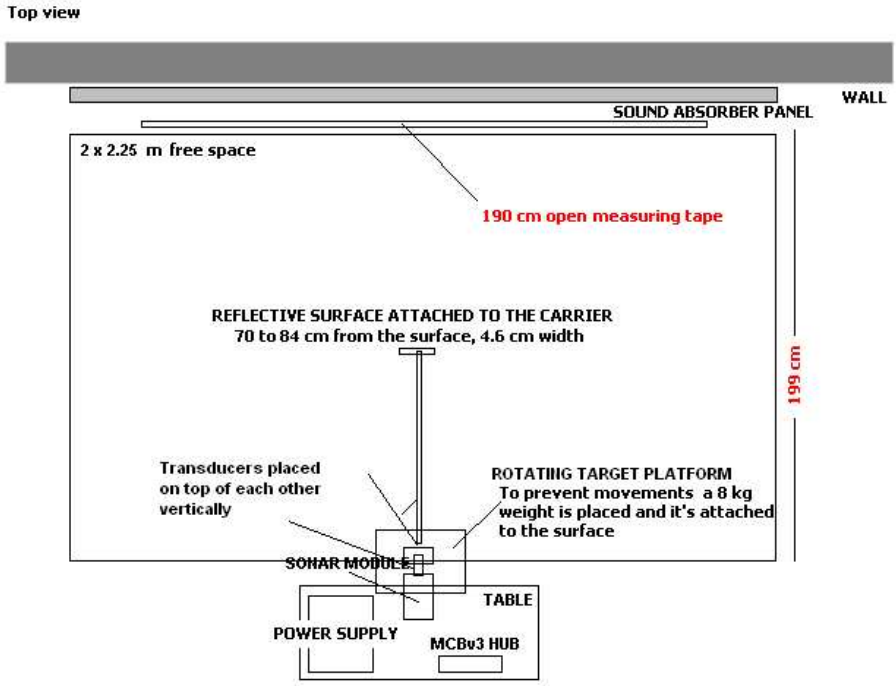

Figure 5.13. Improved experimental setup

- The number of measurement azimuth positions is increased. It is risky to increase the number of measurement positions since the errors introduced by manual reading is no longer an order of magnitude smaller then the step change. It may cause monotonicity errors.

The results are as shown in Table 5.2 and in Table 5.3. Here, let it be noted that the azimuth position 17 corresponds to the azimuth angle 0°. The following observations can be made:

- The standard deviation of the γ values decreases with higher analog gain.
- A close inspection of $\mu(w_1)$ and $\mu(w_2)$ values reveal that measurements with $\theta = 0°$ have the maximal amplitudes.
- The angular accuracies are very promising as indicated in Figure 5.14. We can say that angular accuracies lower that 0.5 degree are easily achievable with this early results. The accuracy increases with increasing azimuth angles. For example, at $\theta = 16.8°$, the accuracy increases to 0.21°.
- The erratic half of the azimuth positions still continues. We conclude that this

Table 5.2. Results for Experiment #9 - Part 1

no	x[cm]	θ[°]	$\sigma(\theta)$	$\mu(\gamma)$	$\sigma(\gamma)$	max(γ)	min(γ)	$\mu(w_1)$	$\mu(w_2)$
1	189	16,8	0,21	2.5505	0.01829	2.5956	2.5004	0.2301	0.0902
2	185	15,7		2,4554	0,01804	2,4983	2,4036	0,2453	0,0999
3	181	14,6		2,3717	0,01174	2,4146	2,3423	0,2564	0,1081
4	176	13,3		2,2840	0,01768	2,3300	2,2408	0,2719	0,1191
5	171	11,9	0,26	2,1873	0,01862	2,2345	2,1291	0,2892	0,1322
6	166	10,5		2,1154	0,01727	2,1679	2,0062	0,3034	0,1434
7	162	9,4		2,0583	0,01446	2,0876	2,0279	0,3120	0,1516
8	158	8,3		2,0039	0,01101	2,0321	1,9681	0,3217	0,1605
9	155	7,4		1,9770	0,00926	2,0142	1,9543	0,3302	0,1670
10	152	6,6		1,9670	0,01274	2,0001	1,9269	0,3365	0,1711
11	149	5,7		1,9283	0,00935	1,9522	1,8982	0,3411	0,1769
12	145	4,6	0,46	1,9010	0,01096	1,9333	1,8720	0,3456	0,1818
13	141	3,5		1,8666	0,01022	1,9052	1,8391	0,3485	0,1868
14	138	2,6		1,8563	0,00978	1,8944	1,8320	0,3524	0,1898
15	135	1,7		1,8520	0,00871	1,8814	1,8266	0,3536	0,1909
16	132	0,9		1,8466	0,01105	1,8744	1,8165	0,3567	0,1932
17	129	0*		1,8470	0,00972	1,8792	1,8239	0,3594	0,1946

error is unsolvable with the current mechanical setup. A new setup with high precision (5000 steps per revolution) step motors and industry class rotating tables is in the plans for design.

Table 5.3. Results for Experiment #9 - Part 2

no	x[cm]	θ[°]	$\sigma(\theta)$	E(γ)	$\sigma(\gamma)$	max(γ)	min(γ)	$\mu(w_1)$	$\mu(w_2)$
18	126	-0,9		1,8406	0,01069	1,8740	1,8115	0,3475	0,1888
19	122	-2,0		1,8148	0,00954	1,8454	1,7923	0,3435	0,1893
20	118	-3,2		1,7884	0,01014	1,8152	1,7611	0,3379	0,1890
21	114	-4,3		1,7883	0,01111	1,8147	1,7624	0,3339	0,1867
22	110	-5,5		1,7762	0,01050	1,8000	1,7494	0,3261	0,1836
24	108	-6,0		1,7921	0,01295	1,1891	1,7538	0,3226	0,1800
23	106	-6,6		1,7815	0,01006	1,8140	1,7561	0,3186	0,1788
25	102	-7,7		1,7869	0,01190	1,8176	1,7566	0,3084	0,1726
26	98	-8,9		1,7801	0,01050	1,8082	1,7507	0,2995	0,1683
27	94	-10,0		1,7581	0,01118	1,7888	1,7275	0,2874	0,1635
28	90	-11,1		1,7886	0,01082	1,8197	1,7592	0,2777	0,1553
29	86	-12,2		1,7829	0,01374	1,8255	1,7502	0,2642	0,1482
30	82	-13,3		1,7949	0,01331	1,8421	1,7511	0,2531	0,1410
31	78	-14,4		1,7904	0,01334	1,8364	1,7614	0,2411	0,1346
32	73	-15,7		1,8197	0,01923	1,8752	1,7693	0,2262	0,1243
33	68	-17,0		1,8487	0,01502	1,8791	1,8077	0,2112	0,1143
34	63	-18,3		1,8592	0,01746	1,8995	1,8180	0,1960	0,1054
35	58	-19,6		1,9155	0,01779	1,9790	1,8693	0,1807	0,0944

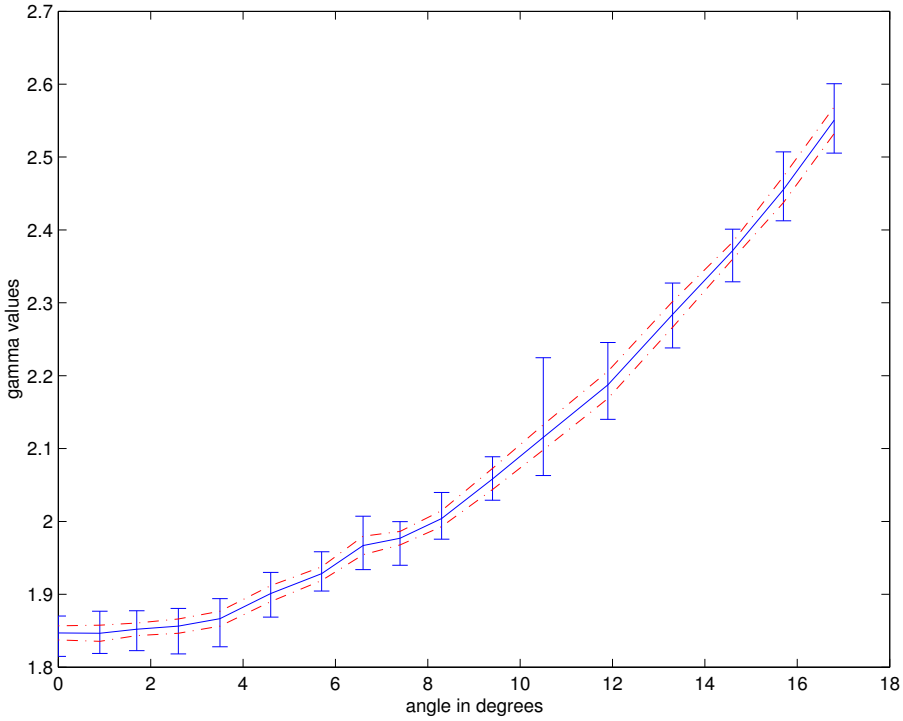

Figure 5.14. Improved setup results: Mean, Mean+σ and Mean-σ curves are drawn and min-max outlier bars are shown at measurement azimuth angles

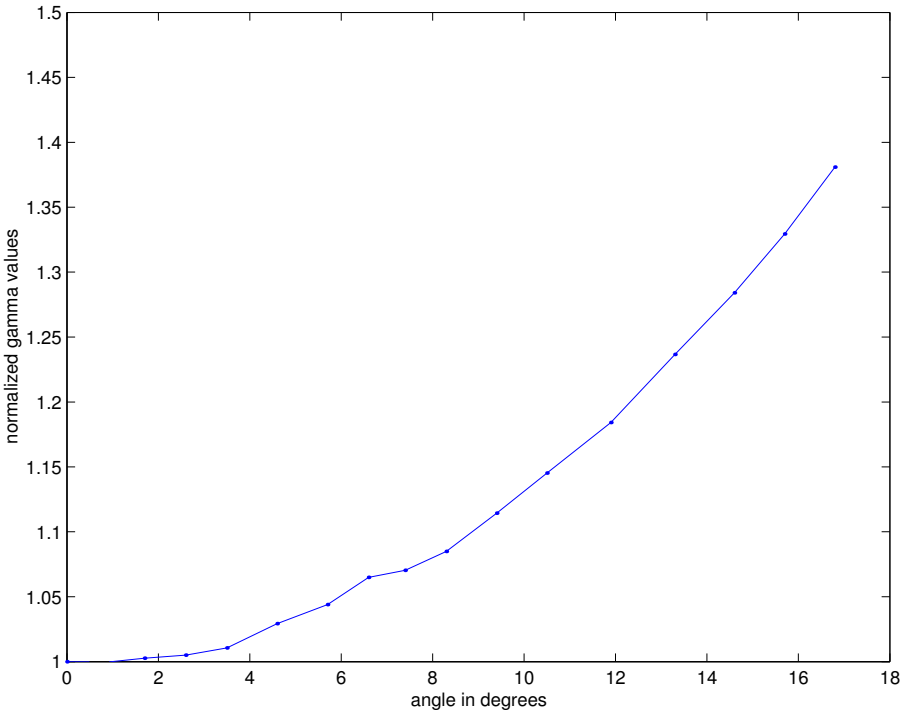

Figure 5.15. Mean γ normalized with respect to 0° γ value

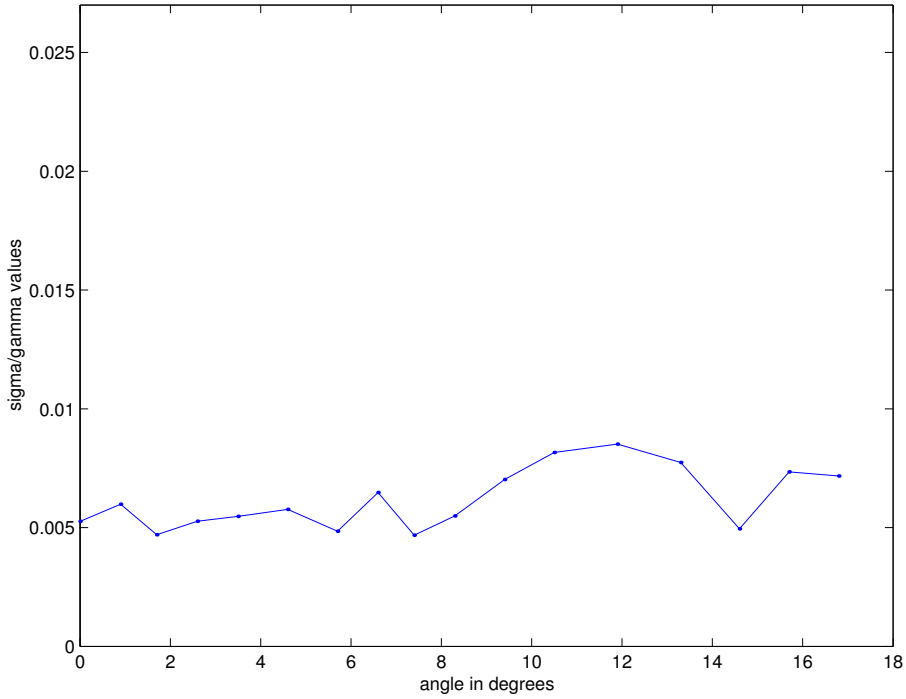

Figure 5.16. Standart deviation over mean curve for experiment #9

5.3.3. Effects of Time Delay Between Consecutive Firings

The quick analysis in Table 5.4 indicates that the responses to signals transmitted close to each other in time are better correlated. Consequently, one is led to the conclusion that such a firing scheme improves accuracy. In the last set of experiments, the time delay between two consecutive firings is investigated in detail. In this analysis, as a figure of merit, standard deviation σ divided by mean μ is adapted as the measure of performance. Two different scenarios are considered:

Case 1 - Large delay between firings of different frequencies: First, 250 measurements of the first transmitted frequency 39215 Hz are taken. Following, those of the second frequency 42553 Hz are taken.

Case 2 - Small delay between firings of different frequencies: The two consecutive signals are of different frequencies 39215 Hz and 42553 Hz respectively with a time delay of 75 ms.

The $\frac{\sigma}{\mu}$ measure of γ is expected to get a lower value for the second case when compared that of the first case.

Table 5.4. Increase in accuracy with close firing

Pos	$\sigma(\omega_1)/\mu(\omega_1)$	$\sigma(\omega_2)/\mu(\omega_2)$	$\sigma(\gamma)/\mu(\gamma)$
Pt 17	0,0072	0,0087	0,0053
Pt 12	0,0087	0,0086	0,0058
Pt 2	0,0061	0,0093	0,0073

Point Pt17 is close to $\theta = 0°$, so the signal amplitudes are relatively high. The second point Pt12 is at an intermediate angle point. For both Pt12 and Pt17, $\frac{\sigma}{\mu}$ for γ shows better accuracy. At Pt2, the accuracy is better than the average. However, it is not better for the lower frequency ω_1. This may be attributed to the reduced utilization of the full ADC input dynamic range and therefore increased effect of quantization noise occurring during digitization. In summary, there is a strong indication that different frequency firings should occur with as minimal time delay as possible.

5.4. Discussions

5.4.1. General Implementation

This section presents a general evaluation of the overall system with respect to implementation:

1. The wave number ka can be optimized for required level of angular resolution versus total angular view angle.
2. The number of quantization levels of the ADC has a direct impact on standard deviation of measured ratios and therefore the accuracy.
3. Wide angle transducers have a couple features which make them quite advantageous:
   - The number of side lobes is much less,
   - The single big major lobe ensures a one-to-one mapping of the γ function in a wider region,
4. Detuning also the transmitter is recommended since thereby it becomes a better radiator for the dual frequency mode of operation,

5. The system beam pattern has a full beamwidth angle nearly takes up 35 dB dynamic range. In order to utilize this, a higher precision ADC (12 bit or more) can be used so that a wider angular span can be processed without switching to another gain setting,
6. In the sine wave testing, the quantization error is partly deterministic and the sample values are strongly interdependent, which makes the sine fit algorithm worse then expected. The LS fit has nice properties, especially when the error sequence is random, zero-mean Gaussian and white. LS fitting does still work, as it usually works, because the error values are more or less scattered. An algorithm is described in [43], which removes pathological bins of the quantizer and improves the determination of the best fitting sine wave. Adding this to current signal processing implementation may further improve the accuracy of the method proposed in this thesis.
7. The use of a pair of transmitting transducers in acoustic doublet configuration may provide higher resolution at low angles,
8. Note that the far field formula gives an idealized pattern. However, in real life some deviations from it are expected since:
    - The original far field model assumes a pulsating circular piston mounted flush with an infinite size baffle. A baffle is a rigid plane boundary with dimensions much greater than a wavelength of sound and which is considered to be a plane of infinite extent. However, in real life, the baffle size is of finite dimensions.
    - Radiation from the back of the pulsating surface that is out of phase with the frontal radiation can get in to the front region.
    - The equal speed/amplitude vibration rule for every point on piston may not be obeyed
    - There is a cone mounted to the center of the bimorph material, and the sound field is modified by the cone.
    - The cone may vibrate.
    - The metal shell around the acoustic membrane and cone structure as well as the metal grid in front of sensor may both affect the generated and received sound waves. However, both are kept in tact during experimental verification

as they are indispensable to ensuring durability in tough environments.

- Separate Tx or Rx optimal transducers are used in order increase the SNR. Although they are spaced as close as possible, the total system beam pattern is not simply the system pattern of a reversible transducer.

Interestingly, despite the fact that the list of possible deviations from the idealized models may is rather long, the results obtained with our adoption of an idealized rigid piston are in reasonably good agreement with observed values.

5.4.2. Advantages & Projected Distinctive Uses

This section gives a summary of advantages along with foresight into future uses:

1. More useful information can be extracted from the environment using minimal hardware, processing power and cost.
2. The effect of distance to the accuracy of angular location estimate given by γ is low when compared to ILD based methods.
3. The use of a single wide angle transducer (utilizing the proposed signal generation and processing methods) as the peripheral vision part of a more complex sensing system as a performance multiplier is possible.
4. The use of a single transducer eliminates the so called *dead zone* - an issue that is critical with narrow angle transducers.
5. The famous correspondence problem does not occur for the target spatial localization by γ.
6. The separation of multiple reflections echoes from direct reflection echoes shall be possible with 2 wide angle transducers.
7. Simultaneous pulse coding of the direction of transmission information for the whole sonified space is very valuable. The extracted stimulus dimension is orthogonal with time.
8. Together with a deconvolving algorithm which is to be designed, the creation of a unconventional high quality air sonar device may be possible. Speech and seismic signal processing background has some critical knowhow in similar problems [44].
9. In previous system, triangulation is achieved by positioning two transducers at a

certain distance from each other and orienting them so that they have an overlapped area of coverage. Trigonometric rules are applied in order to localize the target to a point in the azimuth. The uncertainty may be reduced by introducing a third transducer to the system. The method proposed in this thesis may be applied as an alternative approach – without requiring a third transducer as shown in Figure 5.17.

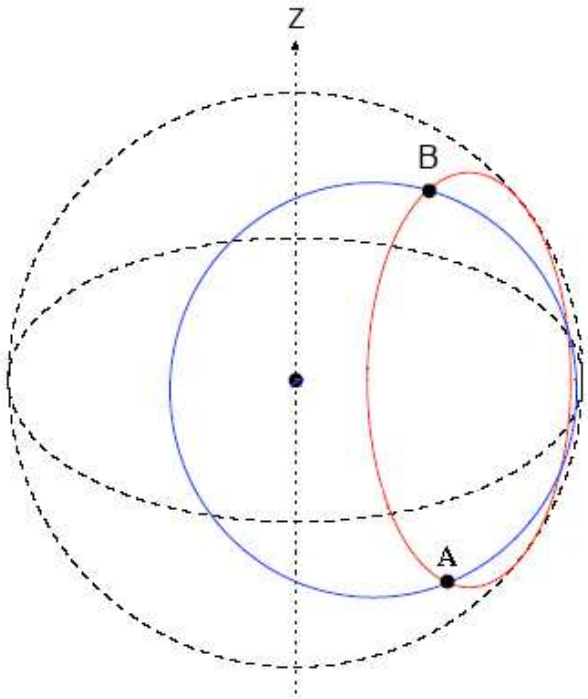

Figure 5.17. The localization solution set for two transducers with γ processing

10. There is an inherent compensation of transmission effects. In the conventional range measurements, the measurements are of absolute nature. Thus, the angle estimation returned from triangulation algorithms is directly affected by the absolute accuracy which is the uncertainty error in the exact distance measurement from the face of the ultrasonic sensor to the target. Uncertainty in the exact sound speed over the entire propagation path usually is the major component of the the inaccuracy in the absolute measurement of the range to the target. Uncertainties in the average value of the speed of sound along the acoustic path can occur for a variety of reasons. A sensor with an built-in temperature probe will obviously have less problem in sound speed approximation than a sensor that does not do a first order compensation of the temperature. In some applications,

however, the temperature along the propagation path between sensor and target can be different from the temperature at the sensor, which therefore will cause an unavoidable error. Also if there is air turbulence along the path from the sensor to the target, then the average speed of sound will randomly change, causing the target range computed by the sensor to randomly vary from pulse to pulse. For an outdoor application, this is important. The γ operator gives an added precision.

6. CONCLUSION

This thesis presents a new complete ultrasound system – inspired by both underlying physics and biological sonar. This system incorporates completely new designs in its electronics as well its accompanying operational software. A novel sonar processing algorithm that is biologically motivated and is based on the physical properties of the sonar transmission is then developed and evaluated on this sytem. The system holds the promise of being a robust, flexible and extendible study platform for further sonar research and applications without requiring any critical modifications. The new ultrasound system has the following contributions:

Hardware: A completely new hardware with an extendible topology of sonar sensors has been designed. The hardware can be interfaced to a desktop computer for sonar theory development or alternatively to a pocket PC in order to mobilize the developed sonar system quickly on a robotic platform. The sensor topology consists of a set of sonar modules – each endowed with enough 'intelligence' as to apply some level of control on the outgoing signal and similarly some level of processing on the incoming signal.

Firmware and Software: A new accompanying software that supports the extendible hardware sensor topology has been designed and programmed. This firmware enables each sensor module to be known to the rest of the system, receive control commands from or send sonar to the central processor. The communication protocol between the host CPU and the sensors is based on a new bus arbitrage method. The accompanying PC software functions as the development environment and handles signal processing and visualisation task during algorithm development.

Dual Frequency Based Bearing Estimation: The newly developed system is then used in the problem of angular position determination. As is well known, sonar sensors provide reliable range estimation, however, their performance in bearing determination is relatively low. This thesis presents a novel approach that is physics-based and biologically inspired. In contrast to most previous methods

that are based on using multiple sensors with a single frequency to improve their angular resolution, this method uses a single transducer with dual frequency beam shaping. Experiments demonstrate that even with minimal hardware, and hence processing power and cost, angular accuracies of order 0.5 degrees are easily achievable.

Future work will continue in two mainstreams. First, the hardware-software bundle will be redesigned and expanded as to allow the miniaturization of sonar modules with increased integration in circuit. The addition of onboard precision laser diodes for precision experimentation are also planned. The accompanying extensions in the associated firmware will need to be made. In particular, we plan to add options for increasing the sampling rates and resolution. Furthermore, the intelligence of each sonar module can be increased by embedding all the algorithms including dual frequency beam shaping method. Secondly, we plan to continue working on the sonar signal analysis and interpretation. The dual frequency beam shaping can be extended to multiple-frequency operation. Furthermore, simultaneous use of multiple sensors will also be investigated.

APPENDIX A: TRANSDUCER SPECIFICATIONS

Air Ultrasonic Ceramic Transducers — 400ST/R160

Dimensions: dimensions are in mm

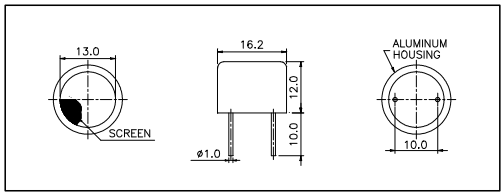

Specification

400ST160		Transmitter
400SR160		Receiver
Center Frequency		40.0±1.0Khz
Bandwidth (-6dB)	400ST160	2.0Khz
	400SR160	2.5Khz
Transmitting Sound Pressure Level at 40.0Khz; 0dB re 0.0002µbar per 10Vrms at 30cm		120dB min.
Receiving Sensitivity at 40.0Khz 0dB = 1 volt/µbar		-65dB min.
Capacitance at 1Khz	±20%	2400 pF
Max. Driving Voltage (cont.)		20Vrms
Total Beam Angle	-6dB	55° typical
Operation Temperature		-40 to 85°C
Storage Temperature		-40 to 85°C

All specification taken typical at 25°C
Closer frequency tolerance can be supplied upon request.

Impedance/Phase Angle vs. Frequency

Tested under 1Vrms Oscillation Level
400SR160 Impedance
400SR160 Phase
400ST160 Impedance
400ST160 Phase

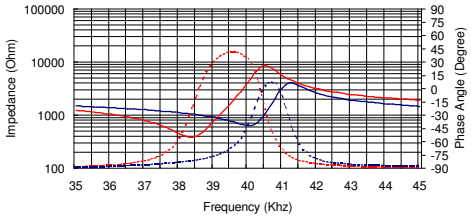

Sensitivity/Sound Pressure Level

Tested under 10Vrms @30cm

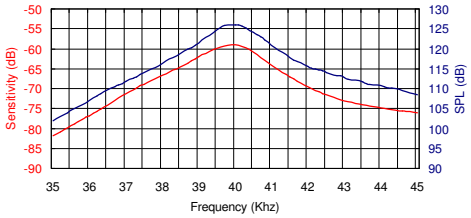

Beam Angle: Tested at 40.0Khz frequency

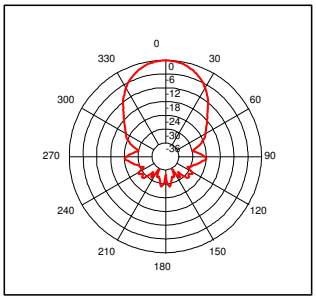

Models available:

1	400ST/R160	Aluminum Housing
2	400ST/R16B	Black Al. Housing
2	400ST/R10P	Plastic Housing
3	400ST/R16F	Al. Housing w/Solid Grid

REFERENCES

1. Kinsler, E. L., A. R. Frey, A.B. Coppens, and J. V. Sanders, "Fundamentals of Acoustics", *Academic Press*, 1980.

2. Cheeke, J. D. N., "Fundamentals and Applications of Ultrasonic Waves", *CRC Press*, 2002.

3. Schnitzler, H.U., C.F. Moss, and A. Denziger, "From spatial orientation to food acquisition in echolocating bats", *Trends in Ecology and Evolution*, Vol.18, No.8, 2003.

4. Middlebrooks, J., and D. Green, "Sound Localization by Human Listeners.", *Annual Review of Psychology*, 42, pp. 135-139, 1991.

5. Brungart, D. S., "Three-Dimensional Auditory Localization of Nearby Sources", Air Force Research Laboratory's Human Effectiveness Directorate, *http://www.afrlhorizons.com/Briefs/0009/HE0002.html*

6. Brungart, D. "Near-Field Auditory Localization.", PhD thesis, *Massachusetts Institute of Technology*, 1998.

7. Wightman, FL., and DJ Kistler., "The dominant role of low-frequency interaural time differences in sound localization", *Journal of the Acoustical Society of America*, 91, pp. 1648-1661, 1992.

8. Ihlefeld, A., and B.G. Shinn-Cunningham, "How natural environments alter spatial information in acoustic cues", *Cosyne (Computational and Systems Neuroscience)*, Salt Lake City, Utah, 2005.

9. Hartman, R., and K. Pohlmann, "High Frequency Effects on Localization and Sound Perception in a Small Acoustic Space", *SAE 2002 World Congress*, 2002.

10. Aytekin, M., E. Grassi, M. Sahota, and C. F. Moss, "The bat head-related transfer function reveals binaural cues for sound localization in azimuth and elevation", *Journal of Acoustic Society of America*, Vol. 116, No. 6, 2004.

11. Kalko, E. K. V., "Insect pursuit, prey capture and echolocation in pipistrelle bats (Microchiroptera)", *Anim. Behav.*, 50, pp. 861-880, 1995.

12. Shimozawa, T., N. Suga, P. Hendler, and S. Schuetze, "Directional Sensitivity of Echolocation System in Bats Producing Frequency-Modulated Signals", *Journal of Experimental Biology 60*, pp. 53-69, 1974.

13. Simmons, J. A., M. J. Ferragamo, and C. F. Moss, "Echo-delay resolution in sonar images of the big brown bat – Eptesicus fuscus", *Proc. Natl. Acad. Sci. USA*, Vol. 95, pp. 1264712652, 1998.

14. Wotton, J.M., and J.A. Simmons, "Spectral Cues and perception of the vertical position of targets by the big brown bat, eptesicus fuscus", *Journal of Acoustical Society of America*, 107(4), pp. 1034-1041, 2000.

15. Mogdans, J., J. Ostwald, and H.-U. Schnitzler, The role of pinnae movement for the localization of vertical and horizontal wire obstacles in the greater horshoe bat, rhinolophus ferrumequinum, *Journal of Acoustic Society of America*, 84(5), 1988.

16. Kampchen, N., "Evolving pinna-like surfaces for a biomimetic sonar head", Ms Thesis in Artificial Intelligence, *University of Edinburgh*, 2000.

17. Fazli, S., and L. Kleeman, "A Low Sample Rate Real Time Advanced Sonar Ring", *Proceedings of the Australasian Conference on Robotics and Automation*, Australia, 2004.

18. "Theory, History and The Advancement of Parametric Loudspeakers Rev. E", *A Technology Review*, American Technology Corporation, 2001.

19. Bererton, C., L.E. Navarro-Serment, R. Grabowski, C. J.J. Paredis, and P. K.

Khosla, "Millibots: Small Distributed Robots for Surveillance and Mapping", *Government Microcircuit Applications Conference*, 2000.

20. Yata, T., A. Ohya, and S. Yuta, "A Fast and Accurate Sonar-ring Sensor for a Mobile Robot", *ICRA*, 1999.

21. Kleeman, L., and A. Heale, "A Real Time DSP Sonar Echo Processor", *IROS*, 2000.

22. Duke, T. C., T. Gunnarsson, P. Mansen, and L. Asplund, "Design of an Ultrasonic Vision System for Environment Perception and Object Recognition in Robot Soccer", *RoboCup 2003 International Symposium*, 2003.

23. Suoranta, R., "Novel Ultrasonic Beamforming Method based on Nonlinear Filtering", *IEEE Ultrasonics Symposium*, Tucson, Arizona USA, 1992.

24. Kleeman, K., and R. Kuc, "Mobile Robot Sonar for target localization and classification", *International Journal of Robotics Research*, pp. 295-318, 1995.

25. Barshan, B., and A.S. Sekmen, "Radius of curvature estimation and localization of targets using multiple sonar sensors", *Journal of Acoustic Society of America*, Vol. 105, No:4 April, 1999.

26. Kleeman, L., and S. Fazli, "A Low Sample Rate Real Time Advanced Sonar Ring", *Proceedings of the Australasian Conference on Robotics and Automation*, 2004.

27. Bank, D., and E. Prassler, "Safe Navigation of Autonomous Mobile Systems by Wide-Range Ultrasonic Environment Coverage", 2002.

28. Kleeman, L., "Advanced Sonar Sensing for Robot Mapping and Localisation", *2nd Workshop on Biomimetic Ultrasound, Valencia*, 2003.

29. Kleeman, L., "Fast and accurate sonar trackers using double pulse coding", *IEEE/RSJ International Conference on Intelligent Robots and Systems*, Kyongju,

Korea, pp. 1185-1190., 1999.

30. Peremans, H., "Tri-aural perception for mobile robots", PhD thesis, *Department of Electronics and Information Systems* , University of Ghent, 1994.

31. Universal Serial Bus Specification, rev 1.1, 1998.

32. The RS485 Communications Authority, *http://www.rs485.com/*, 2006.

33. "AN232B-04 Data Throughput, Latency and Handshaking", *Future Technology Devices International Ltd.*, 2006.

34. "Driving Audio Piezoelectric Transducers", *Maxim Semiconductor Corporation*, 2002.

35. Moss, C.F., and S.R. Sinha, "Neurobiology of Echolocation", *Current Opinion in Neurobiology*, 13, pp. 751-758, 2003.

36. GNU GCC Open Source C Compiler for AVR family Devices, *http://winavr.sourceforge.net/*, 2006.

37. Kuc, R., "Forward Model for Sonar Maps Produced with the Polaroid Ranging Module", *IEEE Transactions On Robotics and Automation*, Vol. 19 NO.2, 2003.

38. Hol, W., "Piezoelectric transducer detuning for bat detectors", *http://bertrik.sikken.nl/bat/detuning.htm*, 2000.

39. Kollar, I., "Improved Residual Analysis in ADC Testing", *13th International Symposium on Measurements for Research and Industry Applications , 9th Workshop on ADC Modelling and Testing*, Athens, Greece, pp. 869-874, 2004.

40. Dou, H., and Y. Chen, "Optimal Features Extraction of Noisy Sinusoidal Signals Using Two-Stage Linear Least Squares Fitting", *technical report*, October 1998.

41. Schmeer, G., *Digitale Signalbearbeitung und statistische Datenanalyse - Teil 6*, 2004.

42. Deyst, J. P., T. M. Souders, and O. M. Solomon, "Bounds on Least-Squares Four-Parameter Sine-Fit Errors due to Harmonic Distortion and Noise", *IMTC*, 1994.

43. Kollar, I., and J. J. Blair, "Improved Determination of the Best Fitting Sine Wave in ADC Testing", *IMTC - Instrument and Measurement Technology Conference*, 2004.

44. Childers, D.G., D.P. Skinner, and R.C. Kemerait, "The Cepstrum: A Guide to Processing", *Proceedings of the IEEE*, Vol. 65, No.10, 1977.